การสร้างอะลูมินาพรุนโดยใช้เรซอซินอล ฟอร์มัลดิไฮด์เจลช่วย

นางสาวภมรรัตน์ จันธรรม

วิทยานิพนธ์นี้เป็นส่วนหนึ่งของการศึกษาตามหลักสูตรปริญญาวิศวกรรมศาสตรดุษฎีบัณฑิต
สาขาวิชาวิศวกรรมเคมี   ภาควิชาวิศวกรรมเคมี
คณะวิศวกรรมศาสตร์   จุฬาลงกรณ์มหาวิทยาลัย
ปีการศึกษา 2554

FORMATION OF POROUS ALUMINA ASSISTED BY
RESORCINOL-FORMALDEHYDE GEL

Miss Pamornrat Chantam

A Thesis Submitted in Partial Fulfillment of the Requirements
for the Degree of Doctor of Engineering Program in Chemical Engineering
Department of Chemical Engineering
Faculty of Engineering
Chulalongkorn University
Academic Year 2011

Thesis Title   FORMATION OF POROUS ALUMINA ASSISTED BY
RESORCINOL-FORMALDEHYDE GEL

By   Miss Pamornrat Chantam

Field of Study   Chemical Engineering

Thesis Advisor   Assistant Professor Varong Pavarajarn, Ph.D.

Accepted by the Faculty of Engineering, Chulalongkorn University in Partial Fulfillment of the Requirements for the Doctoral Degree

………………………………...… Dean of the Faculty of Engineering

(Associate Professor Boonsom Lerdhirunwong, Dr. Ing.)

THESIS COMMITTEE

……………………………………. Chairman

(Professor Paisan Kittisupakorn, Ph.D.)

……………………………………. Thesis Advisor

(Assistant Professor Varong Pavarajarn, Ph.D.)

…………………………………... Examiner

(Assistant Professor Nattaporn Tonanon, Ph.D.)

………………………………….. Examiner

(Assistant Professor Anongnat Somwangthanaroj, Ph.D.)

………………………………….. External Examiner

(Chanchana Thanachayanont, Ph.D.)

ภมรรัตน์ จันธรรม: การสร้างอะลูมินาพรุนโดยใช้เรซอซินอล ฟอร์มัลดิไฮด์เจลช่วย.

(FORMATION OF POROUS ALUMINA ASSISTED BY RESORCINOL-

FORMALDEHYDE GEL) อ.ที่ปรึกษาวิทยานิพนธ์หลัก: ผศ. ดร.วรงค์ ปวราจารย์,

158 หน้า.

การสังเคราะห์อะลูมินาพรุนซึ่งถูกใช้อย่างแพร่หลายในงานรูปแบบต่างๆ ภายใต้อุณหภูมิ สูง จากสารตั้งต้นของอะลูมิเนียมผสมกับอาร์เอฟเจล ด้วยวิธีโซล-เจลร่วมกับปฏิกิริยาโพลิเมอร์ไร เซชั่น ได้ถูกศึกษาโดยพบว่าสารตั้งต้นของอะลูมิเนียมสามารถเกิดปฏิกิริยากับอาร์เอฟเจลได้และยัง สามารถเร่งปฏิกิริยาโพลิคอนเดนเซชั่นได้อีกด้วย อะลูมิเนียม/อาร์เอฟเจลแบบโครงข่ายจะถูก เปลี่ยนเป็นอะลูมินาพรุนหลังจากการเผา โดยที่ความเป็นรูพรุนสูงยังคงถูกรักษาไว้ได้แม้ว่า อุณหภูมิที่ใช้ในการเผาจะสูงถึง 1200 องศาเซลเซียส จากผลการทดลองอะลูมิเนียมอะเซทิลอะเซโต เนตเป็นสารตั้งต้นของอะลูมิเนียมที่เหมาะสมในการสังเคราะห์อะลูมินาพรุน ซึ่งได้พื้นที่ผิวสูงถึง 68 ตารางเมตรต่อกรัม และพบว่าเป็นรูพรุนเมโซพอร์ขนาดใหญ่ นอกจากนี้อะลูมินาที่สังเคราะห์ได้ อยู่ในรูปเฟสอัลฟาซึ่งมีความเสถียรสูง ในงานวิจัยนี้ปัจจัยอื่นๆ เช่น เวลาที่ใช้บ่มเจล สัดส่วนของ อะลูมิเนียมในเจล อุณหภูมิที่ใช้ในการบ่มเจล และชนิดของตัวเร่งปฏิกิริยา ที่มีผลต่อการสังเคราะห์ อะลูมินา จะถูกวิเคราะห์อย่างละเอียด

ภาควิชา   วิศวกรรมเคมี   ลายมือชื่อนิสิต
สาขาวิชา   วิศวกรรมเคมี   ลายมือชื่ออ.ที่ปรึกษาวิทยานิพนธ์หลัก
ปีการศึกษา   2554

5071838721: MAJOR CHEMICAL ENGINEERING

KEYWORDS: FORMATION OF POROUS ALUMINA ASSISTED BY RESORCINOL-FORMALDEHYDE GEL

> PAMORNRAT CHANTAM: FORMATION OF POROUS ALUMINA ASSISTED BY RESORCINOL-FORMALDEHYDE GEL. ADVISOR: ASST. PROF. VARONG PAVARAJARN, Ph.D., 158 pp.

The synthesis of porous alumina, which has been widely used in high temperature applications, from aluminium precursor mixed with RF gel via sol-gel method accompanied with polymerization was investigated. It is found that the aluminium precursor can react with RF and further catalyze the polycondensation. The networked Al/RF gel is transformed into the porous alumina after the calcination step. In addition, high porosity is still maintained even though high calcination temperature of $1200^{o}C$ is applied. From the experimental results, the aluminium acetylacetonate is the suitable aluminium precursor in order to produce the porous alumina achieving high surface area of 68 m^2/g. It is disclosed that the pores are large mesopores. Moreover, the α phase of alumina representing high stable phase is obtained. In this research, other factors, such as aging time, aluminium content in RF gel, aging temperature and catalyst type, affecting the synthesis of the porous alumina will be discussed in detail.

Department: ....Chemical Engineering....   Student's Signature..............................

Field of Study: ..Chemical Engineering..   Advisor's Signature..............................

Academic Year:............2011............

ACKNOWLEDGEMENTS

CONTENTS

LIST OF TABLES

LIST OF FIGURES

Figure **Page**

Figure **Page**

Figure **Page**

Figure **Page**

Figure **Page**

Figure **Page**

CHAPTER I

INTRODUCTION

Porous alumina is an attractive material with broad range of applications. It can be used as adsorbents, membranes, microelectronic refractory materials and catalyst supports (Mahmoud et al., 2010, Yeung et al., 1997) because of the excellent properties such as chemical inertness, good mechanical strength and high hardness, transparency and corrosion resistance, as well as insulating and optical property. Various techniques have been proposed to fabricate the porous alumina having high surface area such as precipitation from solution, sol-gel method and hydrothermal synthesis. One common approach is the use of surfactant as a template during the synthesis (Ray et al., 2007). However, most surfactants decompose at relatively low temperature, for example, around $250^{o}C$ for CTAB (Jirglová and Maldonado-Hódar, 2010), hence they are ineffective toward the prevention of pore collapse during the calcination, especially when high calcination temperature is used, e.g., in the preparation of α-alumina. Moreover, the considerable reduction in surface area may also occur as alumina undergoes phase transformation (Zhang et al., 2009). In such case, the template that can retain its structural integrity at high temperature is needed.

A sol-gel polycondensation of resorcinol (R) and formaldehyde (F) mixtures was firstly proposed that a three-dimensional polymer matrix is arranged according to the method of Pekala (Pekala, 1989). The continuous network of resorcinol/formaldehyde (RF) gel has been proven to achieve high surface area at around 620 m^2/g (Lin and Ritter, 1997). Also, its decomposition due to breaking of C-C bonds in the structure of RF gels (Jirglová and Maldonado-Hódar, 2010) occur at high temperature compared to other kinds of template. The temperature can reach as high as 550°C (Jirglová and Maldonado-Hódar, 2010), thus the porous sample is possible to withstand the structural collapse. Consequently, RF gel is a good candidate to serve as a material template at high temperature. Therefore, it is used in the porous alumina synthesis in this research.

Our basic idea is to use the sol-gel processing to deposit and disperse an aluminium precursor in continuous network of RF gel. It has been recognized that the porous carbon with high specific surface area can be obtained from drying and carbonization of RF gel. Therefore, the porous alumina should also be formed by combining co-polymerization and sol-gel processes using porous network of RF gel as a source for porosity of the alumina. The composites of other materials fabricated by such approach have been proven to obtain the mesoporous structure with high specific surface area. Effects of various factors, such as type of aluminium precursor, type of catalyst, aluminium content and aging time, on the structure and the properties of the obtained product are discussed.

The present study is arranged as follows:

Chapter I is an introduction of this work. In Chapter II, the basic theory about alumina such as the general properties of alumina, sol-gel process, the details of resorcinol-formaldehyde gel and the classification of porous materials are described. Furthermore, literature reviews of the previous works relating to this research are presented in this chapter. Chapter III shows materials and experimental procedures for the alumina preparation assisted by RF gel. Chapter IV presents the experimental results and discussion. In the last chapter, the overall conclusions of this research and recommendations for the future work are given.

CHAPTER II

THEORY AND LITERATURE REVIEWS

The theory relating to synthesis, properties and characterization of alumina and organic resorcinol-formaldehyde gel, as well as definitions and classifications porous structure will be explained in this chapter.

2.1 Alumina

2.1.1 Classification of Alumina

Alumina (Al_2O_3) has been considered as one of the most promising advanced materials for variety of applications such as an adsorbent, a support for catalysts, coatings, and soft abrasives, because of its distinctive chemical, mechanical and thermal properties. Alumina is known to exist in a number of metastable polymorphs in addition to the thermodynamically stable alpha-alumina (α-Al_2O_3) or corundum form. There are six principally metastable phases of alumina designated by the Greek letters, i.e. chi (χ), kappa (κ), eta (η), theta (θ), delta (δ), and gamma (γ), respectively. The metastable alumina can be divided into two groups, i.e. the face-centered cubic (FCC) and the hexagonal close packing (HCP) arrangement of oxygen anion. The distribution of aluminium cations within the structure depends on types of the polymorphs (Garcia-Vergara et al., 2008). The alumina structures based on FCC packing of oxygen include γ-, η-, θ- and δ-phases, whereas those based on HCP packing of oxygen are the α-, κ- and χ-phases.

Most studies on phase transformation of alumina have been conducted by the calcination of alumina precursor. It has been found that the difference in sequence of phase transformation results from the difference in the precursor structure. The sequence of particular type formation under the thermal processing of gibbsite, bayerite, boehmite and diaspore are as follows (Lippens and Steggerdo, 1970).

Gibbsite $\xrightarrow{250C}$ χ-Al_2O_3 $\xrightarrow{900C}$ κ-Al_2O_3 $\xrightarrow{1200C}$ α-Al_2O_3

($Al(OH)_3$)

Bayerite $\xrightarrow{230C}$ η-Al_2O_3 $\xrightarrow{850C}$ θ-Al_2O_3 $\xrightarrow{1200C}$ α-Al_2O_3

($Al(OH)_3$)

Boehmite $\xrightarrow{450C}$ γ-Al_2O_3 $\xrightarrow{600C}$ δ-Al_2O_3 $\xrightarrow{1050C}$ θ-Al_2O_3 $\xrightarrow{1200C}$ α-Al_2O_3

(AlOOH)

Diaspore $\xrightarrow{450C}$ α-Al_2O_3
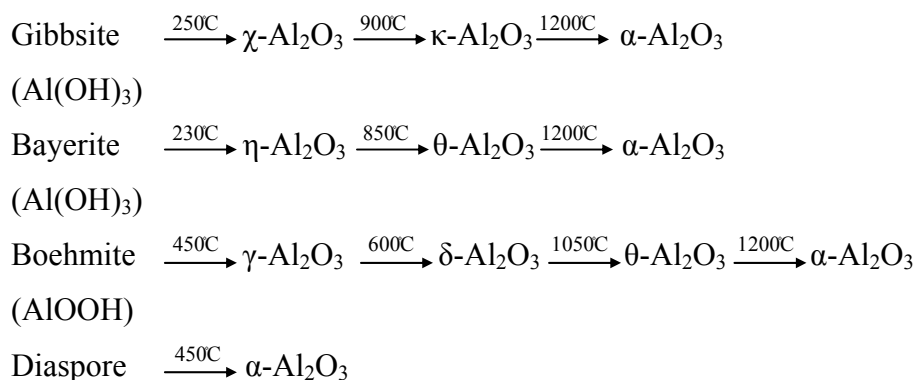
Normally, the sequence of phase transformation starts with aluminium hydroxide ($Al(OH)_3$ or AlOOH) transforming to low-temperature phase of alumina (η and χ) at temperature in the range of 150-500°C, before subsequently transforming to high-temperature phase (δ, θ and κ) at temperature range of 650-1000°C. Finally, the thermodynamically stable phase, α-Al_2O_3, is formed at temperature approximately 1100-1200°C. However, all alumina structures irreversibly transform into α-Al_2O_3 if annealed at high enough temperatures. The transition mechanisms between the starting phases and aluminium hydroxide are of particular interest because the transitions themselves can occur at different temperature depending on the particle size and method of manufacture (Cava et al., 2007). However, an understanding of the structures and an ability to distinguish between the phases is essential.

Many industrial solid catalysts are made up from active centers anchored on transition alumina supports due to the prominent characteristics of the transition alumina such as high porosity, high surface area, good mechanical strength and thermal stability. The excellent stability of alumina makes it an important constituent for many protective oxide scales of the surface of high-temperature metal and alloy. The dominant phase in these scales is α-Al_2O_3, which also contributes to adhesion and coherence of the scales. Normally, transition alumina starts losing the surface area even at temperature below 800°C due to the elimination of micro-pores during heat treatment. However, drastic loss occurs at temperature higher than 1000°C when the crystallization to the thermodynamically stable α-Al_2O_3 occurs (Dynys and Halloran, 1982, Zhang et al., 2009). In term of catalytic activity, high-temperature alumina is less active than low-temperature alumina as a result of lower surface area. Low-

temperature transition alumina, i.e., the metastable phase of low crystallinity indicated as high surface area and open porosity (Morterra and Magnacca, 1996), is in great interest in catalyst industries. In this research, the question how to increase the surface area of high-temperature of materials (stable materials like the α-Al_2O_3) with increasing the porosity is an interesting challenge in the investigation of material chemistry.

2.1.2 Fabrication of Porous Alumina Ceramic

Porous alumina ceramics have attracted significant attention because of their successful uses in a broad range of high-value applications including filters, electronic sensors, catalyst supports in the automotive and in petroleum industries, and construction materials, etc. For most of these applications, the alumina ceramic materials need to fulfill some specific requirements regarding their microstructure, porosity, permeability, mechanical properties, etc (Ishizaki et al., 1998).

Many strategies have been used to fabricate the porous alumina materials such as sol-gel (Khaleel and Al-Mansouri, 2010, Kritikaki and Tsetsekou, 2009), hydrothermal (Tikhov et al., 1999), precipitation (Parida et al., 2009), cation-anion double hydrolysis (Bai et al., 2009) and microemulsion templating method (Zhang et al., 2005). One of these strategies that used in this study is the sol-gel technique.

The sol-gel process has been applied to prepare amorphous and poorly crystalline materials, as porous ceramic with high surface area and small pore size (Brinker and Scherer, 1990). Applying the sol-gel chemistry offers excellent control of mixing (almost on the molecular level) because of its ability to alter the relative precursor reactivity. The precursor in the sol-gel preparation can either be metal salt or alkoxide dissolved in an appropriate solvent. The preparation of relatively stable mesoporous alumina requires strictly controlled synthesis conditions and complicated post-synthesis treatments (Xu et al., 2006).

Homogeneous gel network can be prepared by a simple sol-gel method, directly from aluminium triisopropylate (Brinker and Scherer, 1990). The as-obtained alumina gels have intermediate mechanical properties between the fluids and solids due to the formation of a well ordered spatial structure of solid network with submicronic porosity and non-linear polymeric chains. The controlled densification process achieved during the drying and annealing processes leads to nanoporous alumina with controlled porosity (Boissière et al., 2006, Kim et al., 2007, Tokudome et al., 2007).

The pore size of alumina ceramic made by the sol-gel method can be controlled by varying the processing conditions or using different types of porosity control additives (Jing et al., 2007, Lin and Burggraaf, 1991, Shi and Wong, 1999, Xu et al., 2006). The use of pore-forming agents is one of the frequently used methods to produce porous ceramics with controlled microstructure (porosity and pore size) (Studart et al., 2006). Many compounds are made in monolithic shape with hierarchical pores. These micro-, meso-, and macro-porous monoliths are generally prepared with polymer template method (Maekawa et al., 2003) including the following steps:

1. Preparing macroporous organic foam with a certain shape.
2. Filling the organic foam with precursor sol.
3. Removing the template by calcination or etching.

The resultant monoliths are the replica of the polymer foams, as shown in Figure 2.1, both in microscopic and macroscopic scales, although volume shrinkage takes place to some extent. The shape of the templates can be controlled and molded with mold. Moreover, size of the macropores can be adjusted by changing the volume fraction of the dispersed phase (Maekawa et al., 2003).
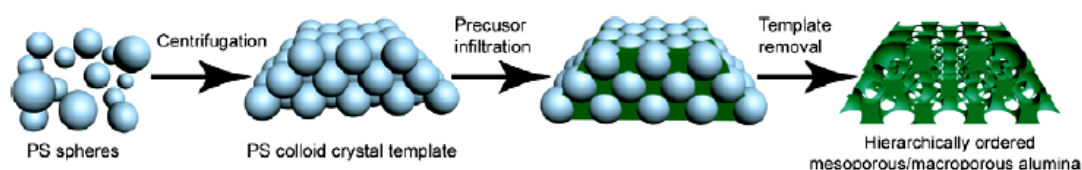
Figure 2.1 Synthesis scheme for the preparation of hierarchically ordered
mesoporous/macroporous alumina using PS colloidal/block co-
polymer dual templates (Maekawa et al., 2003).

Theoretically, if the appropriate template and precursor have been chosen,
macroporous monolith of various compounds can be obtained in any shape with
adjustable macropore sizes. This preparation method has attractive advantages, such
as pore structure controllable and shape moldable as stated above. However, no
reports have been found for the preparation of alumina monolith with hierarchically
porous structure by using this method (Zhang et al., 2009).

2.2 Sol-Gel Chemistry

Sol-gel technology is an important technique for the production of high quality
ceramic at relatively low temperature. Figure 2.2 shows various methods for the sol-
gel process. The sol-gel method is the most promising technique to prepare highly
pure powders with high specific surface area (Dumeignil et al., 2003). For the
formation of α-alumina at low temperature, several studies have employed sol-gel
method (Bahlawane and Watanabe, 2000, Gocmez and Özcan, 2008). In this work,
porous alumina is formed by assistance of organic resorcinol-formaldehyde gel,
which is also prepared by the sol-gel process. There are basically two kinds of the sol-
gel technology that are currently employed to synthesize inorganic materials. The first
one consists of a formation of dispersed colloidal particles in a liquid or sol, which is
then destabilized to produce gel. The second one involves the polymerization of

organometallic compounds such as alkoxides through the removal of stabilizing organic components to produce continuous network of gel.
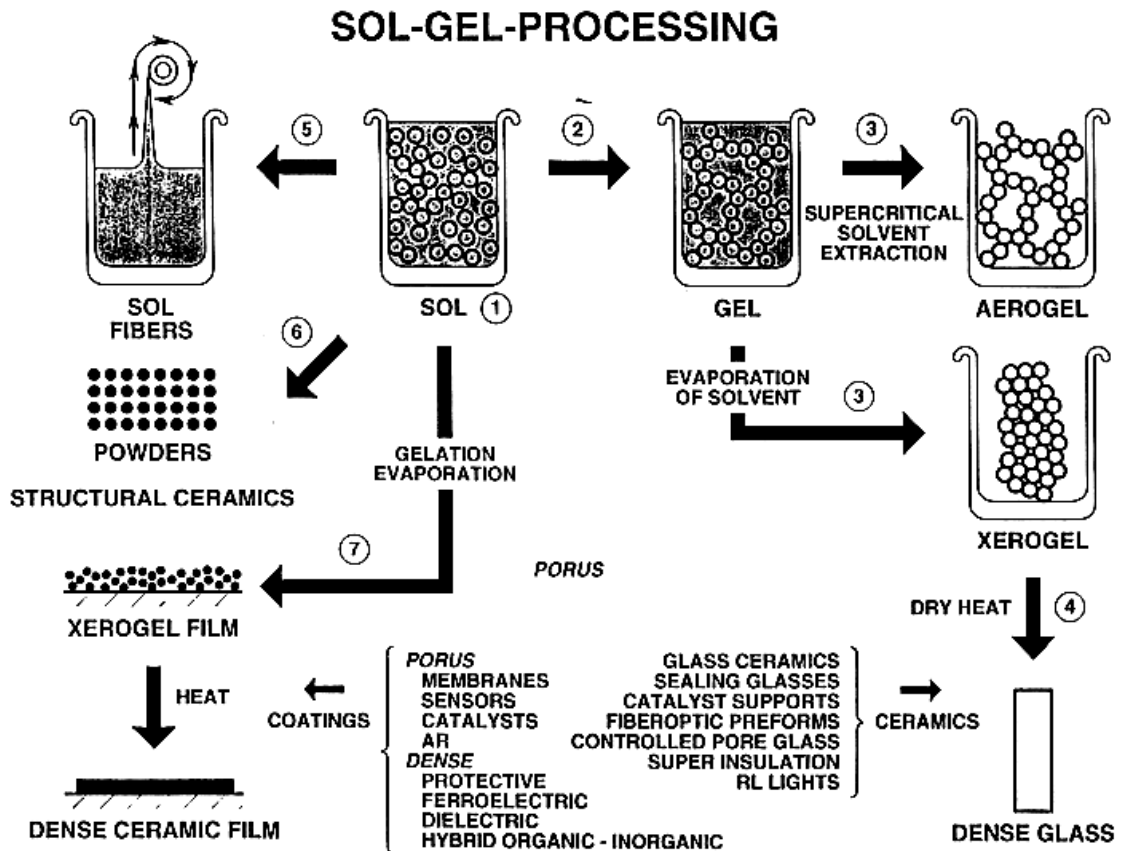
SOL-GEL-PROCESSING

Figure 2.2 Various procedures for processing a sol-gel reaction mixture lead to different types of materials (Brinker and Scherer, 1989).

The sol-gel process involves the formation of sol following by that of gel. A sol is a colloidal suspension of solid particles in liquid. A colloid is a suspension in which the dispersed phase is so small, i.e., particle size ranging from 1 nm to 1 μm, that gravitational forces are negligible and interactions are dominated by short-range effects such as van der waals attraction and electrostatic forces resulting from surface

charges. The sol can be obtained by the hydrolysis and partial condensation of a precursor such as an inorganic salt or a metal alkoxide. Further condensation of sol particles into a three-dimensional network produces gel. A gel can be interpreted to consist of continuous solid and liquid phases of colloidal dimensions. Continuity means that one could travel through the solid phase from one side of the sample to the other without having to enter the liquid; conversely one can make the same trip entirely within the liquid phase. Since both phases are of colloidal dimension, a line segment originating in a pore and running perpendicularly into the nearest solid surface must re-emerge in another pore less than 1 μm away. Similarly, a segment originating within the solid phase and passing perpendicularly through the pore wall must re-enter the solid phase within a distance of 1 μm (Brinker and Scherer, 1989). The gel is a diphasic material with solids encapsulating liquid or solvent. Alternatively, the gel can be produced by destabilizing the solution of preformed sols. In either case, the materials are referred to as aqua-sol (or aqua-gel) if water is used as a solvent, and alco-sol (or alco-gel) if alcohol is used.

In principle, the sol-gel designates process in which the gel is formed from the particles of the sol when attractive forces cause them to stick together in such a way as to form a network. In other words, sol-gel process should imply the formation of the gel by aggregation of particles in the sol. However, the term sol-gel is often used in literature to designate the process that lead to the gel (or sometimes merely to a slurry) from a homogeneous solution of soluble monomer precursors whatever the underlying physico-chemical mechanisms. Indeed, mechanisms other than aggregation have been suggested in various cases. For example, if a monomer can make more than two bonds, then there is no limit on the size of the molecule that can fill the space. If one molecule reaches macroscopic dimensions so that it extends throughout the solution, the substance is said to be the gel and Figure 2.3 shows definition of various species occurred during this process. Another example concerns the mechanism based on the separation of the initial homogeneous solution into two immiscible continuous and interconnected liquid phases, reminiscent of the structure of the gel, and called spinodal phase separation (Brinker and Scherer, 1989).
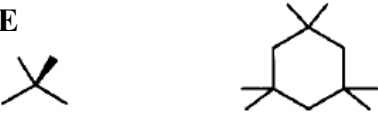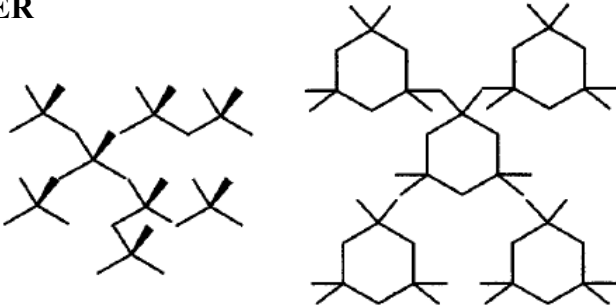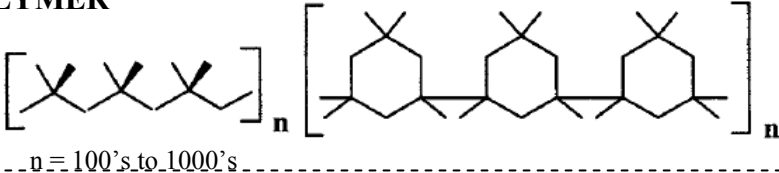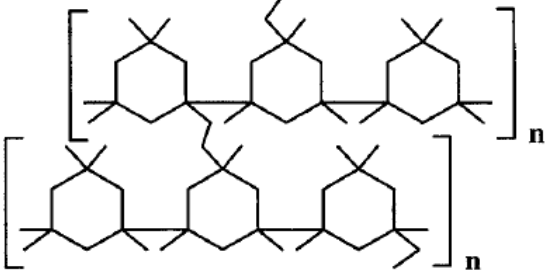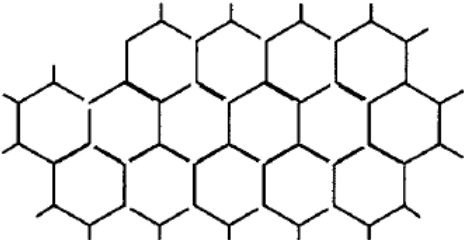
DEFINITIONS		
SMALL MOLECULE		Soluble, meltable, volatile
CLUSTER		Soluble, meltable, low volatile
POLYMER	$n = 100's\ to\ 1000's$	Soluble, meltable, non-volatile
CROSSLINKED SYSTEM		Insoluble (may swell), infusible, non-volatile, thermally reactive
CERAMIC		Insoluble, infusible, non-volatile, hard

Figure 2.3 Definitions of the various species occurred during sol-gel processing (Mark et al., 1989).

Depending on whether the liquid in the wet gel is removed by evaporating drying or by supercritical drying, that is in pressure and temperature conditions beyond the critical point of the liquid, the resulting dry material is named xerogel and aerogel, respectively. Third classes of materials are cryogels dried by freeze-drying or lyophilization.

The single most important characteristic of the sol-gel preparation of inorganic materials is its ease of control that translates into the following advantages:

(i)   the ability to maintain high purity (because of purity of starting materials);

(ii)   the ability to change physical characteristics such as pore size distribution and pore volume;

(iii)   the ability to vary compositional homogeneity at a molecular level;

(iv)   the ability to prepare samples at low temperatures;

(v)   the ability to introduce several components in a single step;

(vi)   the ability to produce samples in different physical forms.

Four key steps in converting a precursor to a particular product form via sol-gel preparation are formation of gel, aging of gel, removal of solvent, and heat treatment. The versatility of this preparative approach lies in the number of parameters that can be manipulated in each of these steps, as seen in the Figures 2.4 and 2.5.

THE NEED FOR CROSSLINKING DURING THERMOLYSIS

Depolymerization or degradation

VOLATILE SMALL MOLECULES

POLYMER   Heat

Crosslinking

NETWORK STRUCTURE   →   **CERAMIC**
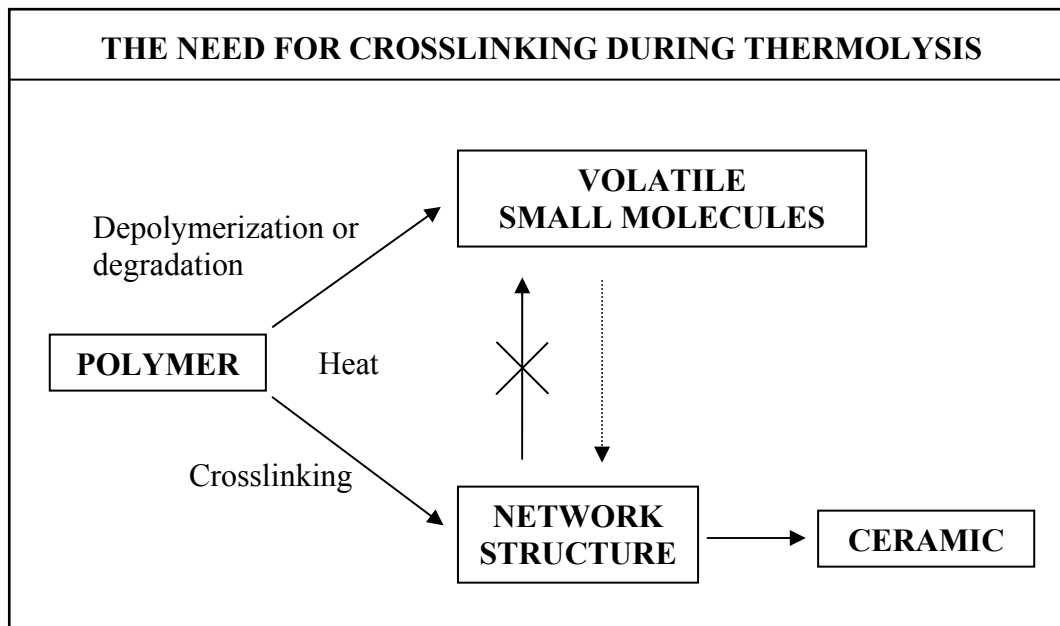
Figure 2.4 Illustrating the crucial need for cross-linking the preceramic polymer at an early stage in the pyrolysis to prevent loss of material in the form of volatile decomposition or depolymerization products (Mark et al., 1989).

The critical crosslinking step

CLUSTER → **NETWORK**

A

MONOMER → **POLYMER** → **NETWORK** → **CERAMIC**

B

C

Loss of carrier

CARRIER POLYMER → **NETWORK**
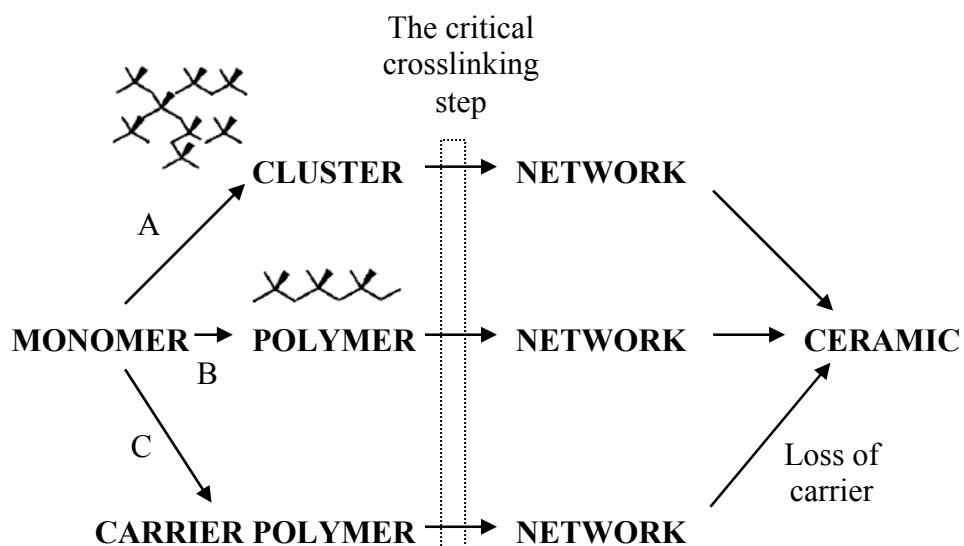
Figure 2.5 Three routes to ceramics all of which proceed through a vital crosslinking process to give a network early in the pyrolysis program. In pathway C the carrier

polymer is decomposed during pyrolysis and the side groups are incorporated into the final ceramic (Mark et al., 1989).

In the sol-gel process, the precursors for synthesis of colloid consist of a metal or metalloid element surrounded by various ligands, as shown in Table 2.1.

Table 2.1 Commonly used ligands (Brinker and Scherer, 1989).

Alkyl		Alkoxy	
methyl	$\cdot CH_3$	methoxy	$\cdot OCH_3$
ethyl	$\cdot CH_2CH_3$	ethoxy	$\cdot OCH_2CH_3$
n-propyl	$\cdot CH_2CH_2CH_3$	n-propoxy	$\cdot O(CH_2)_2CH_3$
iso-propyl	$H_3C(\cdot C)HCH_3$	iso-propoxy	$H_3C(\cdot O)CHCH_3$
n-butyl	$\cdot CH_2(CH_2)_2CH_3$	n-butoxy	$\cdot O(CH_2)_3CH_3$
sec-butyl	$H_3C(\cdot C)HCH_2CH_3$	sec-butoxy	$H_3C(\cdot O)CHCH_2CH_3$
iso-butyl	$\cdot CH_2CH(CH_3)_2$	iso-butoxy	$\cdot OCH_2CH(CH_3)_2$
tert-butyl	$\cdot C(CH_3)_3$	tert-butoxy	$\cdot OC(CH_3)_3$
Other			
acetylacetonate	$H_3COC(\cdot O)CH_2(O\cdot)COCH_3$		
acetate	$\cdot OOCCH_3$		

As mentioned earlier, the precursor in the sol-gel preparation can either be a metal salt/alkoxide dissolved in an appropriate solvent or a stable colloidal suspension of preformed sols. Metal alkoxides have been the most extensively used because they are commercially available in high purity and their solution chemistry has been documented. At its simplest level, sol-gel chemistry with metal alkoxides can be described in terms of two classes of reactions:

$$\text{Hydrolysis:} \quad \text{-M-OR} + H_2O \longrightarrow \text{-M-OH} + ROH$$
$$\text{Condensation:} \quad \text{-M-OH} + \text{XO-M-} \longrightarrow \text{-M-O-M-} + XOH$$
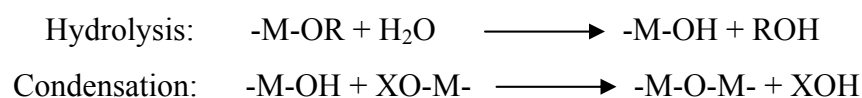
where X can either be H or R (an alkyl group).

Such a description oversimplifies the overall process because it does not correctly represent the molecular formulas of intermediates and end products, nor does it depicts the simultaneous occurrence of the two reactions. However, this oversimplification captures the key phenomenological idea that a three-dimensional gel network comes from the condensation of partially hydrolyzed species. Any parameters that affect either or both of these reactions are thus likely to impact on the properties of the product and Figure 2.6 reveals the different porous alumina product from the different hydrolysis method. In fact, the important variables are the reaction rates of hydrolysis and condensation.
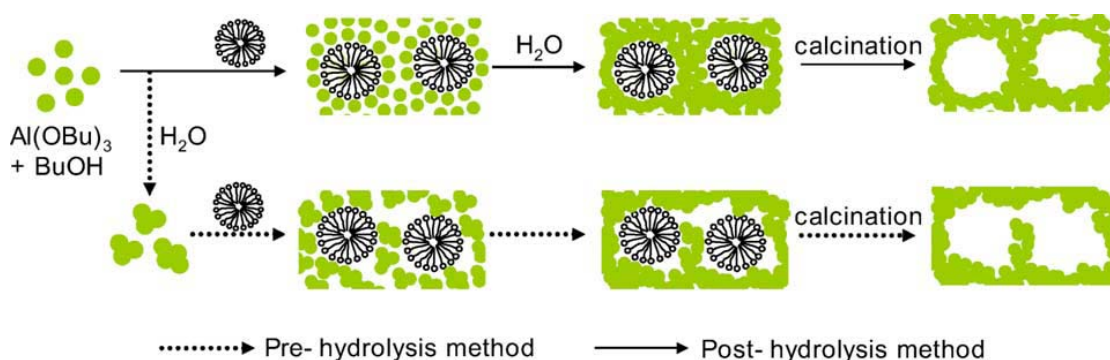
Figure 2.6 Comparison of pre- and post- hydrolysis methods for the synthesis of mesoporous alumina (Kim et al., 2005).

Because hydrolysis and condensation are both nucleophilic displacement reactions, the reactivity of metal alkoxides depends on the positive partial charge of the metal atom and its coordination number. For example, TEOS, which contains small positive partial charge on silicon, is the least reactive among the common alkoxides. In general, the longer and bulkier the alkoxide group attached to a particular metal atom is, the less reactive that precursor is in hydrolysis and

condensation. Changing of the type of precursor and/or its concentration are thus effective means of controlling the reaction rates.

The amount of water used in sol-gel preparation and the rate by which it is added also influence gel characteristics. The former is usually expressed in terms of the hydrolysis ratio h, defined as the moles of water per mole of metal alkoxide, $M(OR)_m$. There are three specific regions of interest:

(i) $h < 1$: An infinite network seldom forms due to the low functionality of the precursor towards condensation. Because there are few M-OH groups for cross-linking, gelation or precipitation cannot occur when there is no local excess of water.

(ii) $1 < h < m$: Polymeric gels can form.

(iii) $h < m$: Cross-linked polymers, particulate gels, or precipitates can form when an excess of water is added to the alkoxides.

For a given amount of water, another level of control comes from the rate of addition. Common approaches to slow addition of water are: using a micropipette, absorbing moisture from a controlled humidity environment, and generating water in the solution with another chemical reaction.

Moreover, two other important sol-gel parameters are temperature and type of solvent. Both hot and cold plates are commercially available and can be used to increase or decrease the reaction rate, respectively. Varying the temperature is most effective when it can alter the relative rate of competing reactions. Solvent can change the nature of an alkoxide or can affect the condensation reaction directly. It is also possible to prepare gel without solvent as long as another mean, such as ultrasound irradiation, is used to homogenize an otherwise immiscible alkoxide/water mixture.

Using preformed sols instead of metal alkoxides as precursors is an attractive alternative in sol-gel preparation because recent advances in inorganic colloidal dispersions allow some control over the characteristic of the starting sols. Colloidal

suspension of sol particles is often stabilized (i.e. prevented from flocculation) by pH adjustment. Thus, pH of the solution, which can be changed by the addition of either acid or base, is the single most important parameter in obtaining gel from preformed sols. Other parameters that influence gel quality are size and concentration of the starting sol particles.

To summarize, the basic chemistry associated with formation of a typical sol-gel material such as silica gel is given in very simplified from in the following Figure 2.7.
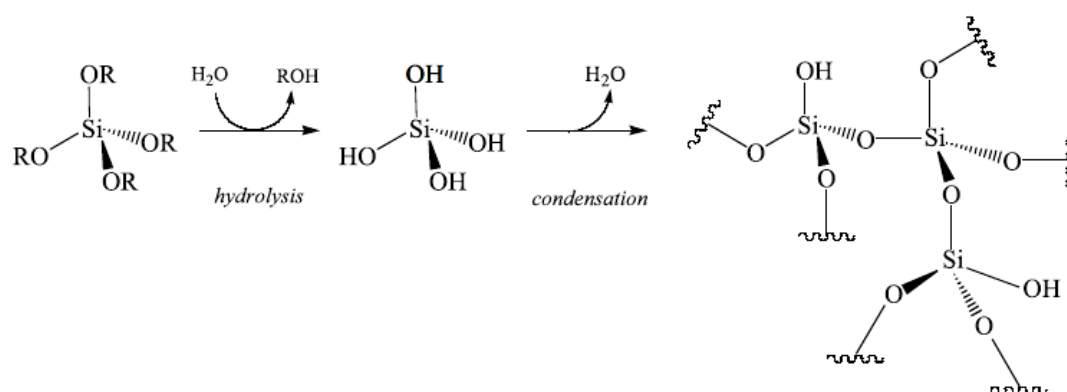
Figure 2.7 Basic steps of a typical sol-gel process from a metal alkoxide.

In the case of silicon alkoxides, hydrolysis occurs by the nucleophilic attack of the oxygen contained in water on the silicon atom and is most rapid and complete when acid (e.g. HCl, CH_3COOH and HF) or basic (e.g. NH_3, KOH and amines) catalysts are employed. Under acidic conditions, it is likely that an alkoxide group is protonated in a rapid first step. Electron density is withdrawn from silicon, making it more electrophilic and thus more susceptible than attacked by water. Under basic conditions it is likely that water dissociates to produce nucleophilic hydroxyl anions in a rapid first step. Then, the hydroxyl anion attacks the silicon atom. Polymerization to form siloxane bonds occurs by either a water-producing condensation reaction or

an alcohol-producing condensation reaction and Figure 2.8 shows the effect of pH condition on the property of gel. Depending on condition, a complete spectrum of structures ranging from molecular networks to colloidal particles may result. Although the condensation of silanols can proceed thermally without involving catalysts, the use of acid or basic catalysts, similar to those used for hydrolysis, is often helpful and various mechanisms have been suggested to explain the role of the catalysts.
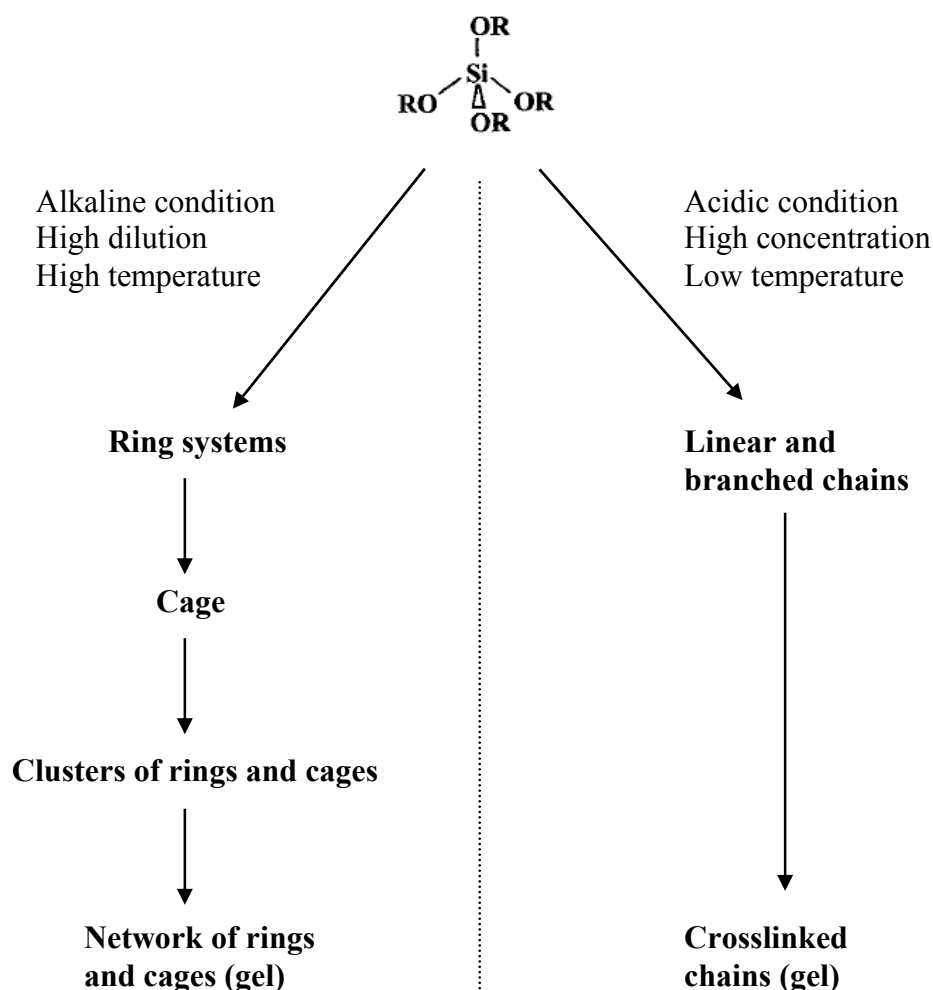
Figure 2.8 Reaction conditions exert a strong influence on the course of a sol-gel polymerization reaction. Basic pH, high temperature, and great dilution favor the formation of rings and ring clusters, as shown in the pathway on the left. Acidic pH,

low temperatures, and high concentrations favor the formation of chains and dendritic structures (Mark et al., 1989).

An important advantage of sol-gel chemistry over conventional oxide preparation techniques is the possibility it offers to prepare mixed oxides, such as SiO_2-Al_2O_3 with an excellent control of mixing because of its ability to adjust the relative precursor reactivity. Mixed oxides are interesting catalysts or catalyst supports because they often display acid strengths that are significantly higher than either of the component oxides. In a mixed oxide MO_x-$M'O_y$, the acidic properties are related to the homogeneous mixing of the two component oxides in terms of a number of available M-O-M' linkages. The key condition to obtain molecularly homogeneous mixed oxides is to adjust the relative reactivity of the precursors in such a way that they have similar rates of hydrolysis and/or condensation. The matching of precursor reactivity can be accomplished using various strategies including the use of a precursor containing a different alkoxy group, the prehydrolysis of a less reactive precursor, the slowing down of a more reactive precursor by replacing some of its alkoxy groups with different ligands or by stabilizing it by using an appropriate solvent, and the modification of synthesis temperature. For prepared SiO_2-TiO_2 mixed oxides with low titania crystallization tendency by using single-source precursors containing both $-Si(OR)_3$ and $-Ti(OR)_x$ (X=2 or 3) moieties linked by an organic group.

From the hydrolysis and condensation reactions presented above as a starting point, various theories corresponding to various physico-chemical mechanisms have been suggested to explain the formation of the wet gel. According to several authors who investigated how inorganic polymer systems, such as SiO_2, TiO_2 and ZrO_2, are formed. The materials are obtained via the formation of elementary building blocks that, in a secondary stage, aggregate until the resulting clusters fill the space. This is the aggregation theory. According to that theory, the large variety in structures results from differences in the details of the building blocks and in their aggregation mechanisms, which are governed by the nature of the precursor and by the synthesis condition. It must be noted that the building block notion is sometimes confusing in

literatures since it designates now a monomer molecule, now silica, alumina and titania particle of about several tens nanometer, that is a large macromolecule. However, the aggregation mechanism implies most often first the formation of inorganic particles by polycondensation followed by their aggregation.

For any of the sol-gel parameters discussed so far, its effect on gel properties can often be observed by an experimental parameter known as gel time. Gel time is defined as the time that the solution undergoes rapid rise in viscosity which is corresponding to the transition from viscous fluid to elastic gel. At the gel point, the solid phase forms a continuous structure that reflects the formation and branching of particles under specific growth condition. This particular phase is an important because it is the genesis of structural evolution that takes place in all subsequent processing steps.

For the synthesis of alumina via sol-gel technique, the process starts with the mixing aluminium alkoxide (Yoldas, 1975) or inorganic aluminium salts (Ramanathan et al., 1994) with alcohol or water. Acid aqueous solution is subsequently added to the mixture (Ecsedi et al., 2008). This technique can be adapted by using ultrasonic vibrations to aid dispersion (Yao et al., 2002), which can make result in alumina with higher surface area than alumina prepared by using stirring method. The average crystal size of alumina synthesized by ultrasonic vibrations method has been reported to be in the range of 10 – 20 nm and BET surface area in the range of 50-170 m^2/g (Ecsedi et al., 2008), depending on calcinations temperatures. However, the limitation of this method is strong reactivity of alkoxide toward water that often results in uncontrolled precipitation.

2.3 Resorcinol-Formaldehyde Gel

Beside gels composed of a metal oxide skeleton, sol-gel process is also a powerful tool for synthesizing porous organic three-dimensional networks in a solvent. The increasing popularity of these organic materials is largely due to their unique and controllable properties. They open up new horizons for obtaining highly porous tailor-made carbon catalyst supports since, after drying, organic gels can be converted into carbon gels by pyrolysis (Lin and Burggraaf, 1991, Pekala, 1989).

Porous carbon gels have been prepared by polycondensation of hydroxylated benzene (phenol, catechol, resorcinol, hydroquinone or phloroglucinol) and aldehyde (formaldehyde, furfural) in a solvent followed by drying and pyrolysis have been extensively studied for the past fifteen years (Saunders, 1988). Various carbon materials whose texture depends on the nature of the precursors, the gelation conditions and the drying method can be obtained. The most common precursors are resorcinol (1,3-dihydroxybenzene) and formaldehyde (CH_2O). The polymer is usually synthesized using water as solvent and sodium carbonate (Na_2CO_3) as catalyst (Pekala, 1989).

The reaction of resorcinol with formaldehyde to produce resorcinol-formaldehyde (RF) resins is well known. RF resins have a wide rang of industrial applications particularly in wood and rubber industry. These resins have been used as room temperature curable adhesives to bond wood products and widely used to enhance the adhesion between various synthetic fibers, i.e. steel, polyester, nylon, rayon, glass and rubber compounds (Durairaj, 2005).

The organic sol-gel polymerization chemistry involving a reaction between phenol and formaldehyde has been widely studied for a long time (Saunders, 1988). The reaction of resorcinol with formaldehyde is similar to that of phenol. However, the reactivity of resorcinol with formaldehyde is completely different, and therefore the products formed from the reaction can be different. With phenol, complete reactivity and mechanistic studies have been made and well documented (Grenier-

Loustalot et al., 1996a, Grenier-Loustalot et al., 1996b, 1996c, Grenier-Loustalot et al., 1994, Grenier-Loustalot et al., 1996d). On the other hand, the resorcinol-formaldehyde reaction may not be understood and properly documented.

Resorcinol has two hydroxyl groups that are located at the 1- and 3-positions in the benzene ring, as shown in Figure 2.9.
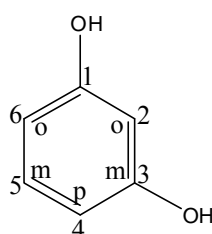
Figure 2.9 Molecular structure of resorcinol.

The reaction sites or positions in the resorcinol molecule for various chemical reactions, including formaldehyde, are 2-, 4- and 6-. Of these three, the 2-, 4- and 6-positions are located at either "ortho" (adjacent) or "para" (opposite) to the two hydroxyl groups. The electron density of δ (delta) and π (pi) electrons of resorcinol molecule contributes to the electrophilic substitution of protons at the 2-, 4- and 6-positions of the benzene ring. Resorcinol can undergo all of the typical reactions of phenol, but at a much faster rate because of the enhanced electron density at the 2-, 4- and 6-positions. The ratio of electron density at the 2-position (ortho) to the 4- or 6- (ortho-para) position is about 5.8 (Šebenik et al., 1981), which higher at the 2-position, it is sterically hindered by the adjacent hydroxyl groups and therefore the substitutions primarily occur at the 4- and 6-positions.

Because of the high electron density at 2-, 4- and 6- reactive positions, resorcinol can react with formaldehyde at room temperature without any catalysts, meaning under neutral conditions, and at a fast rate. The pH of the solution depends on their molar ratios and the reaction can be faster at the pH conditions approximately

4.0 (Raff and Silverman, 1951). From quantitative ^{13}C NMR analysis of previous report, it was observed that uncatalyzed RF reaction at room temperature and a pH of 4.0 produced only methylene bridged substitutions (Werstler, 1986). The absence of methylol groups in the uncatalyzed RF reaction product strongly suggests a very fast reaction that occurred between resorcinol and formaldehyde at room temperature condition.

The resorcinol is more reactive because of the electron-donating, ortho- and para- directing affects of the attached hydroxyl groups (Varagnat). As illustrated in Figure 2.10, the resorcinol-formaldehyde polymerization mechanism including the formation of resorcinol anions by hydrogen abstraction (enhanced by OH-) (step 1a), the formaldehyde addition to obtain hydroxymethyl derivatives ($-CH_2OH$) of resorcinol (mono-, di-, and tri-substituted methylolphenols) (step 2), and the condensation of the hydroxymethyl derivatives (catalyzed by H^+) to form methylene ($-CH_2-$) and methylene ether ($-CH_2OCH_2-$) bridged compounds which leads to cluster growth (step 3) (Pekala et al., 1991, Regalbuto, 2006).
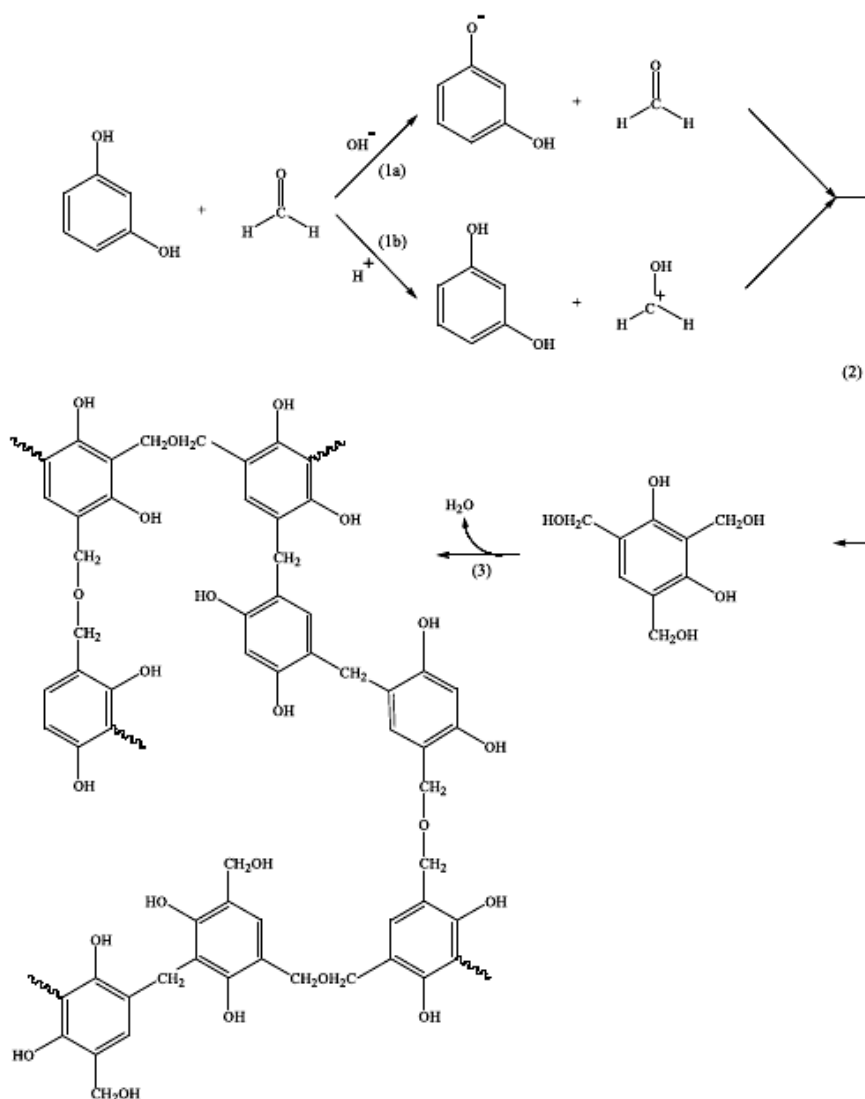
Figure 2.10 Resorcinol-formaldehyde polymerization mechanisms (Regalbuto, 2006).

The mechanism of step 1a is questionable in acidic solutions, because of the very low amount of charged species (resorcinol anions) present at the beginning of the polymerization reaction. In this case, the charged species activate the addition reaction that is probably the protonated form of formaldehyde, $(CH_2-OH)^+$ (step 1b), which is more sensitive to resorcinol addition than molecular formaldehyde.

Note that the often used sodium carbonate is not a catalyst strictly speaking. Indeed, its primary role is to increase the acidic pH of the resorcinol-formaldehyde aqueous solution by increasing the OH^-/H^+ ratio. Sodium cations (Na^+) have no direct role in the polymerization reaction whereas carbonate anions (CO_3^{2-}) basify the solution. In fact, the pH changing can be achieved by addition of any base that does not react with resorcinol or formaldehyde such as sodium hydroxide (Tamon and Ishizaka, 2000). In all cases, the concentration of activated species and the condensation rate are controlled by the pH of the solution.

According to Yu et al. (Yu et al., 1996) who examined the polymerization of 1,4 benzenedimethanol ($HOCH_2$-ph-CH_2OH) in a concentrated H_2SO_4 medium, the condensation of hydroxymethyl derivatives is catalyzed by H^+ according to the presumed following mechanism: in the presence of a proton, such molecules lose their -OH groups to form a benzyl-type cation (-ph-CH_2^+). The cation then undergoes an electrophilic reaction with the benzene ring of another molecule to connect the two benzene rings with a methylene bridge (-CH_2-) (Streitwieser and Heathcock, 1976, Yu, Kaneko, Yoshimura and Otani, 1996). Pekala et al. (Pekala, Alviso and LeMay, 1991) also showed that the cation can react with a hydroxymethyl group of another molecule to form a methylene ether bridge. In the case of the hydroxymethyl derivatives of resorcinol, successive repetitions of such a condensation reaction lead to the three-dimensional cross-linked polymer.

Since the texture of the final material obtained after drying and pyrolysis that is strongly influenced by the reaction mechanism which is itself influenced by pH, the latter is a key variable for controlling texture. Indeed, depending on the pH interval used for synthesis, micro-macroporous, micro-mesoporous, only microporous or totally non-porous carbon materials can be obtained (Job et al., 2004, Lin and Ritter, 1997, Pekala et al., 1991).

The various mechanisms proposed in literatures to explain the formation of inorganic gels are also encountered in the case of organic gels. However, in the latter case, the mechanism based on phase separation and particularly spinodal phase

separation is most often suggested as the polymerization proceeds, the molecular weight of clusters consisting of branched polymeric species increases which makes them immiscible and induces a phase separation, the polymer-rich phase becoming the precursor of the final organic gel skeleton (Pekala and Schaefer, 1993, Schaefer et al., 1995). Beside the phase separation mechanism, the clusters formation followed by aggregation mechanism is suggested by some authors (Tamon and Ishizaka, 1998).

RF gel was first synthesized by Pekala via sol–gel polycondensation of resorcinol (R) and formaldehyde (F) with sodium carbonate (C) as catalyst (Pekala, 1989). A polycondensation reaction between resorcinol and formaldehyde results in a three-dimensional polymer matrix called the RF hydrogel. Then, mesoporous carbon gel, which is consisted of solid carbon skeleton, can be formed by heat treatment of the RF gel after solvent exchange and drying (Lin and Burggraaf, 1991, Pekala, 1989).

The major reactions between resorcinol and formaldehyde including (1) an addition reaction to form hydroxymethyl derivatives ($-CH_2OH$) of resorcinol, and (2) a condensation reaction of the hydroxymethyl derivatives to form methylene ($-CH_2-$) and methylene ether ($-CH_2OCH_2-$) bridged compounds (Lin and Ritter, 1997). Figure 2.11 illustrates a brief mechanism of the sol-gel polymerization of resorcinol with formaldehyde.

1. Addition Reaction
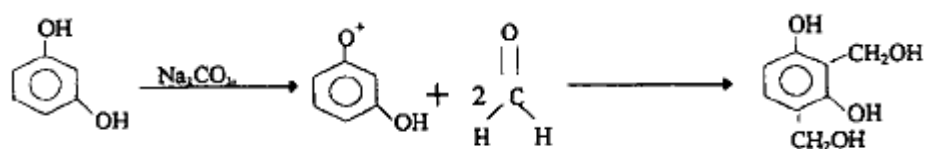
2. Condensation Reaction
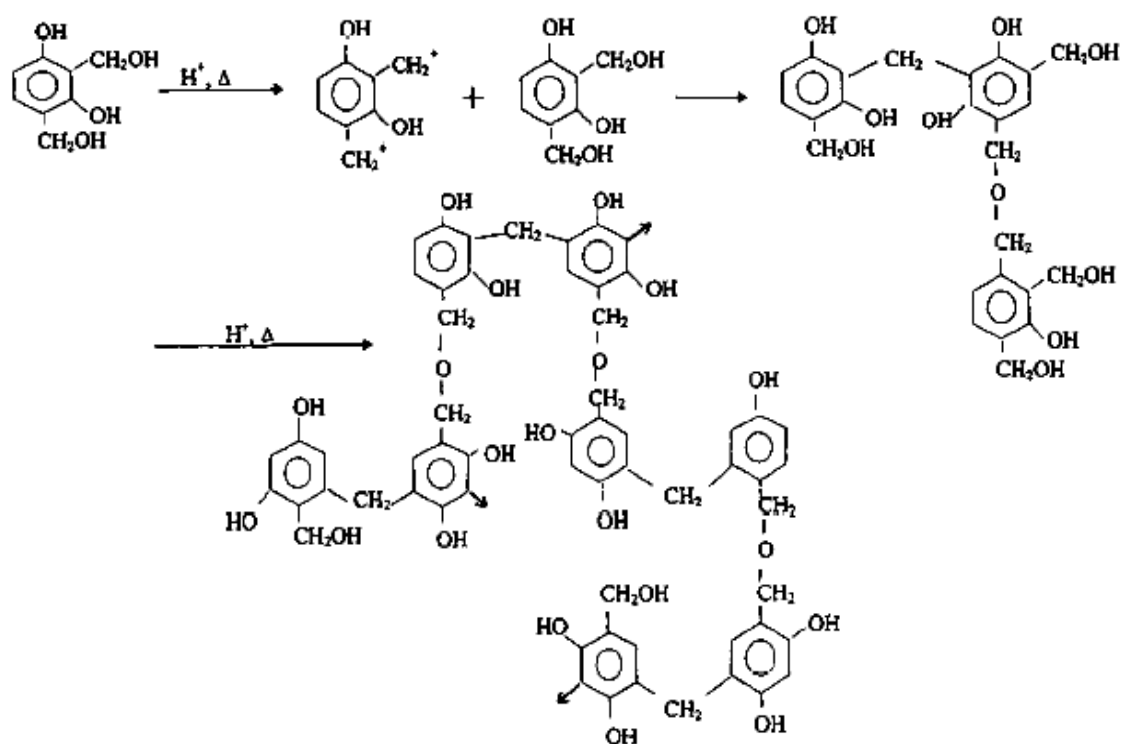
Figure 2.11 Reaction mechanism of the sol-gel polymerization of resorcinol
with formaldehyde (Lin and Ritter, 1997).

2.3.1 Factors Influencing Polymerization Reaction of RF Gel

The properties of the wet RF gel are affected and can be tailored through controlling the concentrations of the main ingredients (resorcinol and formaldehyde), catalyst type and concentration, initial solution pH, the curing time and temperature. Details on these factors and their effects on the structural properties as summarized in Table 2.2.

Table 2.2 Effects of various synthesis conditions on the corresponding properties of organic gels (ElKhatat and Al-Muhtaseb, 2011).

Factor Type	Factor Condition	Resulting Properties
Mass ratio (M=percentage of the mass of monomers to the total mass of the starting solution)	Increasing	Increasing the micropore surface area and volume Increasing the BET surface area of the CA spheres Decreasing the mesopore area, the mesopore volume and average pore diameter Producing homogeneous gels Giving monolithic gels
R/C ratio	Increasing	Longer gelation times Forming bigger particles Increasing the monomer particle size Pore volume and BET surface area appearing to increase

Table 2.2 Effects of various synthesis conditions on the corresponding properties of
organic gels (continued) (ElKhatat and Al-Muhtaseb, 2011).

Factor Type	Factor Condition	Resulting Properties
R/C ratio	Decreasing	Shorter gelation times Decreasing the size of the carbon-nano particles Decreasing the surface area and pore volume
Initial pH solution	Increasing	Decreasing gelation times abruptly At initial pH between 6.5 and 7.5, color of RF wet gels becomes darkish red indicating high degree of cross linking, small particles synthesized at high pH
	Decreasing	Increasing gelation times abruptly At initial solution pH less than 6, color of synthesized RF wet gels were yellowish brown indicating low degree of cross linking

Table 2.2 Effects of various synthesis conditions on the corresponding properties of organic gels (continued) (Al-Muhtaseb and Ritter, 2003).

Factor Type	Factor Condition	Resulting Properties

Factor: Acidic catalyst solutions

    Effect: At low RF concentrations: small, smooth, fractal aggregates of particles with wide PSDs.

    At high RF concentrations: no fractal aggregates, very narrow PSDs may reduce gelation time.

Factor: Alkaline catalyst solutions

    Effect: High concentrations: polymeric gels (small polymer particles interconnected with large necks, high surface areas, high mechanical strengths), reduces gelation time.

    Low concentrations: colloidal gels (large particles interconnected with narrow necks, low surface areas, low mechanical strengths).

For the formation of carbon gel, pH of the solution during RF gel synthesis is one of the most crucial factors affecting gelation time of the RF gel and properties of the resulting carbon gel. On measuring the gelation time at various pH values, these data points were plotted and a bell-shaped curve was obtained, as shown in Figure 2.12. The initial pH of RF solution had effects on surface area, pore volume, pore size distribution and nanostructure of the gel. A lower initial pH yields carbon gel with higher surface area and pore volume. If the initial pH was too high, the condensation reaction was hindered, resulting in a less cross-linked RF structure that would collapse during drying and pyrolysis, leading to carbon gel with lower surface area and pore volume (Lin and Ritter, 1997).
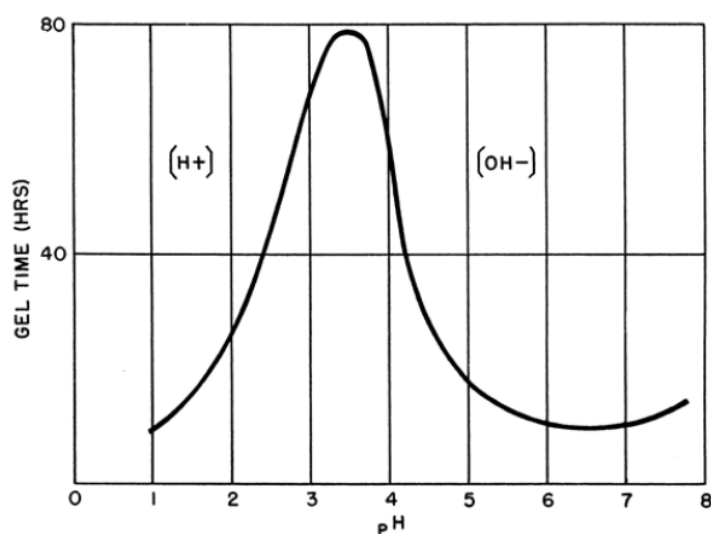
Figure 2.12 Resorcinol-formaldehyde gelation time versus pH (Durairaj, 2005).

The base catalyzed resorcinol-formaldehyde reaction and its mechanism were shown in Figure 2.13 and Figure 2.14, respectively. For the mechanism under basic conditions, the first step in the RF reaction is the formation of a resorcinol anion from the resorcinol and hydroxide ion. This resorcinate ion now activates the benzene ring, and the electron density at the 4- (or 6-) increases for the formaldehyde attack and

formation methylol group (as shown in Figure 2.14). The dimethylol resorcinol can be formed from the reaction of a monomethylol resorcinol with formaldehyde. This reaction might have occurred from the delocalization of electrons by the resorcinate anion.

Simultaneously, due to the presence of the methylol group and resorcinate anion in the same benzene ring, the formation of quinone methide structure (an intermediate) can be expected by the elimination of a hydroxyl group from the molecule. A compound having a quinone methide structure is very unstable and highly reactive. Therefore it can react fast with another resorcinol molecule or reactive sites present in the resorcinol to produce a methylene bridged structure.
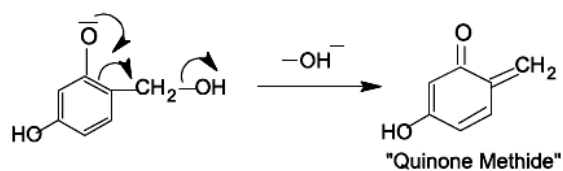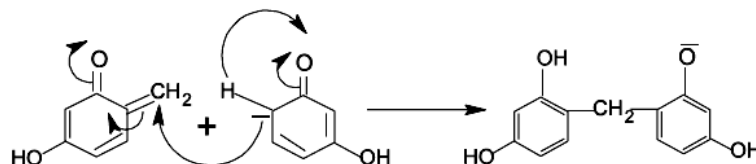
Figure 2.13 Base catalyzed resorcinol formaldehyde reaction.
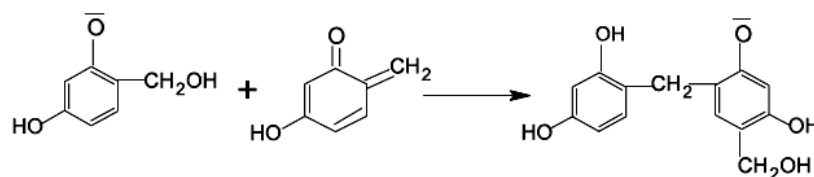
Figure 2.14 Mechanisms of base catalyzed resorcinol formaldehyde reaction (Durairaj, 2005).

Based on published information, it was understood that resorcinolic resoles could exist only under dilute solution conditions and their stability was limited. The methylol groups were formed by the reaction of formaldehyde with resorcinol could react with an additional formaldehyde molecule to form the hemiformal structure and the benzyl ether group could also be formed from the reaction of methylol groups as shown in Figure 2.15.
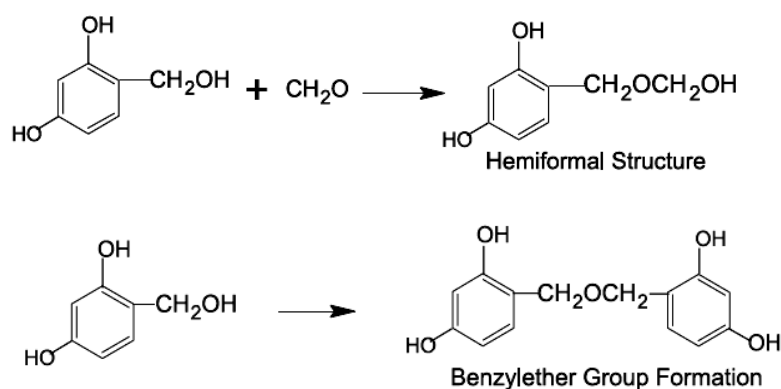
Figure 2.15 Mechanisms of base catalyzed resorcinol formaldehyde reaction
(with additional formaldehyde molecule) (Durairaj, 2005).

Since the formation of hemiformal and benzyl ether structures should come from the methylol groups, they were considered very unstable structures and their formation was questionable because when the methylol groups were formed in the RF reaction, due to instability and high reactivity were immediately converted into carbonium ion (with acid catalysts) and quinone methide (with base catalysts) intermediates (Pizzi et al., 1979). These reactive intermediates could react very quickly with the reactive positions in the resorcinol molecule to produce methylene bridged structures.

The hemiformal and benzyl ethers of resorcinol form and disappear at a faster rate at elevated temperatures. They are instability and the difficulty in isolating them

from the RF reaction mixture. Though the benzyl ether structures formed from the phenol and formaldehyde that can be stable up to 130°C, with resorcinol the formation and decomposition of such structures can happen even at room temperature condition.

The acid catalyzed resorcinol-formaldehyde reaction and its mechanism were shown in Figure 2.16 and Figure 2.17, respectively. In the presence of an acid catalyst the formaldehyde is activated by the protonation reaction. This protonated formaldehyde reacts with resorcinol to produce an unstable methylol or hydroxymethyl intermediate at the resorcinolic reactive sites. On further protonation of the methylol group, it forms a benzyl carbonium ion as the reactive intermediate, which immediately reacts with another resorcinol molecule to form the methylene bridged resorcinolic structure.
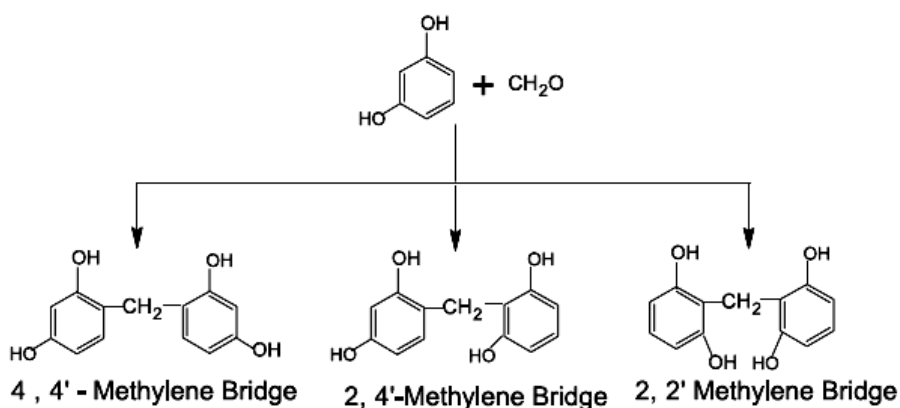
Figure 2.16 Acid catalyzed resorcinol formaldehyde reaction (Durairaj, 2005).
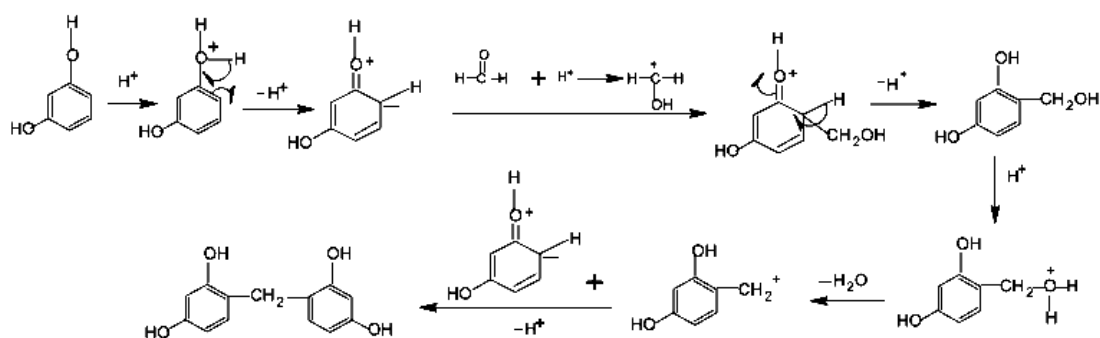
Figure 2.17 Mechanisms of acid catalyzed resorcinol formaldehyde reaction
(Durairaj, 2005).

Pore structure and surface area of the final carbon gel depend not only on the conditions of RF gel synthesis, but also on the drying and carbonizing techniques. Three kinds of drying techniques are available to convert the hydrogel to a solid RF gel. The first method is drying in an inert atmosphere, which gives a RF xerogel (Pekala, 1989). A second method is freeze-drying, which yields a RF cryogel (Tamon and Ishizaka, 2000). The third method employs supercritical extraction with carbon dioxide, which results in a RF aerogel (Lin and Ritter, 1997).

The method of drying RF gels also influences the structure of carbon gels. Xerogel, obtained by heating the RF hydrogel in an inert atmosphere, has the most compact structure with the lowest specific surface area (<900 m^2/g). The highest surface area is found in the gel lyophilized after freeze-drying in *t*-butanol (>2500 m^2/g), but the resulting carbon cryogel is not structurally stable, i.e. the measured surface area decreases with time. Supercritical extraction with carbon dioxide yields aerogel with an intermediate value for the surface area (ca. 1000 m^2/g) (Czakkel et al., 2005).

2.4 Definition and Classification of Porous Materials

The term of a porous material is used for all materials that are full of pores, channels, vessels, holes, or cavities which are deeper than they are wide and permit the movement of fluids or gases. An example of a porous material is sponge. Porous materials were created by nature or by synthetic design have found great utility in all aspects of human activities. Their pore structures are usually formed in the stages of crystallization or subsequent treatment and consist of isolated or interconnected pores that may have similar or different shapes and sizes.

Porous materials with small pore diameters (0.3 nm to 10 μm) are being studies for their molecular sieving properties. The pore shape can be roughly approximated by any of the following three basic pore models, i.e. cylindrical pores having circular in cross section, ink-bottled pores having a narrow neck and wide body, and slit-shaped pores with parallel plates, as seen in the Figure 2.18.

(a)   **(b)**   **(c)**
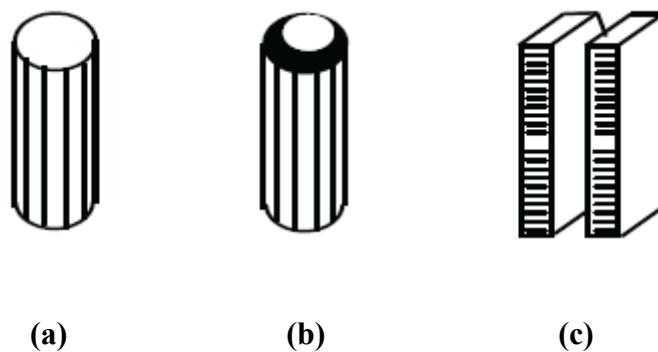
Figure 2.18 Pore shapes; (a) cylindrical pores, (b) ink-bottled pores and (c) slit-shaped pores.

Pores in solids are classified as shown in Table 2.3, intraparticle and interparticle pores on the basis of their origin, micro-, meso- and macro-pores on the basis of their size, open and closed pores on the basis of their state, and rigid and flexible pores on the basis of their strength.

Table 2.3 Classification of pores in solid materials (Inagaki, 2009).

1) Based on their origin		
	Intraparticle pores	Intrinsic intraparticle pores
		Extrinsic intraparticle pores
	Interparticle pores	
2) Based on their size		
	Micropore <2 nm	Ultramicropores <0.7 nm
		Supermicropores 0.7-2 nm
	Mesopores 2-50 nm	
	Macropores >50 nm	
3) Based on their state		
	Open pores	
	Closed pores (Latent pores)	
4) Based on their strength		
	Rigid	
	Flexible	

In addition, Figure 2.19 gives a few examples of porous materials that fit into these pore size regimes.
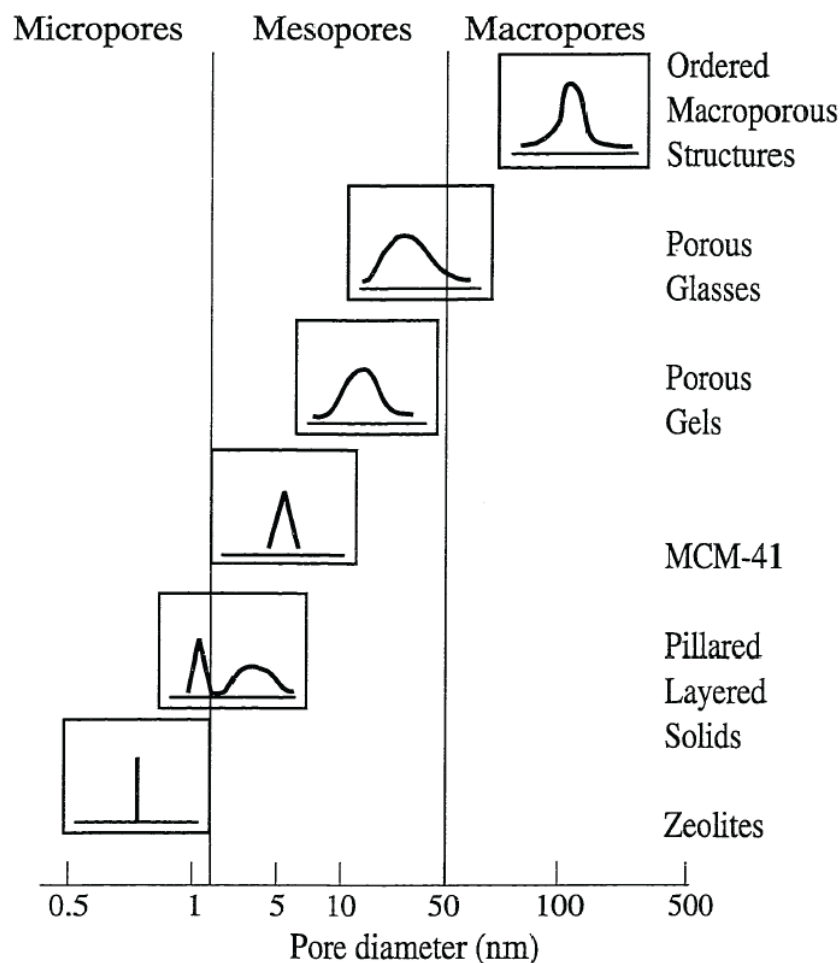
Figure 2.19 Schematic illustrating pore size distributions of some porous materials.

As indicated, the pore size is generally specified as the pore width which is defined as the distance between the two opposite walls. Obviously, pore size has a precise meaning only when the geometrical shape is well defined. Porosity of a material is usually defined as the ratio of the volume of pores and voids to the volume occupied by the solid.

Pores types in porous materials have been identified by different techniques depending mostly on their sizes. The techniques for the identification and the characterization of pores in materials are summarized in Figure 2.20 and Table 2.4.
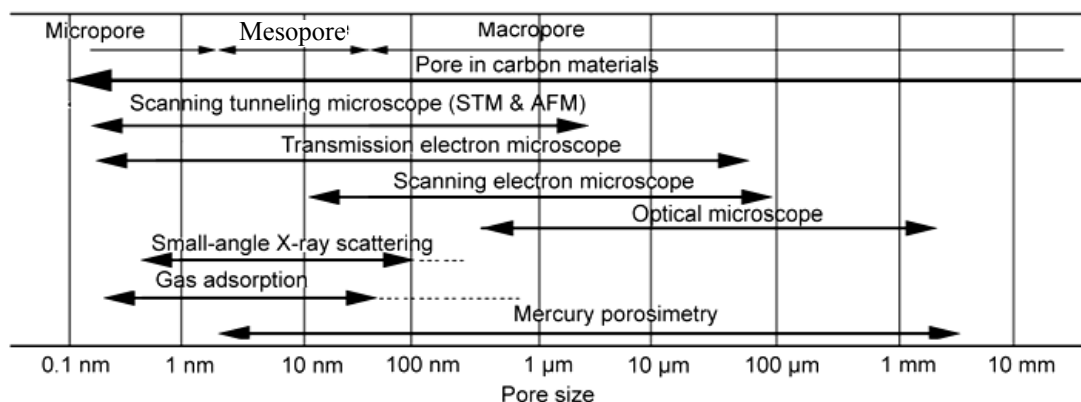
Figure 2.20 Identification techniques of pores in porous materials (Inagaki, 2009).

Table 2.4 Techniques for characterization of pores in porous materials
(Inagaki, 2009).

Characterization technique	Comments (advantages and disadvantages)
Adsorption/desorption of N_2 gas at 77 K	
BET method	Give overall surface area (SS)
s plot	Give microporous and external SSs separately Give micropore volume
BJH method	Differentiate microporous and mesoporous SSs and volumes Give pore size distribution in mesopore range
DFT method	Give pore size distribution in a wide range of size
HK method *etc.*	Give pore size distribution
Adsorption/desorption isotherm of various gases (H_2, He, CO_2, CO)	Give the information molecular sieving performance
X-ray small-angle scattering	Detect micropores, either open or closed pores

Table 2.4 Techniques for characterization of pores in porous materials (continued).

Characterization technique	Comments (advantages and disadvantages)
Transmission electron microscopy	Detect nano-sized pores, even less than 0.4 nm size Give localized information, need statistical analysis of data
Scanning tunneling microscopy	Detect only pore entrances on the surface Give morphological information of the pore entrance Need statistical analysis with criteria
Scanning electron microscopy	Detect only macropores
Mercury porosimetry	Detect mostly macropores Difficult to apply for fragile materials

Porous materials are also defined in terms of their adsorption properties. The term adsorption originally denoted the condensation of gas on a free surface as opposed to its entry into the bulk, as in absorption. However, this distinction is frequently not observed, and the uptake of a gas by porous materials is often referred to as adsorption or simply sorption, regardless of the physical mechanism involved. Adsorption of a gas by a porous material is described quantitatively by an adsorption isotherm, the amount of gas is adsorbed by the material at fixed temperature as a function of pressure. Porous materials are most frequently characterized in terms of pore sizes derived from gas sorption data, and IUPAC conventions have been proposed for classifying pore sizes and gas sorption isotherms that reflect the relationship between porosity and sorption. The IUPAC classification of adsorption isotherms is illustrated in Figure 2.21. The six types of isotherm are characteristic of adsorbents that are microporous (Type I), nonporous or macroporous (Types II, III, and VI), or mesoporous (Types IV and V) (Sing et al., 1985).

The reversible *Type I* isotherm, sometimes referred to as Langmuir isotherms, is concave to the p/p_o axis and surface excess amount approaches a limiting value as $p/p_o \rightarrow 1$. Type I isotherms are given by microporous solids having relatively small external surfaces, the limiting uptake being governed by the accessible micropore volume rather than by the internal surface area.

The reversible *Type II* isotherm is the normal form of isotherm obtained with a non porous or macroporous adsorbent. Type II isotherm represents unrestricted monolayer adsorption. Point B, the beginning of the almost linear middle section of the isotherm, is often taken to indicate the stage at which monolayer coverage is complete and multilayer adsorption about to begin.

The reversible *Type III* isotherm is convex to the p/p_o axis over its entire range and therefore it does not exhibit a Point B. Isotherm of Type III are not common, but there are a number of systems which give isotherms with gradual curvature and an indistinct Point B. In such cases, the adsorbate-adsorbate interactions play an important role.

Characteristic features of the *Type IV* isotherm are its hysteresis loop, which is associated with capillary condensation taking place in mesopores, and the limiting uptake over a rang of high p/p_o. The initial part of the Type IV isotherm is attributed to monolayer-multilayer adsorption since it follows the same path as the corresponding part of a Type II isotherm obtained with the given adsorptive on the same surface area of the adsorbent in a non-porous form. Type IV isotherm is given by many mesoporous industrial adsorbents.

The *Type V* isotherm is uncommon; it is related to the Type III isotherm in that the adsorbent-adsorbate interaction is weak, but it is obtained with certain porous adsorbents.

The *Type VI* isotherm, in which the sharpness of the steps depends on the system and the temperature, represents stepwise multilayer adsorption on a uniform

non-porous surface. The step-height now represents the monolayer capacity for each adsorbed layer and, in the simplest case, remains nearly constant for two or three adsorbed layers.
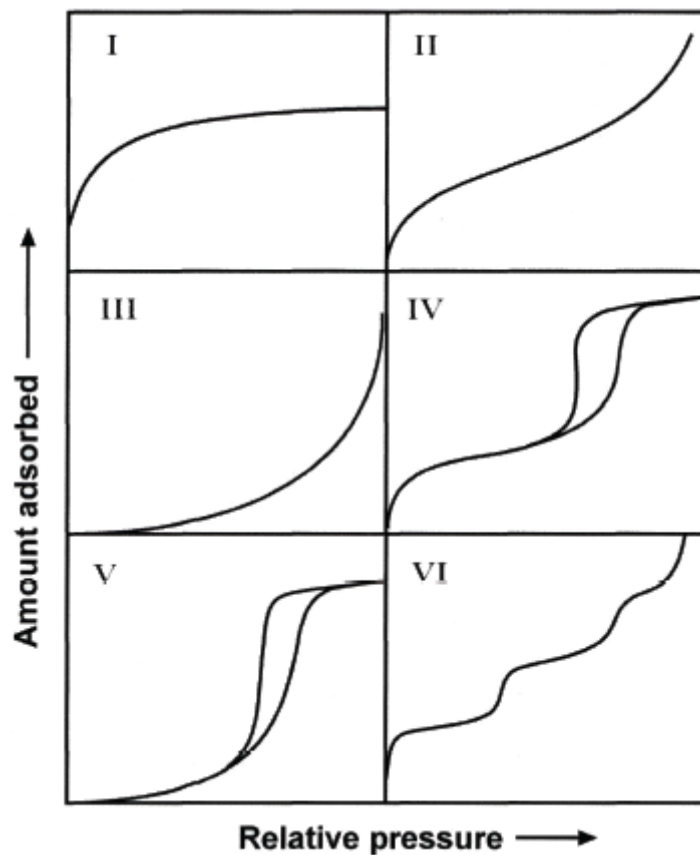
Figure 2.21 The IUPAC classification of adsorption isotherms showing both the adsorption and desorption pathways. Note the hysteresis in types IV and V (Sing, Everett, Haul, Moscou, Pierotti, Rouquerol and Siemieniewska, 1985).

The adsorption hystereses in Figure 2.21 (IV and V) are classified and are widely accepted that there are a correlation between the shape of the hysteresis loop

and the texture (e.g., pore size distribution, pore geometry and connectivity) of a mesoporous material. An empirical classification of hysteresis loops is given by the IUPAC, which is based on an earlier classification of hysteresis by De Boer.
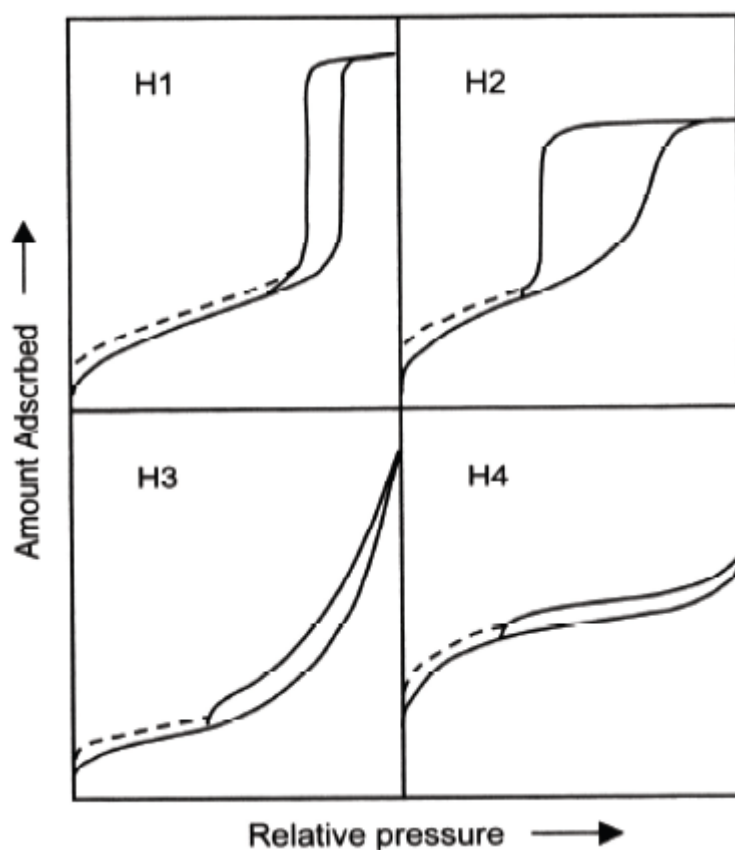
Figure 2.22 The relationship between the pore shape and the adsorption-desorption isotherm (Sing et al., 1985).

Figure 2.22 shows the IUPAC classification and according to the IUPAC, Type H1 is often associated with porous materials consisting of well-defined cylindrical-like pore channels or agglomerates of approximately uniform spheres. Type H2 ascribes materials that are often disordered, and the distribution of pore size and shape are not well defined and also indicate of bottleneck constrictions. Materials that give rise to Type H3 hysteresis have slit-shaped pores (the isotherms revealing

Type H3 do not show any limiting adsorption at high P/P^0, which is observed with non-rigid aggregates of plate-like particles). The desorption curve of Type H3 hysteresis contains a steep associated with a forced of the hysteresis loop, due to the so-called tensile strength effect which is a phenomenon occurs for nitrogen at 77 K in the relative pressure rang from 0.4 to 0.45. However, Type H4 hysteresis is also often associated with narrow slit pore.

With many systems, especially those containing micropores, low pressure hysteresis (indicated by the dashed lines in Figure 2.22), may be observed extending to the lowest attainable pressures. Removal of the residual adsorbed material is then possible only if the adsorbent is outgassed at higher temperatures. This phenomenon may be associated with the swelling of a non-rigid porous structure or with the irreversible uptake of molecules in pores (or through pore entrances) of about the same width as that of the adsorbate molecule or in some instances with an irreversible chemical interaction of the adsorbate with the adsorbent (Sing et al., 1985).

Porous materials can be structurally amorphous, polycrystalline, or crystalline. Amorphous materials, such as silica gel or alumina gel, do not possess long range order, whereas polycrystalline solid, such as γ- or η- Al_2O_3 are quasiordered as evidenced by the broad peaks on their X-ray diffraction patterns. Both classes of materials exhibit a broad distribution of pores predominantly in the mesoporous range. This broad pore size distribution limits the shape-selectivity and the effectiveness of the adsorbents, ion-exchangers, and catalysts prepared from amorphous and polycrystalline solids. The only class of porous materials possessing narrow pore size distributions or uniform pore sizes includes crystalline zeolites and related molecular sieves.

Macroporous solids are not widely used as adsorbents and catalysts due to their low surface area and large non-uniform pores. Microporous and mesoporous solids, however, are widely used in adsorption, separation technology and catalysis. Owing to the need for higher accessible surface area and pore volume for efficient chemical processes, there is a growing demand for new highly stable porous materials.

CHAPTER III

EXPERIMENTAL

The synthesis of porous alumina assisted by resorcinol-formaldehyde gel via sol-gel polycondensation process is explained in this chapter. The samples preparation including lists of chemical agents and preparation procedure are also presented. In addition, various characterization techniques such as FTIR, XRD, SEM, and N_2 sorption analysis are described as well.

3.1 Preparation of Porous Alumina Assisted by Resorcinol-Formaldehyde Gel

3.1.1 Materials

The chemical agents used in this research are as follow:

1. Resorcinol (99.8%, Fluka)
2. Formaldehyde (37% aqueous solution with 8-10% methanol as stabilizing agent, Ajax Finechem)
3. Sodium carbonate (99.8%, Ajax Finechem)
4. Aluminium acetylacetonate (99%, Sigma-Aldrich)
5. Aluminium nitrate (99.9%, Sigma-Aldrich)
6. Aluminium acetate (99.9%, Aldrich)
7. Tartaric acid (99.5%, Ajax Finechem)
8. Oxalic acid (99.5%, Ajax Finechem)
9. Acetic acid (99.8%, QRëC)
10. Formic acid (85%, QRëC)
11. Acetylacetone (98%, s.d.fine-chem limited)

All chemicals were used as received without further purification. The chemical structures of some agents are shown in Tables 3.1 and 3.2.

Table 3.1 Chemical structures of starting material that were used in this study.
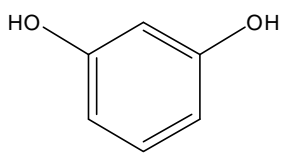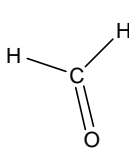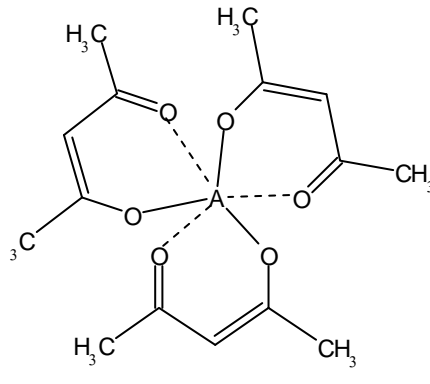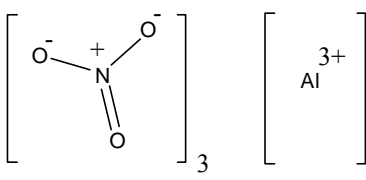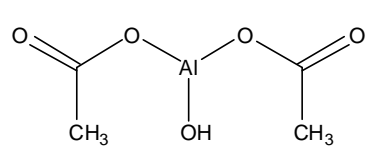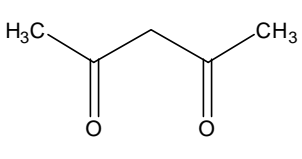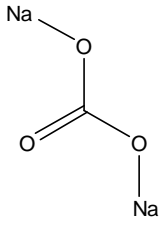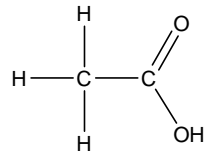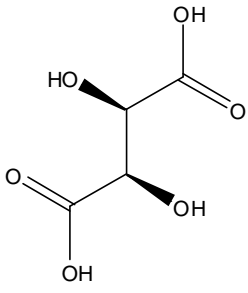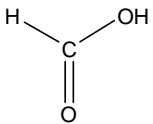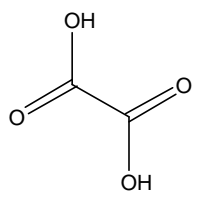
Chemical name (Designation)	MW	Chemical structure
Resorcinol (R) $C_6H_4(OH)_2$	110.1	
Formaldehyde (F) CH_2O	30.03	
Aluminium acetylacetonate $(Al(acac)_3)$ $Al(CH_3COCHCOCH_3)_3$	324.31	
Aluminium nitrate (AN) $AlN_3O_9 \cdot 9H_2O$	375.13	
Aluminium acetate (AA) $C_6H_9AlO_6$	162.08	
Acetylacetone (Acac) $C_5H_8O_2$	100.13	

Table 3.2 Chemical structures of acid and base agents that were used in this study.

Chemical name (Designation)	MW	Chemical structure
Sodium carbonate Na_2CO_3	105.99	
Acetic acid CH_3COOH	60.05	
Tartaric acid $C_4H_6O_6$	150.087	
Formic acid CH_2O_2	46.03	
Oxalic acid $C_2H_2O_4$	90.03	

3.1.2 Preparation Procedures

The synthesis of porous alumina assisted by resorcinol (R) and formaldehyde (F) gel was done in four steps as illustrated in Figures 3.1 and 3.2. Firstly, the RF template with aluminium precursor was prepared, according to the modification of the previously reported RF gel preparation method (Tonanon et al., 2005). The starting agents were resorcinol, formaldehyde, distilled water (W), sodium carbonate as a polymerization catalyst (C), and aluminium precursor (A). The ratios of R/F, R/W, and C/w were 0.5 mol/mol, 0.15 mol/mol and 10 mol/m^3, respecrtively, whereas that of A/R was varied from 0.005 to 0.1. For the preparation in general, 9 g of resorcinol and 0.01 g of sodium carbonate were dissolved in 10 ml distilled water. After homogenizing, 12.5 ml of formaldehyde was added and the mixture was stirred at room temperature for 15 min to obtained RF template solution. After that, 1.3254 g of aluminium acetylacetonate (Al(acac)$_3$), i.e., for the A/R = 0.05, as a source of aluminium, was added into the RF mixture. The Al(acac)$_3$/RF solution was stirred at room temperature for 30 min to obtain a homogeneous light yellow color solution, as shown in Figure 3.1.

Secondly, i.e., aging of the Al(acac)$_3$/RF solution, the sample gel was aged in a closed system (uncontrolled relative humidity (RH) condition) at room temperature for 3 days.

Thirdly, i.e., drying process, a conventional drying was performed at 110°C in an oven for 24 hours. The Al(acac)$_3$/RF xerogel was then obtained, as shown in Figure 3.2.

Finally, i.e., heat treatment of the xerogel sample, the dried product was heated to 600°C at the heating rate of 5°C/min to remove the RF template. In order to convert the amorphous product to crystalline product, after the process of template removal, the white alumina products were finally formed by calcinating at designed temperature ranging from 800 to 1200°C in a box furnace with the same heating rate and maintaining at this temperature for 2 hours.

In this study, there are several factors affecting the characteristic of the alumina product. However, the interesting points in four steps of preparation that were focused on and investigated are listed as follows:

Step 1:

- the effect of type of polymerization catalyst (Figure 3.1 (a))

- the effect of aging time of RF template (Figure 3.1 (b))

- the effect of type of aluminium precursor (Figure 3.1 (c))

Step 2:

- the effect of aging condition (Figure 3.1 (d))

> For this case, the relative humidity in the system in the range of 8-100% was controlled. In addition, for controlling the relative humidity at room temperature (25°C), the agents used were silica gel (8%), saturated solution of $Mg(NO_3)_2$ (52.9%), saturated solution of NaCl (75.3%) and water (100%) (Soykeabkaew et al., 2004).

- the effect of aging temperature (Figure 3.1 (e))

- the effect of aging time (Figure 3.2 (a))

Step 4:

- the effect of calcination temperature (Figure 3.2 (b))

> For this case, the phase transition as a result of this effect was also investigated.
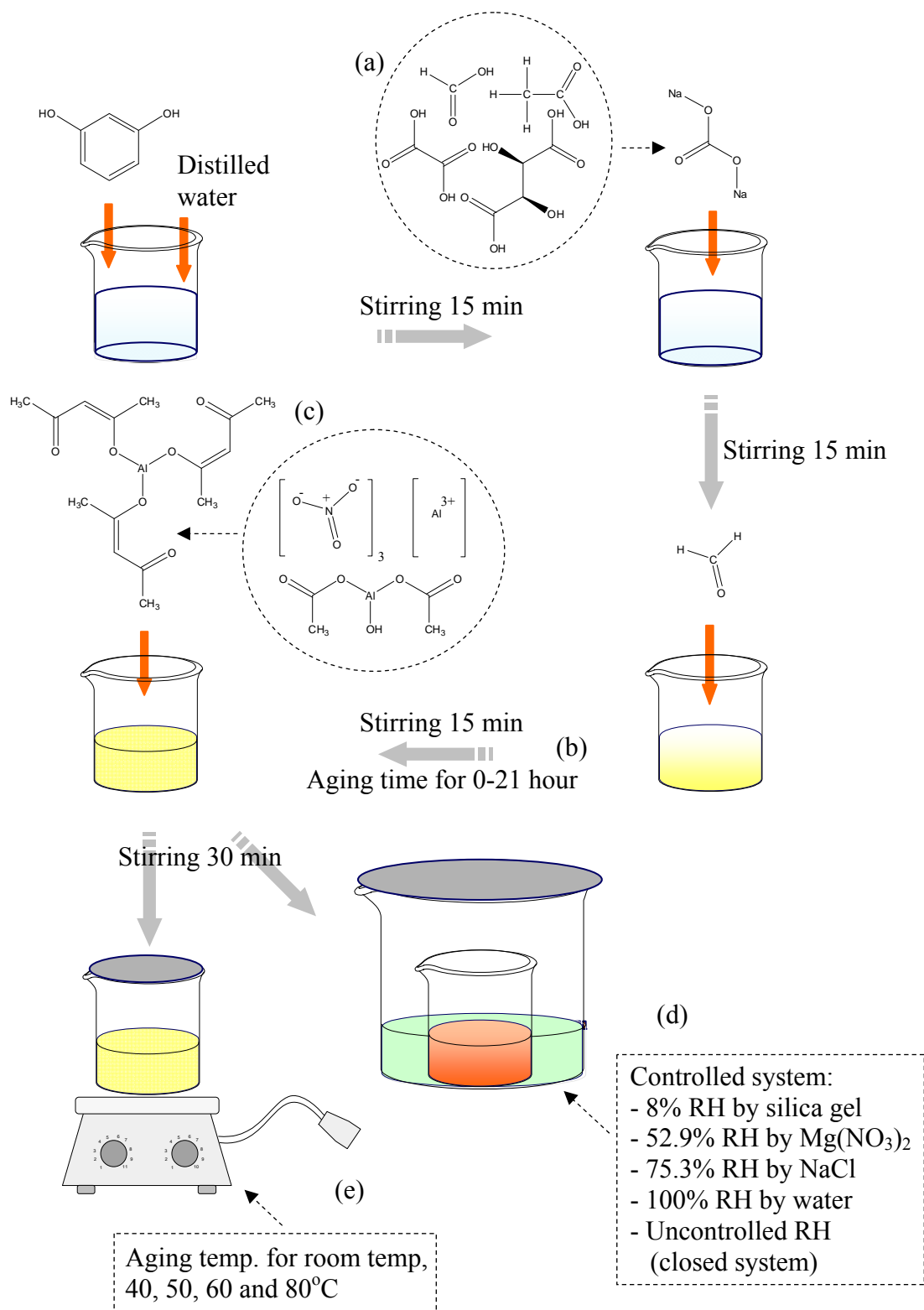
Figure 3.1 Scheme for the preparations of the aluminium/RF gel.

Controlled system:
- 8% RH by silica gel
- 52.9% RH by $Mg(NO_3)_2$
- 75.3% RH by NaCl
- 100% RH by water
- Uncontrolled RH
  (closed system)

Aging temp. for room temp, 40, 50, 60 and 80°C

(a)
Aging time for 0-72 hour

Conventional dry at 110°C for 24 hour

(b)

Calcination at 600°C for template removal and designed temperature, i.e., 800, 1000, 1100 and 1200°C for phase transition study
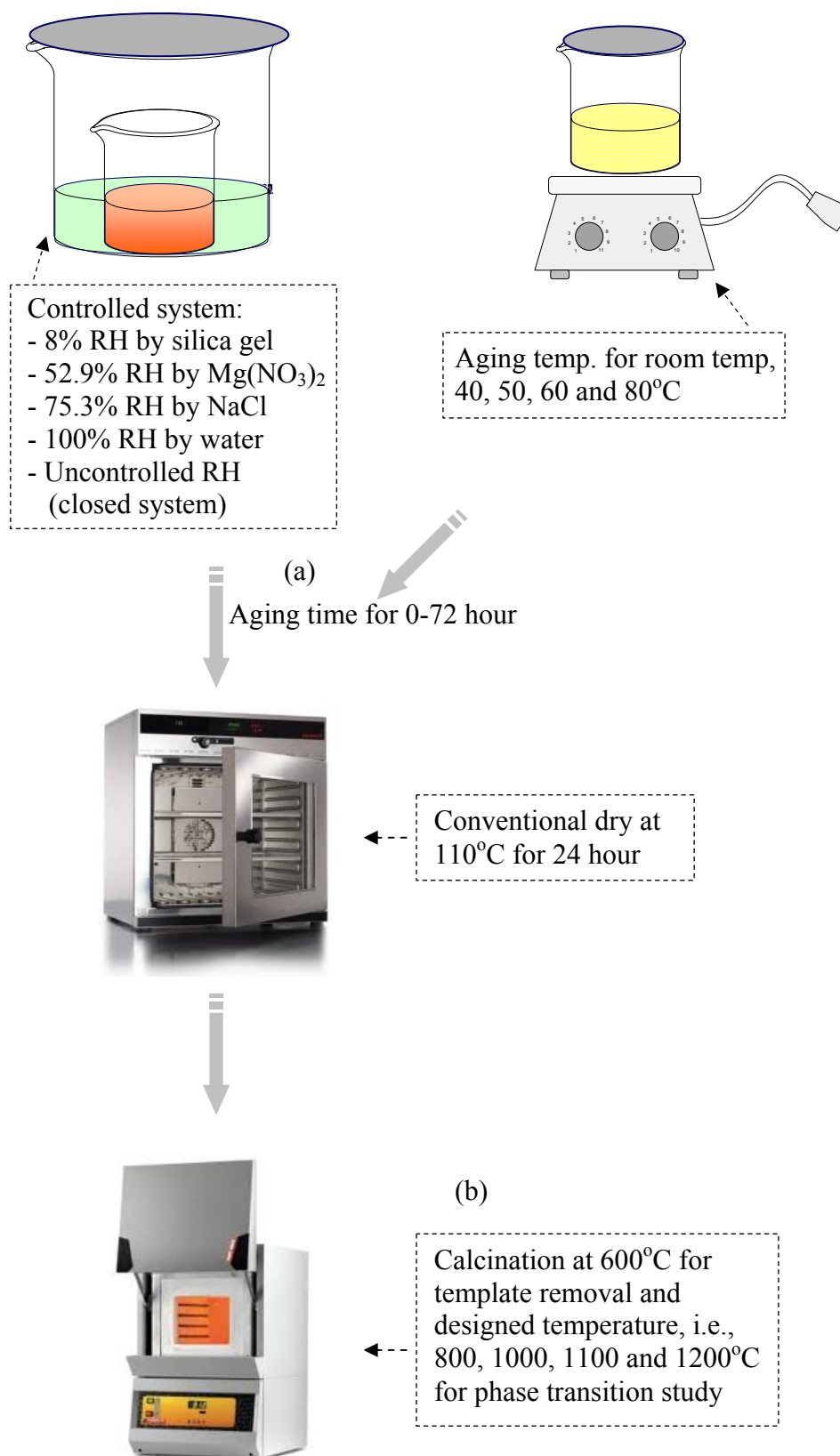
Figure 3.2 Scheme for the calcinations of the porous alumina assisted via RF gel.

3.2 Characterizations of Products

The chemical and physical characterizations of the samples were performed by various techniques. To study the chemical nature of the polymeric gel and polymeric xerogel, many techniques including fourier transform infrared spectroscopy (FTIR), raman spectrometer, nuclear magnetic resonance (NMR), and thermogravimetric analyzer-differential scanning calorimeter (TGA-DSC) were performed. In addition, the crystalline phase and the porous properties of the products were elucidated by X-ray diffraction (XRD) and nitrogen physisorption measurement, respectively. Furthermore, the morphologies of the xerogel and the alumina product were studied by scanning electron microscopy (SEM) and transmission electron microscopy (TEM).

The pictures and the operating conditions of the instrument are shown in this chapter and some related theories are explained in the appendix of the research.

3.2.1 X-ray Diffraction (XRD)

The crystalline phases of the obtained alumina product were identified by using a Siemens D5000 X-ray diffractometer as seen in the Figure 3.3. The measurement was carried out by using Ni-filtered CuKα radiation, operated in the 2 theta range of 20-80 degree at scanning step of 0.04 degree. The crystallite size was estimated from line broadening of the main XRD peak, according to the Scherrer equation, using α-Al_2O_3 as standard.
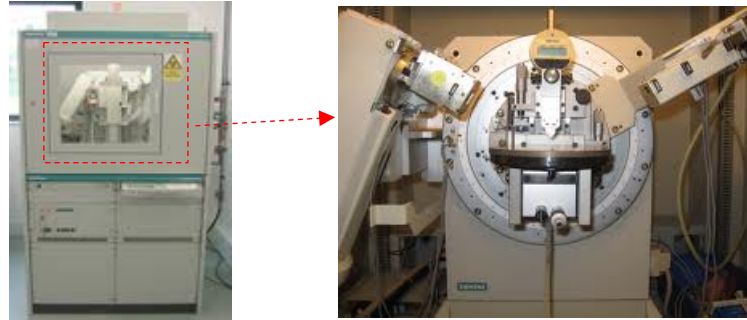
Figure 3.3 Instrument of X-ray diffraction.

3.2.2 Scanning Electron Microscopy (SEM)

Surface morphology of product was observed by a Hitachi S-3400N scanning electron microscopy as seen in the Figure 3.4, which was operated at 15 kV. Samples were coated by thin film of palladium prior to the analysis.

Figure 3.4 Instrument of scanning electron microscopy.

3.2.3 Transmission Electron Microscopy (TEM)

The transmission electron microscope and selected area electron diffraction was JEOL JEM-2010 as seen in the Figure 3.5, with an accelerating voltage of 120 kV. The sample powder was dispersed in absolute ethanol and sonicated for about 15 min before dropping on a copper grid (with Formvar film) or carbon grid.

Figure 3.5 Instrument of transmission electron microscopy.

3.2.4 N_2 Adsorption-Desorption Analysis

The BET surface area, N_2 adsorption-desorption isotherm and pore size distribution were measured at 77 K by a Micromeritics ASAP 2020, Figure 3.6, using nitrogen as the adsorbate. The sample was degassed at $200^{o}C$ for 3 hour under vacuum before the adsorption of nitrogen. The specific surface area was calculated using the BET adsorption-desorption method (Coleman and Hench, 2000) and pore size distribution was calculated by BJH (Barrett-Joyner-Halenda) desorption branch analysis.

Figure 3.6 Instrument of nitrogen physisorption measurement.

3.2.5 Thermal Analysis

The thermogravimetric analyzer and differential scanning calorimeter (TGA-DSC) analysis was performed with a SDT Q600 instrument as seen in the Figure 3.7. 5-10 mg of sample was put in a 90 μl of Al_2O_3 cup and heated to 1000^oC with a heating rate of $10^oC/min$, under nitrogen or oxygen flowing at 400 ml/min.

Figure 3.7 Instrument of thermogravimetric analyzer-differential scanning calorimeter.

3.2.6 Fourier Transform Infrared Spectroscopy (FTIR)

Functional groups of sample were identified by a Nicolet 6700 fourier transform infrared spectroscopy as seen in the Figure 3.8. Infrared spectra were recorded between the wave number of 4000 and 400 cm^{-1} with resolution of 2 and the data spacing was 0.964 cm^{-1} by using KBr mode.

Figure 3.8 Instrument of fourier transform infrared spectroscopy.

3.2.7 Raman spectrometer

Raman spectra was recorded by a Nicolet 6700 raman spectrometer as seen in the Figure 3.9, with the 1,064 nm line of an Nd-YAG laser source. The exciting laser power was about 200-500 mW. The sample was pressed into the sample holder and measured with resolution of 2 cm^{-1} from 200-3500 cm^{-1}.
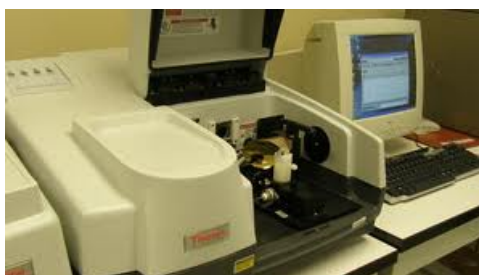
Figure 3.9 Instrument of raman spectrometer.

3.2.8 Nuclear Magnetic Resonance (NMR)

^1H, ^{13}C and ^{27}Al nuclear magnetic resonance spectra in liquids were recorded with a Bruker 400 UltraShield spectrometer as seen in the Figure 3.10. The following conditions were used to record spectra: pulse angle 90° (12.9 μs ^1H, 8.5 μs ^{13}C); digital resolution 0.098 Hz/pt (^1H) and 0.367 Hz/pt (^{13}C) were corresponding to a spectral length of 6400 Hz (^1H) and 24000 Hz (^{13}C). Sample was dissolved in deuterated dimethylsulfoxide (DMSO). ^{13}C chemical shifts were measured with respect to tetramethylsilane (TMS) as internal standard, δ (DMSO-d_6) = 39.5 ppm.

Figure 3.10 Instrument of nuclear magnetic resonance.

CHAPTER IV

RESULTS AND DISCUSSION

This study fabricates a porous alumina having high surface area, by sol-gel technique and using resorcinol-formaldehyde hydrogel as a template. The various conditions such as aging temperature, aging time, moisture content, type of catalyst, type of aluminium precursor and aluminium content were found to play an important role in producing a product by this method. Their effects were investigated and explained in the following sections. In addition, the interaction between aluminium precursor and resorcinol-formaldehyde gel was also elucidated.

4.1 Interaction between RF Gel and Aluminium Acetylacetonate

In this topic, a source of alumina was incorporated into RF gel by adding $Al(acac)_3$ into resorcinol-formaldehyde mixture during the sol-gel polycondensation process. As the time elapsed, the gelation spontaneously proceeded in a closed system at room temperature (25^oC). After aging for 3 days, the $Al(acac)_3$/RF gel was dried at 110^oC for 24 hours and calcined at 1200^oC for 2 hours in order to obtain the porous alumina product.

4.1.1 Morphology and Textural Properties of Alumina Product

Morphology and N_2 adsorption-desorption isotherm of the obtained product, compared with those of alumina synthesized without the aid of RF gel are shown in Figures 4.1 and 4.2, respectively. It could be seen that morphology and porosity of alumina synthesized with and without the RF gel are significantly different. The product synthesized without the RF gel appeared as nonporous aggregates with low surface area of 10 m^2/g (Figure 4.1 (a) and 4.2 (d)). On the other hand, by using the RF gel, the obtained products were found to have interconnected porous structure with the surface area as high as 68 m^2/g, even after the calcination at 1200°C.

The adsorption isotherm was classified as type IV with H3 hysteresis loop indicating a mesoporous structure with large pore diameter (Figures 4.1 (b) and 4.2 (c)).
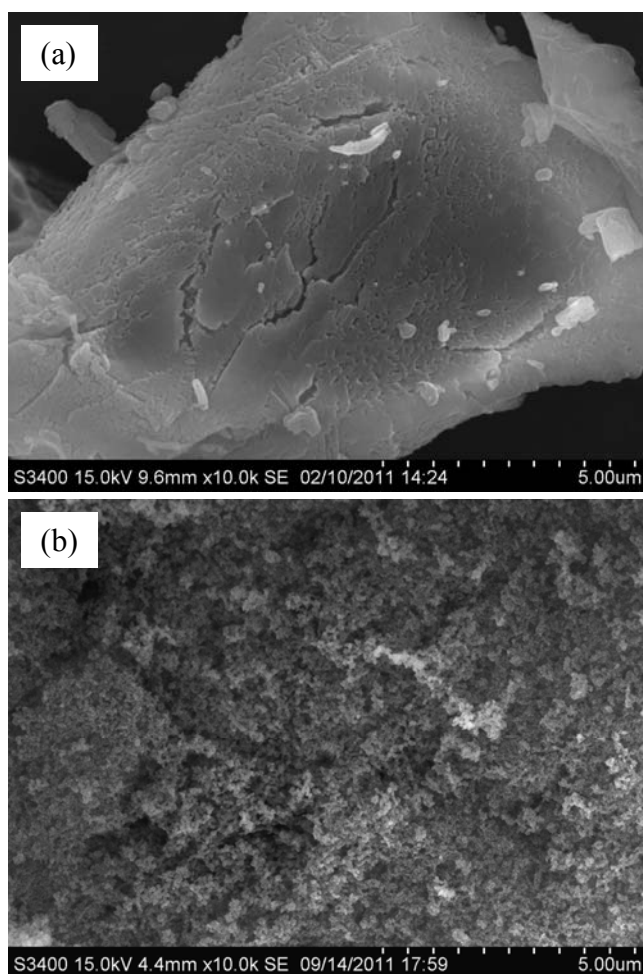
Figure 4.1 SEM micrographs of alumina products synthesized without (a) and with (b) the aid of RF gel, after calcination at 1200°C for 2 hours.
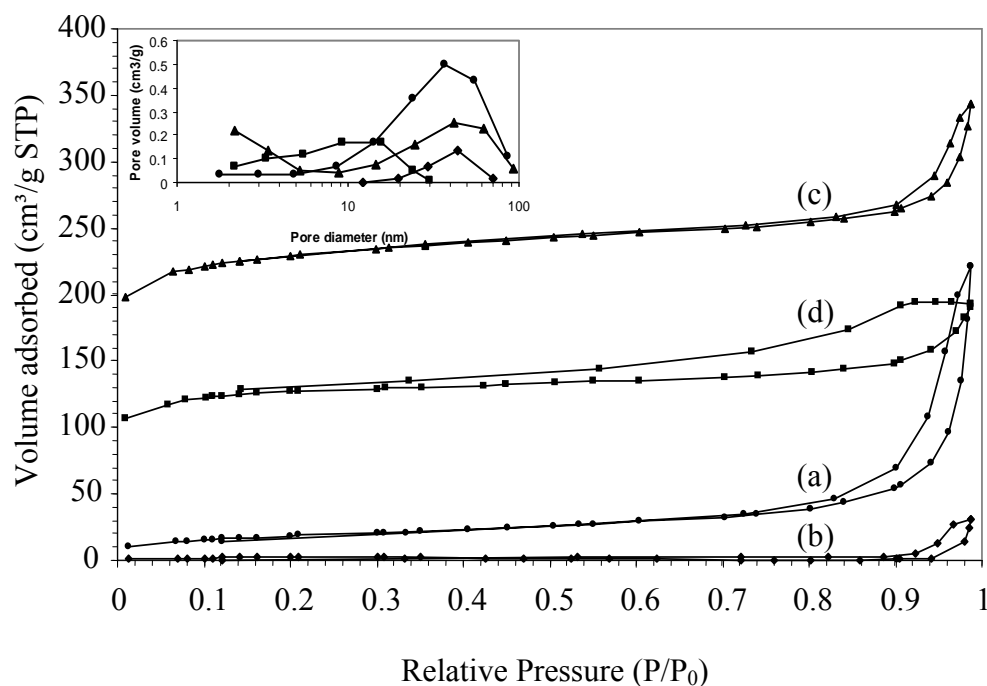
Figure 4.2 Nitrogen adsorption-desorption isotherms of alumina products synthesized with (a) and without (b) the aid of RF gel after being calcined at 1200°C for 2 hours, compared with those of the gel synthesized with (c) and without (d) the Al(acac)$_3$ after being pyrolyzed at 750°C for 4 hours. The inset shows the corresponding pore size distributions.

Although, the use of RF gel as a template in the synthesis of porous alumina could significantly increase porosity of the product, the process was not direct templating of aluminium precursor within pores of the RF gel network. Interaction between Al(acac)$_3$ and the RF mixture was observed. It was detected by means of FTIR technique that will be exhibited in more detail in Section 4.1.2. One obvious evidence was the fact that the Al(acac)$_3$/RF mixture becomes gel much faster than the conventional RF gel. According to the measurement of viscosity during the aging period, the gelation time of the Al(acac)$_3$/RF mixture was only 509 minutes (Figure 4.3 (b)), while that of the neat RF gel was 2195 minutes (Figure 4.3 (c)). However, the explanation of the reduction in gelation time relating to the Al(acac)$_3$ and RF interaction will be disclosed in detail in Section 4.1.2.
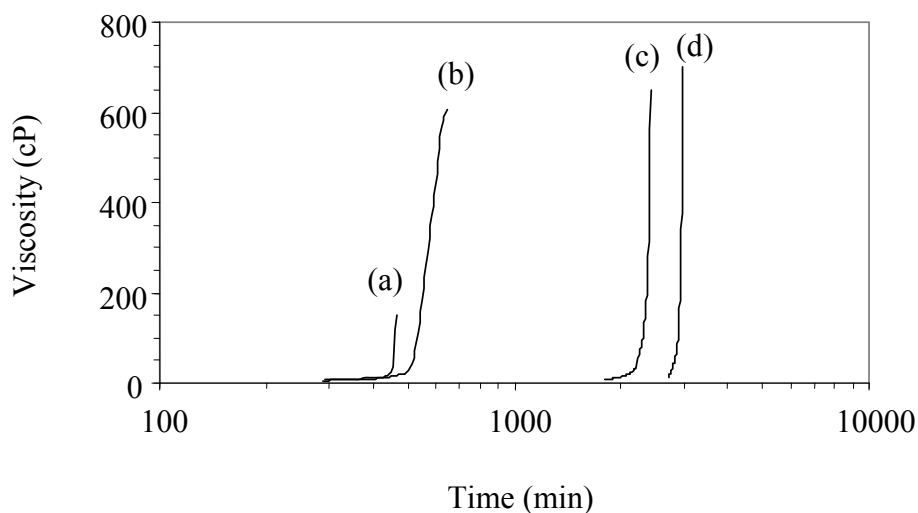
Figure 4.3 Viscosity evolution of: (a) uncatalyzed Al(acac)$_3$/RF gel, (b) Al(acac)$_3$/RF gel, (c) neat RF gel and (d) AcacH/RF gel.

Further investigation was done by characterizing pore structure of the gels that were pyrolyzed under nitrogen atmosphere at 750°C for 4 hours, comparing between the RF gels with and without Al(acac)$_3$. The results in Figure 4.2 reveal that the N$_2$ adsorption-desorption isotherms of both pyrolyzed products are similar, i.e., a mixed mode of type I and type IV, indicating the presence of both micropores and mesopores in the samples. However, shape of the hysteresis loop shifts from type H2 (Figure 4.2 (b)) to H3 (Figure 4.2 (a)) when Al(acac)$_3$ was added to the RF mixture which indicats that pore structure of the RF gel is affected by the interaction between the RF gel and Al(acac)$_3$.

Moreover, thermal behaviors of alumina precursor (Al(acac)$_3$), RF gel and Al(acac)$_3$/RF gel were also investigated by TG/DTA in nitrogen flow (400 ml/min) at heating rate of 5°C/min, as shown in Figure 4.4. Considering the TG/DTA profiles, it could be seen that pure Al(acac)$_3$ powder decomposes from 190°C in only one step with the formation of 2.5% solid residue and the DTA signal revealed that there are two endothermic peaks at 195°C and 231°C, corresponding to the melting and the evaporation from the melt (Gairola et al., 2009). For the neat RF gel, there are three changes of slope in the TG profile. First slope that takes place at temperature below 200°C is attributed to the evaporation of water product from polycondensation reaction and light solvent residue, while other changes of slope occur around 350°C and 550°C corresponding to the breaking of C-O and C-H bonds in the RF networks, respectively (Lin and Ritter, 1997). Nevertheless, when the Al(acac)$_3$ was mixed in the RF gel, the decompositions of Al(acac)$_3$ (at around 195°C) and that of typical RF gel (at around 350°C and 550°C) are retarded. Thus, it could be implied that there is the interaction between Al(acac)$_3$ and RF gel.
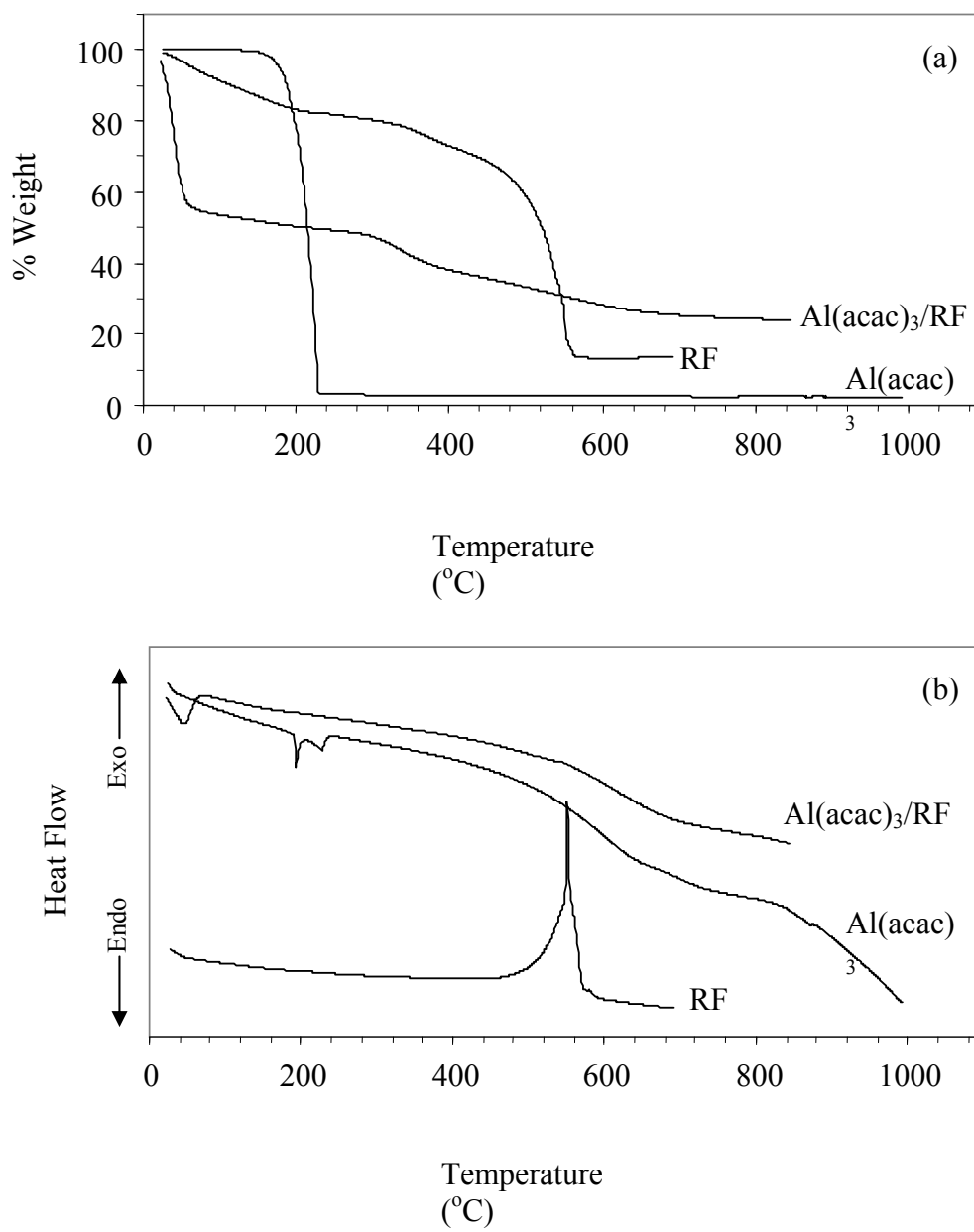
Figure 4.4 TG (a) and DTA (b) analysis of Al(acac)$_3$ powder, RF gel and Al(acac)$_3$/RF gel.

Figure 4.5 shows XRD patterns of $Al(acac)_3$ powder, $Al(acac)_3/F$ xerogel and $Al(acac)_3/RF$ xerogel. It is found that the $Al(acac)_3$ is highly crystalline with main narrow diffraction peak at 24.1^o, while this peak is not observed for $Al(acac)_3/F$ xerogel and $Al(acac)_3/RF$ xerogel. This result reveals that the crystallinity of the $Al(acac)_3$ disappears when it is mixed with formaldehyde and RF gel. In other words, the crystal structure of $Al(acac)_3$ might be changed by dissolving or reacting with that gel.
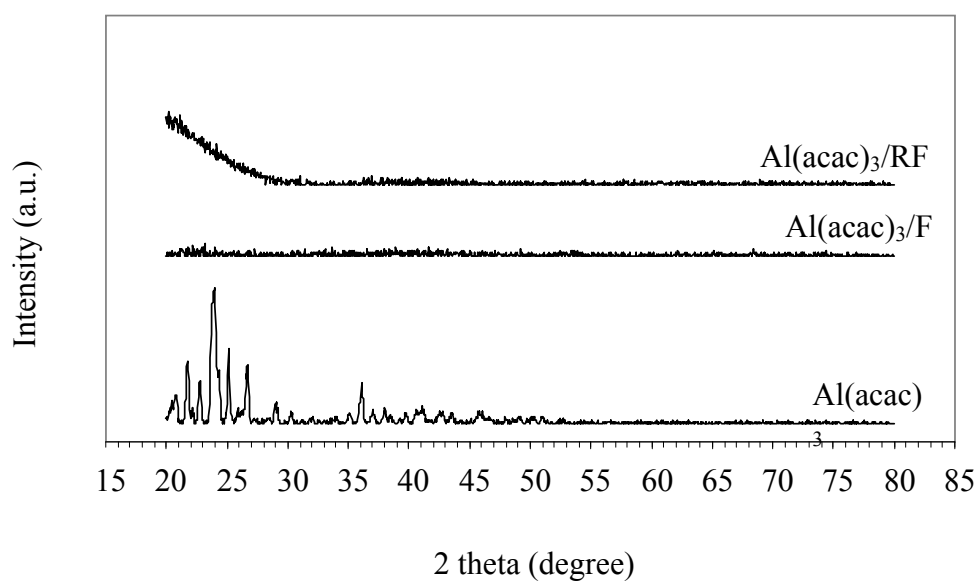
Figure 4.5 XRD patterns of $Al(acac)_3$ powder, $Al(acac)_3/F$ xerogel and $Al(acac)_3/RF$ xerogel.

Phase transition and crystallite size and surface area of the products calcined at temperature in the range of 800 to 1200°C were investigated by XRD analysis as shown in Figure 4.6. The crystallite sizes were calculated from the XRD line broadening using the Scherrer equation, while surface area was analyzed from BET model, as listed in Table 4.1. Both products synthesized with and without the RF gel are amorphous when the calcination temperature is lower than 800°C (results not shown). At the calcination temperature of 800°C, γ-alumina is formed with the crystallite size of 5 nm. For the product prepared without the RF gel, the γ-to-α phase transformation takes place at temperature around 1000°C as witnessed from the emergence of weak signals of α-alumina mixed with those of γ-alumina. The phase transformation is complete when the product is calcined at 1100°C and the crystallite size of α-alumina becomes bigger to around 46 nm. On the other hand, for alumina synthesized with the aid of the RF gel, γ-phase is stable up to 1100°C, whereas the crystallite size could be maintained at 5 nm. By using the RF gel, the γ-to-α phase transformation temperature could be shifted up to 1200°C. At 1200°C, α-alumina is the major phase observed with the crystallite size of 50 nm. These results reveal that the use of the RF gel in the synthesis of porous alumina is effective not only in enhancing porosity of the product, but also in retarding the transformation to α-alumina because it can prevent the crystallite growth and inhibit the aggregation of γ-alumina to reach the critical crystallite size that can initiate the phase transformation to α-alumina (Cava et al., 2007).

Table 4.1 Surface area and crystallite size analyses as a function of calcination temperature.

Calcination temperature (°C)	Al$_2$O$_3$ synthesized with RF gel		Al$_2$O$_3$ synthesized without RF gel	
	BET (m^2/g)	Size (nm)	BET (m^2/g)	Size (nm)
800	154	5	174	5
1000	106	5	120	5
1100	96	5	80	39
1200	67	50	13	46
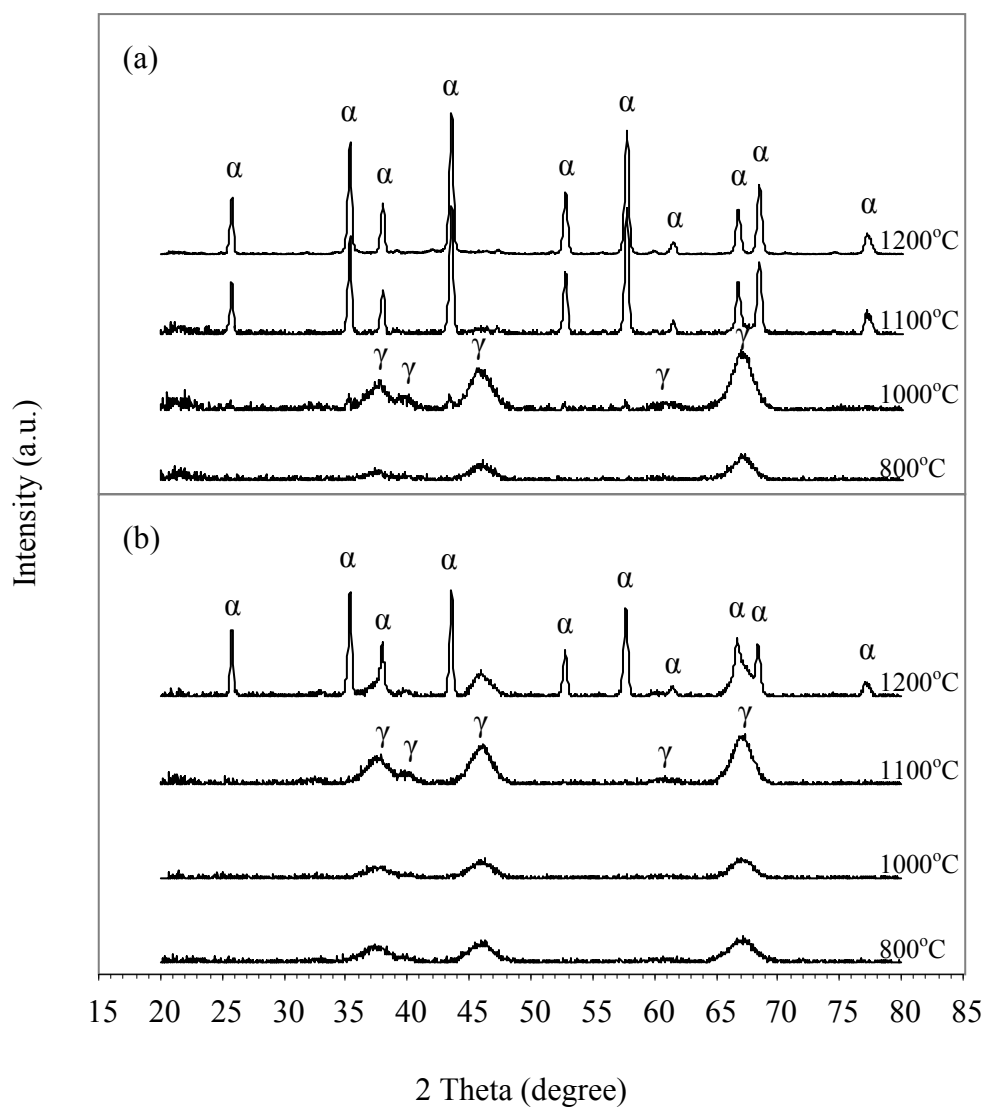
Figure 4.6 XRD patterns of alumina products synthesized without (a) and with (b) the aid of RF gel, after being calcined at various temperatures.

4.1.2 Proposed Interaction between Resorcinol-Formaldehyde Gel and Aluminium Acetylacetonate

To investigate the interaction between aluminium precursor and RF gel, Al(acac)$_3$ was mixed with RF solution. The mixture was then kept in a closed system at room temperature. The solution gradually transformed to the Al(acac)$_3$/RF hydrogels as a result of the sol-gel polymerization and its color changed from clear to deep red via yellow and orange depending on the aging time. The spectroscopic study of the Al(acac)$_3$/RF mixture during aging was performed using FTIR analysis.

Figure 4.7 shows the FTIR spectra of Al(acac)$_3$/RF gel, comparing with those of neat RF gel and the starting agents, i.e. Al(acac)$_3$, resorcinol and formaldehyde. The details of the IR bands of starting agents are listed in Tables 4.2 and 4.3. After 45 hours of aging the RF gel and Al(acac)$_3$/RF gel, all important features of the typical RF gel are presented in Al(acac)$_3$/RF gel, with bands at 1617.0, 1473.3, 1294.9, 1164.5 and 1017.7 cm^{-1} corresponding to aromatic ring stretching vibration, CH$_2$ stretching vibration, C-O stretching vibration, C-H in plane deformation of the RF mixture and C-OH bonding of formaldehyde (Liang et al., 2000), respectively, are found. The strong absorption bands at 1221.8 and 1090.0 cm^{-1} associating with C-O-C stretching vibrations of methylene ether bridges between resorcinol molecules (Liang et al., 2000) are also observed. These FTIR results indicate that the reaction between resorcinol and formaldehyde in the RF structure in this work is the same as reported elsewhere (Liang et al., 2000).

Moreover, there is a new strong absorption peak appearing at 1687.4 cm^{-1}. This band is not present in the spectrum of neat RF gel or that of pure Al(acac)$_3$. Since it clearly appears after mixing both compounds together, it suggests that the presence of this absorption band is the result from the interaction between RF gel and Al(acac)$_3$. However, the characteristic of the interaction for this absorption peak will be mentioned and explained later in this section.
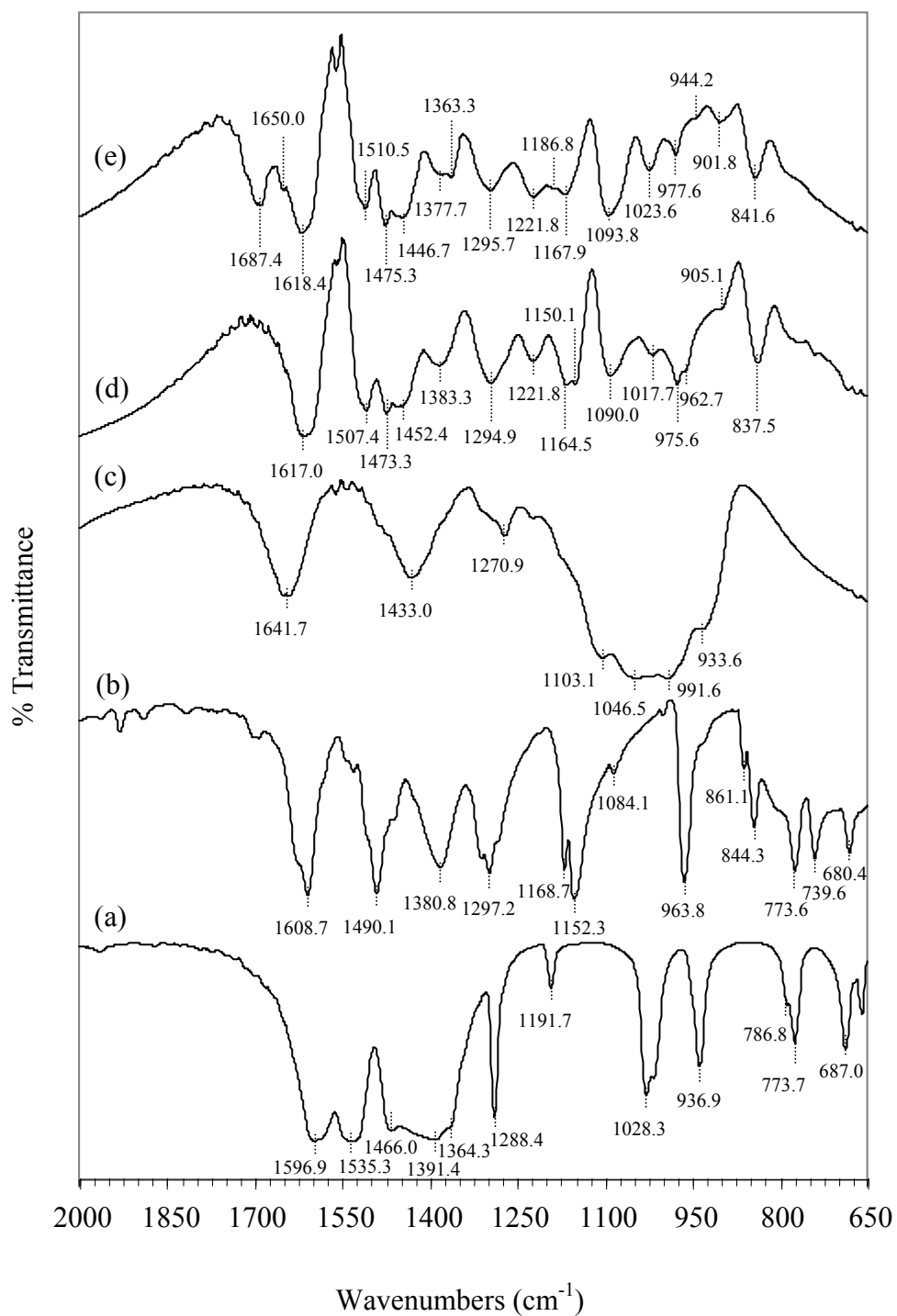
Figure 4.7 FTIR spectra of: (a) Al(acac)$_3$, (b) resorcinol, (c) formaldehyde, (d) RF gel aged for 45 hours and (e) Al(acac)$_3$/RF gel aged for 44 hours.

Table 4.2 FTIR peak assignment for resorcinol and formaldehyde.

Wavenumber (cm^{-1})	Peak assignment	References
Resorcinol		
1608.7	C=C aromatic ring	[1,2]
1490.1	C=C aromatic ring	[1,2]
1380.8	OH in-plane bend	[1,2]
1297.2	C-C-O asymmetric stretch	[1]
1168.7	CH aromatic, in-plane	[1]
1152.3	C-O stretch	[1,2]
1084.1	-C-OH	[1]
963.8	-C-H out of plane	[1,2]
861.1	-C-H	[1]
844.3	asymmetric stretch of phenolic C-C-OH	[1]
773.6	CH aromatic, out-of-plane	[1,2]
739.6	CH aromatic, out-of-plane	[1,2]
680.4	C-C out of plane, ring bend	[1,2]
Formaldehyde		
1641.7	C=O stretch (overlapped with OH scissors of water)	[1]
1433.0	C-H bend	[1]
1270.9		
1103.1	-C-OH	[1]
1046.5	-C-OH	[1]
991.6	C-H	[1]
934.0		
615.0		

[1] (Poljanšek and Krajnc, 2005)

[2] (Reddy et al., 2009)

Table 4.3 FTIR peak assignment for aluminium acetylacetonate.

Wavenumber (cm^{-1})	Peak assignment	References
Aluminium acetylacetonate (Al(acac)$_3$)		
1596.9	C=O, C=C stretch	[1]
1535.3	C=C stretch, C=CH bend	[1]
1466.0	C=O stretch	[1]
1391.4	C=O, C=C stretch	[1]
1364.3	CH$_3$ bend	[1]
1288.4	C=C, C-CH$_3$ stretch	[1]
1191.7	C=O stretch, C=CH bend	[1]
1028.3	C=O stretch, ρ(CH$_3$) rock, π_{ring}	[1]
936.9	C-CH$_3$ stretch	[1]
786.8		
773.7	π(C-H)	[1]
687.0	π_{ring}	[1]
658.8	C-CH$_3$ stretch, $\rho\pi_{ring}$	[1]
594.5	Al-O stretch	[1]
578.8	Al-O stretch, C=O-Al, CH$_3$-C=O bend	[1]

[1] (Diaz-Acosta et al., 2000)

In order to investigate the reaction, a brief explaination of precursor structure is also introduced. The molecular structures of Al(acac)$_3$ precursor and AcacH ligand are shown in Figure 4.8. According to the XRD analysis (Figure 4.5), it has been well-known that Al(acac)$_3$ powder was crystalline in the monoclinic space group (Shirodker et al., 2010). The unit cell dimension, the bond lengths and the bond angles of AcacH ligand have also been documented in the literature (Shirodker et al., 2010). The central metal atom, i.e., aluminium, is hexa-coordinated and is linked to six oxygen atoms from three bidentate acetylacetonate ligands (Shirodker et al., 2010), as seen in Figure 4.8.

(a)

Al
O
C
H

(b)

Keto tautomer   Enol tautomer
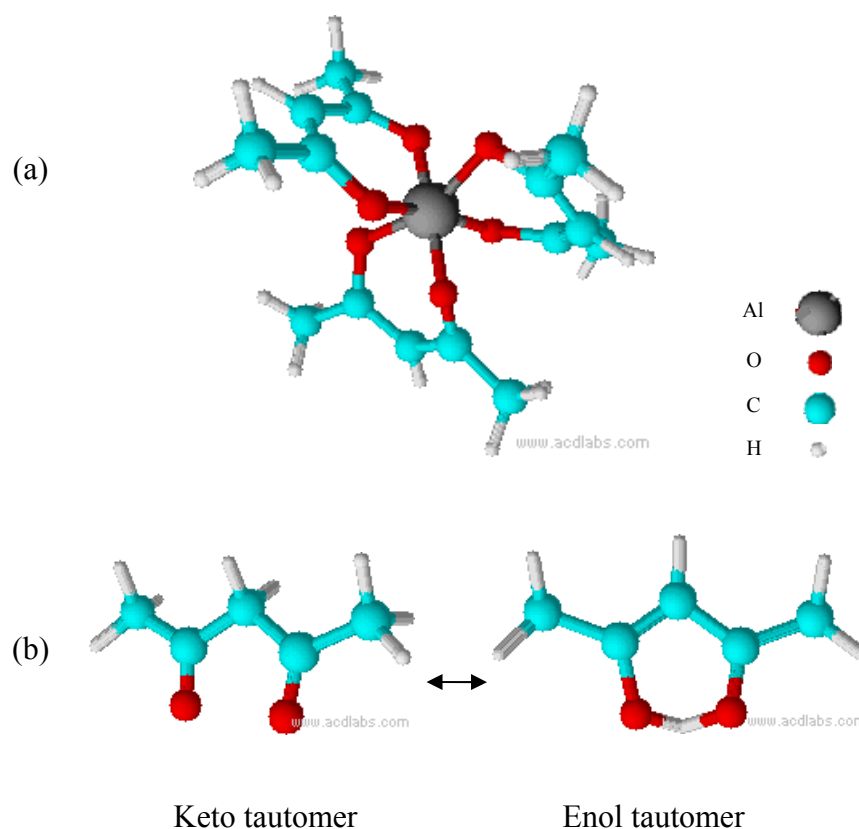
Figure 4.8 Molecular structure of: (a) aluminium acetylacetonate (Al(acac)$_3$) and (b) acetylacetone (AcacH).

In considering of the interaction between the RF gel and aluminium precursor, i.e., Al(acac)$_3$, FTIR spectra of acetylacetone (AcacH), AcacH in formaldehyde, Al(acac)$_3$ and Al(acac)$_3$ in formaldehyde were firstly gathered. These spectra are illustrated in Figure 4.9.
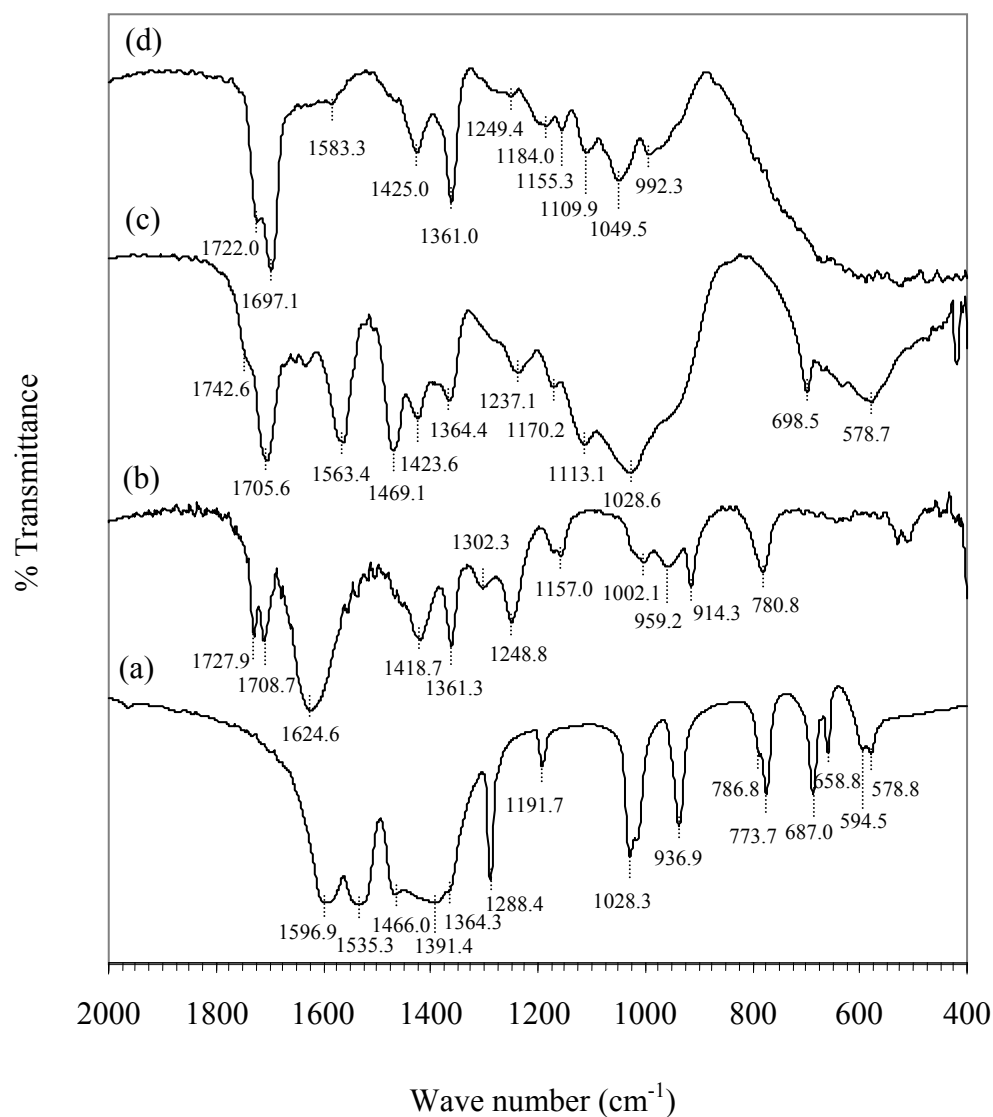
Figure 4.9 FTIR spectra of: (a) Al(acac)$_3$, (b) AcacH, (c) Al(acac)$_3$ in formaldehyde and (d) AcacH in formaldehyde.

In the infrared spectrum of pure Al(acac)$_3$, two characteristic absorption bands at 1596.9 and 1535.3 cm^{-1} are assigned to the C=O stretching vibrations of acetylacetonate moieties bonded to aluminium atoms as bidentate ligand (Slabzhennikov et al., 2006). These bands disappear when Al(acac)$_3$ is added to the formaldehyde, while a new sharp band at 1705.6 cm^{-1} is observed. Regarding to the infrared spectrum of pure AcacH, it display a doublet at 1727.9 and 1708.7 cm^{-1} attributing to the C=O stretching vibration of keto and enol form, respectively (Shen and Shaw, 2010). Moreover, the C=C stretching vibration of the enol form reveals as a strong band at 1624.6 cm^{-1} (Shen and Shaw, 2010). Generally, AcacH or β-diketones exhibit tautomerization in form of keto and enol mixtures. The details of the IR bands of pure AcacH are listed in Table 4.4.

When the AcacH is mixed with formaldehyde, the strong band of C=C stretching vibration disappears and the C=O stretching in both of keto and enol forms shift to 1722.0 and 1697.1 cm^{-1}, respectively. Considering the FTIR spectra of Al(acac)$_3$ or AcacH after mixing with formaldehyde, the existence of the new peak in the former might be possibly ascribed to a part of the latter. In addition, it is obviously noticed that the former is similar to the latter. It is indicated that the reaction of Al(acac)$_3$ and formaldehyde behaves like when the AcacH ligand reacts with formaldehyde. For the interaction between AcacH and formaldehyde, it has been previously proposed in the literature (Amin and Zareh, 1996) as shown in Figure 4.10.

Therefore, it is reasonable to suggest that the reaction between Al(acac)$_3$ and formaldehyde possibly takes place at AcacH ligand position. Nonetheless, this reaction might take place in different pathways from the previous investigation as further proposed in this study.
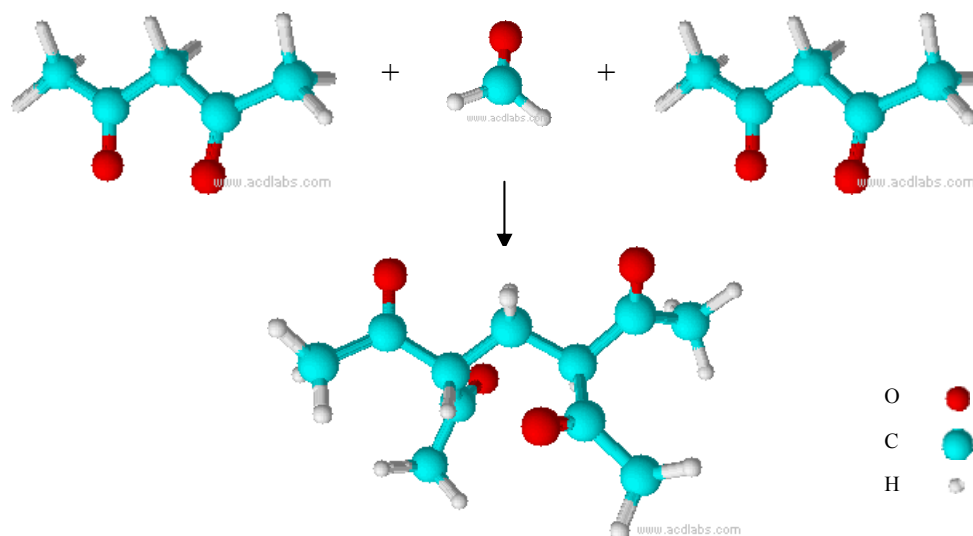
Figure 4.10 Scheme for the reaction of acetylacetone and formaldehyde (Amin and Zareh, 1996).

Although the formaldehyde is proposed to react with $Al(acac)_3$ precursor at AcacH ligand position, the absorption band at 578.7 cm^{-1},which is associated with the vibration of Al-O=C bond (Diaz-Acosta et al., 2000, Shirodker et al., 2010) is observed in Figure 4.9 (c). This presumably means that acetylacetonate ligands are still coordinated to aluminium atoms to form $Al(acac)_3$-formaldehyde species.

Table 4.4 FTIR peak assignment for acetylacetonate.

Wavenumber (cm^{-1})	Peak assignment	References
Acetylacetonate (AcacH)		
1727.9	C=O, C=C stretch	[1]
1708.7	C=O stretch	
1624.6	C=C stretch	[1]
1418.7	C-C C-O + C-CH$_3$ stretch + CH + OH bend	[2]
1361.3	CH$_3$ bend	[2]
1302.3	C-C C-O + C O stretch + OH bend	[2]
1248.8	C-C C + C-CH$_3$ stretch + OH bend	[2]
1157.0	CH	[2]
1002.1	CH$_3$	[2]
959.2	OH rock	[2]
914.3	C-CH$_3$ + C-O stretch	[2]
780.8	C-H rock	[2]
529.3		
510.5		

[1] (Sohn and Lee, 1997)

[2] (Tayyari and Milani, 2000)

To clarify the formation of Al(acac)$_3$-formaldehyde species, the FTIR spectrum of Al(acac)$_3$ with formaldehyde were measured at various time as shown in Figure 4.11. The characteristic absorption peaks of Al species at 699.5 cm^{-1} (Al-O=C stretching) and 591.0 cm^{-1} (Al-O stretching) are observed after aging the mixture for 12 hours. The intensity of these peaks increases with the progress in aging. These results confirm that there is a new species of Al(acac)$_3$-formaldehyde as a result from the reaction between Al(acac)$_3$ and formaldehyde.
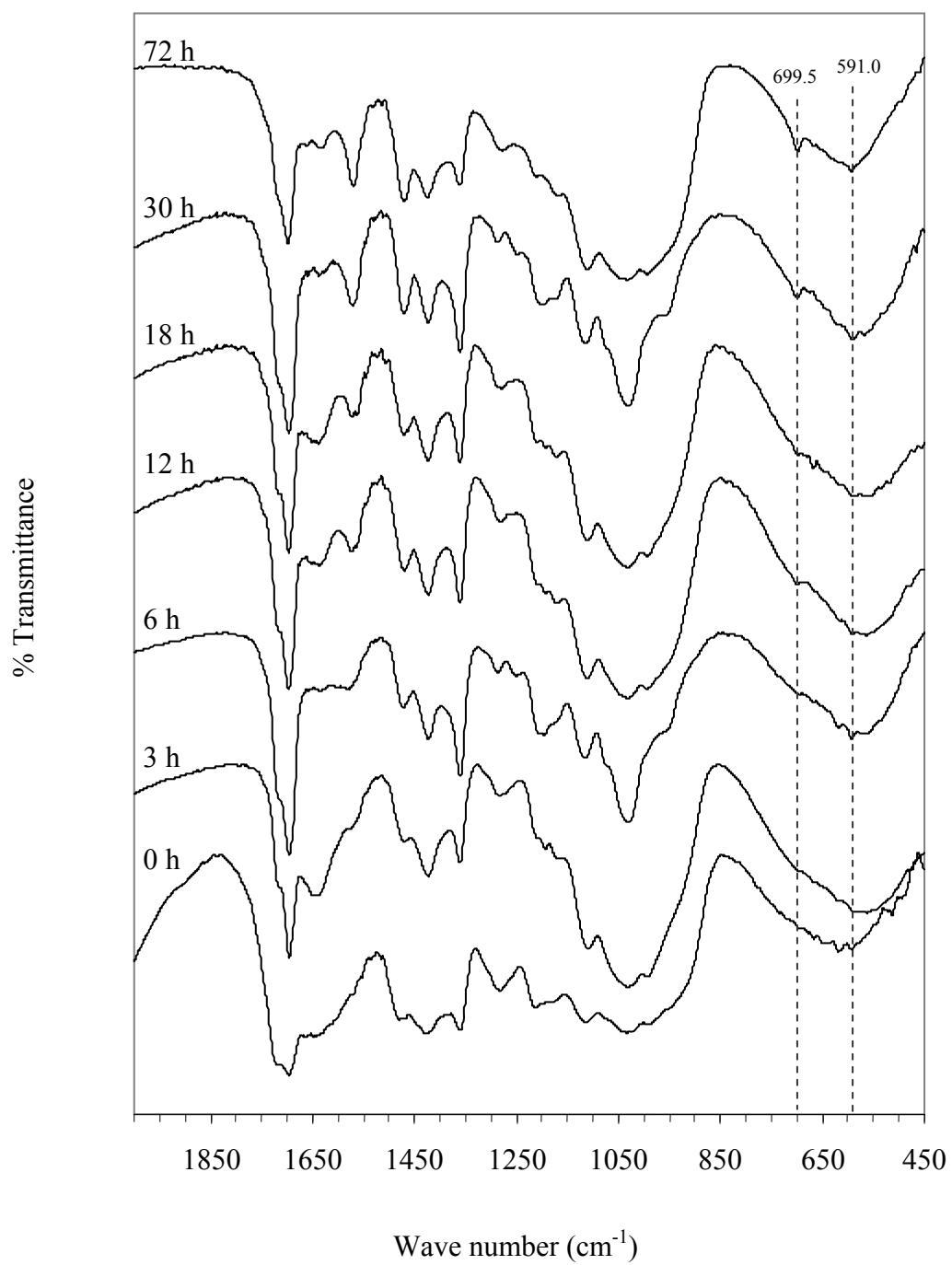
Figure 4.11 FTIR spectra of Al(acac)$_3$ mixed with formaldehyde at various aging time.

Considering the interaction between resorcinol and AcacH, the FTIR spectrum of AcacH, resorcinol in water, and the mixture of AcacH and resorcinol with and without water were collected. For the study of chemical reaction in that mixture, it is based on either the disappearance of one type of group or the appearance of another. According to the Figure 4.12, the presence of new band at 1019.4 cm^{-1} in the resorcinol mixed with AcacH and the missing of C-C C stretching vibration at 1248.8 cm^{-1} for pure AcacH are observed. Thus, it could be presumed that the AcacH molecules have ability to incorporate with resorcinol molecules. However, the phenomenon disappears when the water is added to the system.

One of the possible reasons is that the solubility of resorcinol in water is as high as 110 g/100 ml which is higher than that of resorcinol in AcacH. The resorcinol molecule consists of two hydroxyl groups in the structure leading to hydrophilic nature. This is the reason why resorcinol can be dissolved in water more than in AcacH. Conversely, AcacH molecules are slightly soluble in water as low as 16 g/100 ml. Therefore, it is suggested that the AcacH molecules may not chemically react with resorcinol in aqueous system.
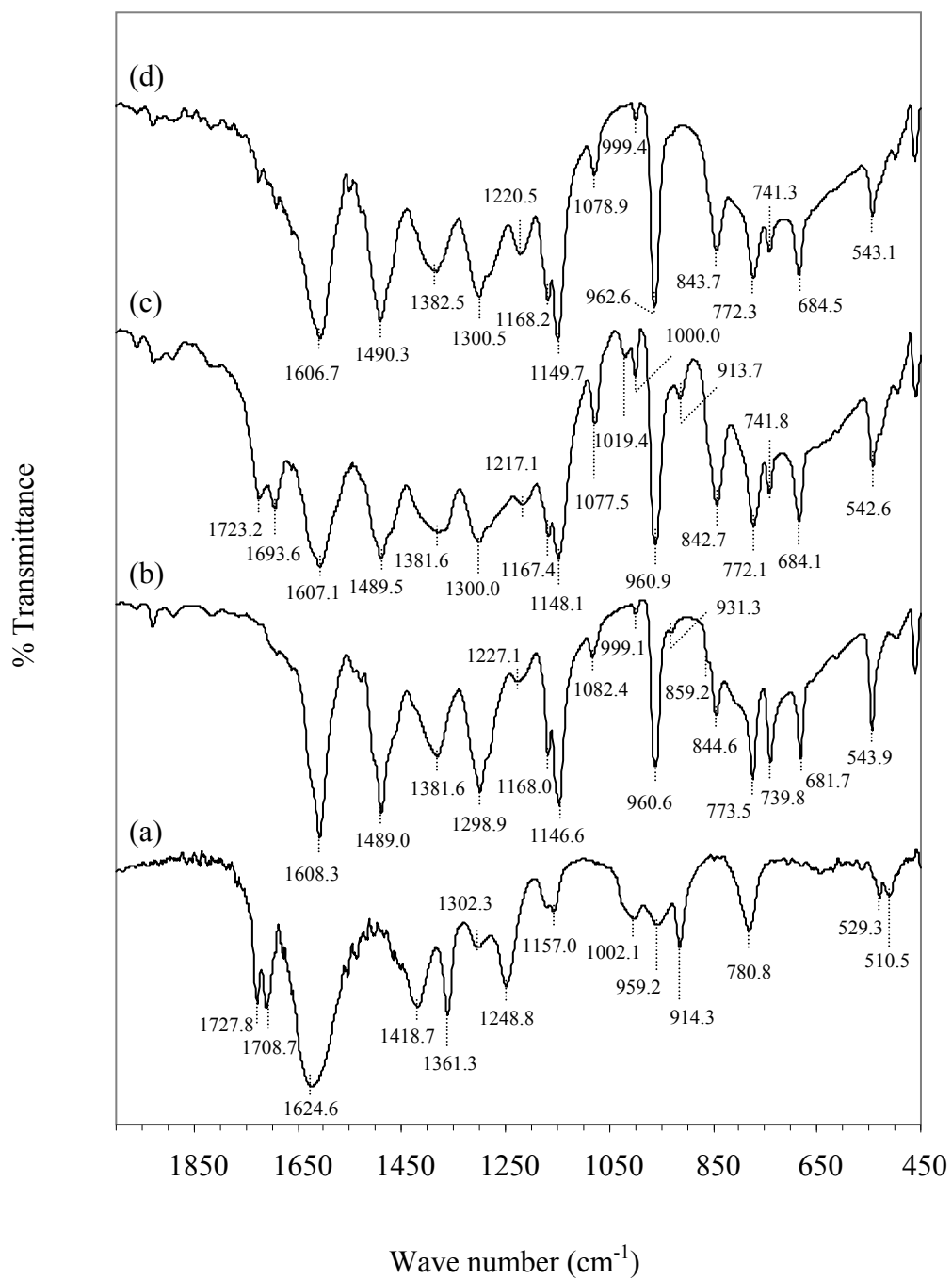
Figure 4.12 FTIR spectra of: (a) AcacH, (b) resorcinol in water, (c) resorcinol in AcacH and (d) mixing of resorcinol with AcacH in water.

The sol-gel polycondensation of sodium carbonate catalyzed resorcinol-formaldehyde gel added with AcacH was also investigated by FTIR technique as depicted in Figure 4.13. The IR spectrum of AcacH/RF gel show the same features to that of Al(acac)$_3$/RF gel (Figure 4.7). It is apparent that the absorption bands at 1606.4, 1469.9, 1298.3 and 1166.0 cm^{-1} are corresponding to aromatic ring stretching vibration, CH$_2$ stretching vibration, C-O stretching vibration and C-H in plane deformation of the RF mixture, while the absorption band at 1020.0 cm^{-1} is assigned to C-OH bonding of formaldehyde. During the aging of the AcacH/RF mixture, it is found that the IR bands at 1222.8 and 1096.4 cm^{-1} associated with C-O-C stretching vibrations of methylene ether bridges between resorcinol molecules are intensified.

Nevertheless, the viscosity measurement in Figure 4.13 reveals that the gelation of AcacH/RF occurs slower than that of both neat RF and Al(acac)$_3$/RF. The gelation time of the Al(acac)$_3$/RF and the neat RF mixture is 509 and 2195 minutes, respectively, while that of the AcacH/RF mixture is as slow as 2812 minutes. Owing to the slowest gelation time of AcacH/RF, it might be caused by steric hindrance from the bonding creation of acetylacetone with resorcinol, resulting in slow rate of RF polymerization. These results give a good agreement with the result of FTIR analysis, as shown in the Figure 4.13, such that the absorption bands at 770.4, 742.4 and 686.6 cm^{-1} which are characteristic of C-H aromatic ring bending vibration and C-C aromatic ring bending vibration (Poljanšek and Krajnc, 2005, Reddy et al., 2009), are still detected even after aging that gel for 47 hours. At the same aging time, for other gels, there are no absorption peaks in those ranges presented.

As the results, no evidence for free molecules of AcacH ligands in the system of Al(acac)$_3$/RF gel is observed. It means that aluminium atoms are still linking to AcacH ligands. This effect is also explained by a strong interaction between aluminium atom and acetylacetonate ligand (Charles and Pawlikowski, 1958).
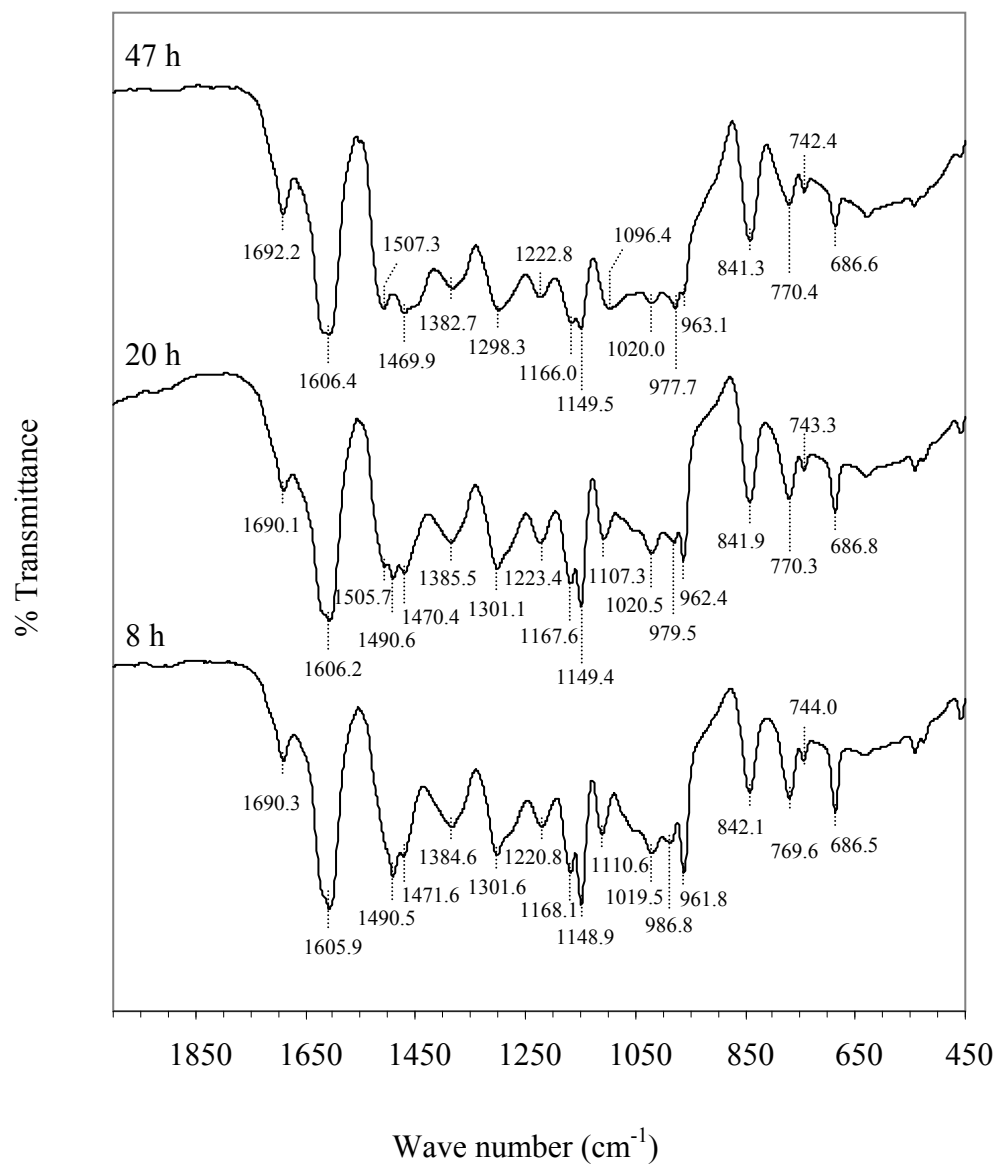
Figure 4.13 FTIR spectra of AcacH/RF gel at various aging times.

The spectra of RF gel comparing with those of uncatalyzed and catalyzed Al(acac)$_3$/RF gel are shown in Figure 4.14. It is observed that all important bands in both spectra of RF gel and Al(acac)$_3$ gel also appear in the spectrum of uncatalyzed Al(acac)$_3$/RF gel. However, as a matter of fact, the uncatalyzed Al(acac)$_3$/RF mixture becomes gel faster than both the conventional RF gel and the Al(acac)$_3$/RF gel, as seen from the viscosity measurement in Figure 4.3. The gelation time of the uncatalyzed Al(acac)$_3$/RF mixture is only 455 minutes, while that of the Al(acac)$_3$/RF mixture and the neat RF mixture are 509 and 2195 minutes, respectively. Therefore, it is interesting to note that Al(acac)$_3$ not only reacts with the RF mixture but also catalyzes the polymerization of that mixture.

In order to clarify the aluminium coordination of Al(acac)$_3$ precursor, the ^{27}Al NMR was employed. The NMR spectra of RF mixture, Al(acac)$_3$ mixed with formaldehyde and Al(acac)$_3$ mixed with RF gel are illustrated in Figure 4.15. For the RF mixture, no peak was observed due to an absence of the aluminium atom in that mixture, while both mixtures of Al(acac)$_3$/F and Al(acac)$_3$/RF show only one broad peak in the range of 5-10 ppm that is assigned to six-coordinated aluminium atom (Fessi and Ghorbel, 2000). Moreover, it was found that the broad peak can be deconvoluted into two peaks in both cases of Al(acac)$_3$/F and Al(acac)$_3$/RF mixtures, attributing to more than one type of bond coordinating with aluminium atom.

From these results, it is considered that aluminium atom can not only bond to AcacH as monodentate ligand, but also react with other molecule to fully form six coordinated aluminium atom. As mentioned earlier, there was no free AcacH ligand in the mixture. Therefore, the ligands are likely attached to the aluminium metal center. Considering the molecular structure of Al(acac)$_3$ in Figure 4.8, it is possible to have three AcacH ligands accompanied with three unoccupied aluminium bonds.

One of the possible reactions of Al(acac)$_3$ and RF is that the Al(acac)$_3$, which consists of C=O group, is capable of forming adducts via hydrogen bonding with resorcinol at the hydroxyl functional positions.

Another possible reaction is that, when Al(acac)$_3$ is mixed with formaldehyde, three acetylacetonate ligands might form monodentate bonding with aluminium metal center and other three unoccupied aluminium bonds could further react with resorcinol. These are in a good agreement with previous literature (Dhere et al., 2011, Durairaj, 2005, Zhang, 1997) and are presented in Figure 4.16. Regarding to six-coordinated aluminium atom of Al(acac)$_3$ precursor, three unoccupied aluminium bonds and three AcacH ligands could potentially form the hydrogen bonding with hydroxyl group in the compound such as resorcinol. As a result of these bonding, it could induce the resorcinol to come closer and surround the Al(acac)$_3$ precursor. Consequently, it helps generating the RF network and it could eventually reduce the gelation time.
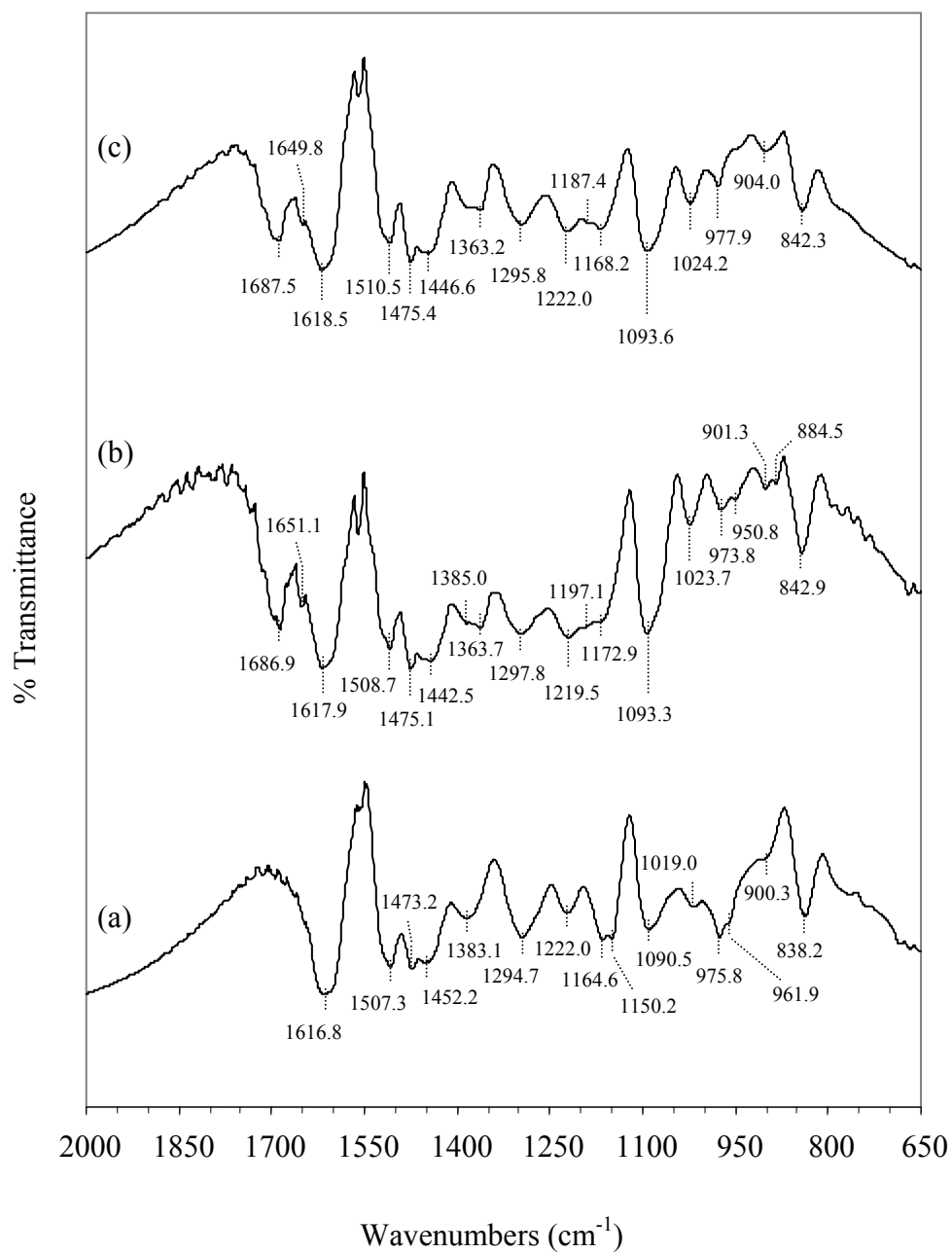
Figure 4.14 FTIR spectra of: (a) RF gel aged for 45 hours, (b) uncatalyzed Al(acac)$_3$/RF gel aged for 45 hours and (c) Al(acac)$_3$/RF gel aged for 44 hours.

Al(acac)$_3$/F

Al(acac)$_3$/RF

RF

ppm
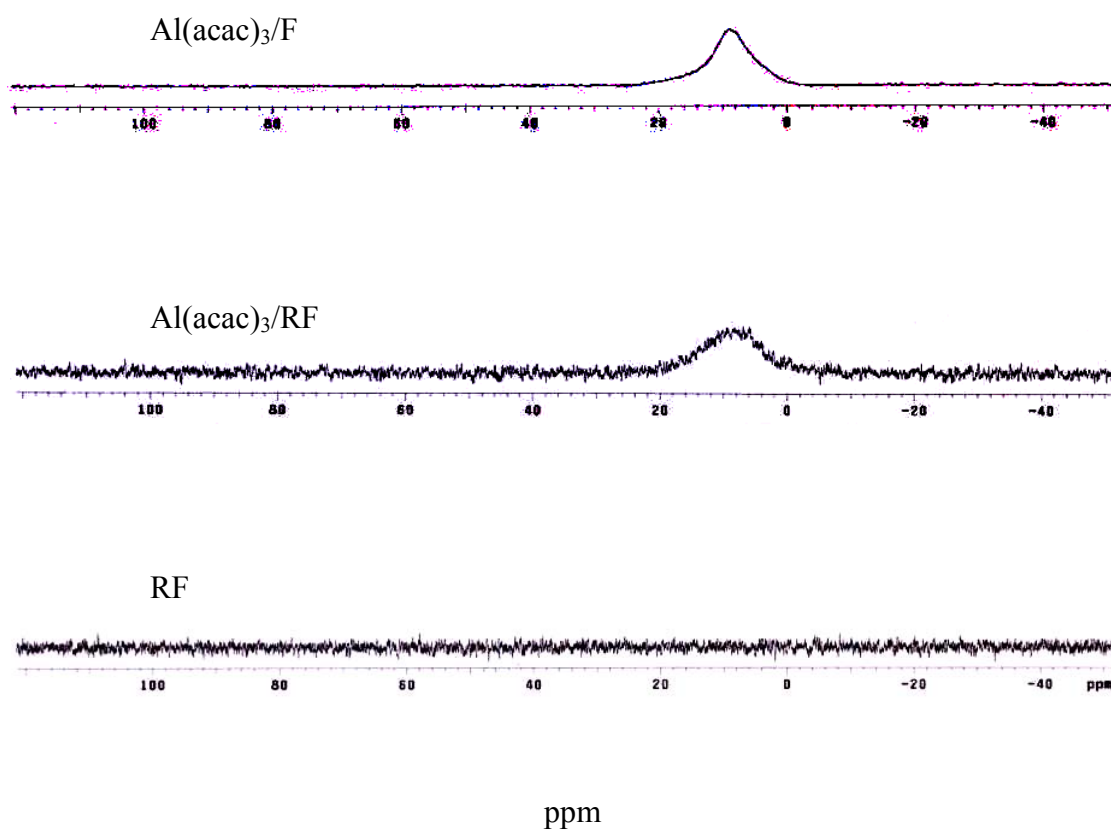
Figure 4.15 Solution ^{27}Al NMR of Al(acac)$_3$/F, Al(acac)$_3$/RF and RF gel.

$$\text{Al(acac)}_3 + {}^+\text{H-}{}^-\text{O-[ ]} \quad \rightarrow \quad \text{Al(acac)}_3 \; \text{H}^+ \dots {}^-\text{O-[ ]} \qquad \text{(a)}$$

$$\text{AcacH} + {}^+\text{H-}{}^-\text{O-[ ]} \quad \rightarrow \quad \text{AcacH} \; \text{H}^+ \dots {}^-\text{O-[ ]} \qquad \text{(b)}$$
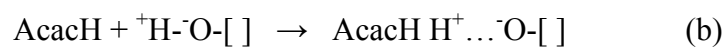
Figure 4.16 Proposed the possible interaction of (a) Al(acac)$_3$ and (b) AcacH with hydroxyl group in this system (Dhere et al., 2011, Zhang, 1997).

In summary of the Al(acac)$_3$/RF gel formation section, the possible structure is proposed in three dimensional features as shown in Figure 4.17.
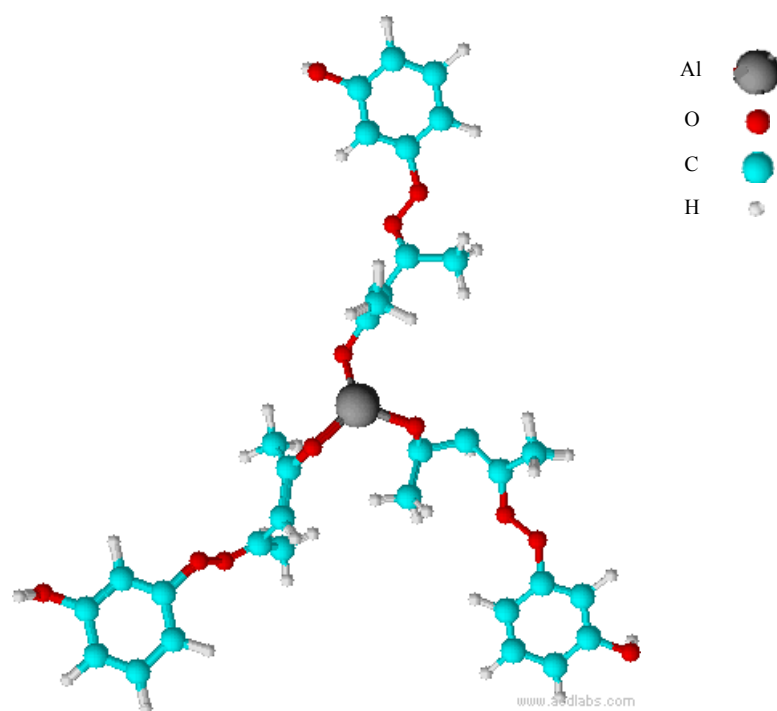
Figure 4.17 Optimized geometries of Al(acac)$_3$ bonded with resorcinol performed by ACDLABS 12.0.

4.2 Effect of Aging Time

In order to investigate the effect of aging time on the morphology of RF gel and alumina product, the Al(acac)$_3$ precursor was mixed with RF solution and the mixture then was aged in a closed system at room temperature. During the sol-gel polycondensation process, the Al(acac)$_3$/RF gel was collected to analyze the gel at the aging time of 0, 7, 15, 25, 40, 50 and 72 hours. The details of the morphology and the chemical properties relating to the aging time were typically studied by means of scanning electron microscopy (SEM) and fourier transform infrared spectroscopy (FTIR). From the method mentioned above, the white alumina product was obtained after the Al(acac)$_3$/RF gel was dried and calcined.

Generally, morphology of the RF gel was spherical-like shape (Jirglová and Maldonado-Hódar, 2010). However, it could be changed to other shapes, relying on the additive agent. For example, the lamellar structure of modified RF gel was obtained when the anionic surfactant, e.g., sodium dodecylbenzensulfonate, was added (Jirglová and Maldonado-Hódar, 2010) into the RF mixture. The characteristic of the final gel strongly depend on the presence of the additive agent in the synthesis as well.

In this study, the Al(acac)$_3$ representing as an additive agent was added into the RF mixture. The sampled gel was investigated at the aging time in the range of 0-72 hours. For the gel aged longer than 72 hours, it could be presumed that the complete gelation has occurred. For the next step, the drying process that generally affects the morphology was carried out.

There are several drying processes that can be applied for this work. However, the conventional drying process (stagnant air at 110°C) and the freeze drying process were taken into account because the differences in the heat treatment of both drying processes might influence the morphology. Typically, the gels after being dried by means of conventional and freeze drying process are so-called xerogel and cryogel, respectively. Concerning at the state of complete gel (aging time of 72 hours), the

morphologies of Al(acac)$_3$/RF xerogel and cryogel were compared as illustrated the SEM images in Figure 4.18. The insets show the corresponding images at high resolution. It is observed that the morphologies, in microscopic view, of both Al(acac)$_3$/RF xerogel and cryogel are quite similar, exhibiting the formation of particle aggregates structure with the particle size around 250 nm.
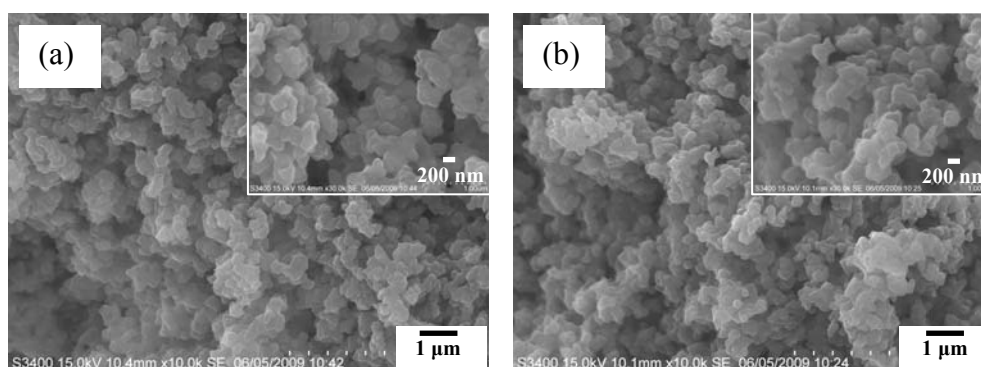
Figure 4.18 SEM micrographs of the aluminium acetylacetonate/resorcinol-formaldehyde gels after aging for 72 hours which were further dried by freeze (a) and conventional drying processes (b).

Even though the change in the morphologies of the complete gel according to the different drying processes was not observed, it might not be the case for the incomplete gel (aging time of 0-7 hours). In addition, it could be examined from the morphology of the alumina product as well. The morphologies of the alumina products obtained from Al(acac)$_3$/RF xerogel and cryogel aged at various aging time are presented in Figures 4.19 and 4.20.

Regarding the alumina synthesized from the xerogel, it is found that there is no significant difference in the morphology for all studied aging time. The alumina particles, which form into an aggregated product, are worm-like in shape with the particle size around 110 nm. For the alumina produced from freeze drying process, differences in the surface morphologies (Figure 4.20) could be apparently observed from the samples aged in the range of 0-7 hours. This phenomenon does not occur in the case of the conventional drying. A possible explanation might be that the heat treatment of the conventional drying can help catalyzing the polymerization reaction leading to a possibility of forming a complete gel. On the other hand, this reaction is instantly stopped after starting the freeze drying process.

Considering the surface morphology of the alumina products fabricated via freeze drying (Figure 4.20), it is found that the incomplete particle appears at the beginning (0 hour). After aging the gel for 7 hours, the alumina is formed as aggregates of large particles around 200 nm. The product from gel aged longer than 15 hours exhibits similar morphology to the alumina product obtained by applying the conventional drying. Moreover, it also shows the same particle size, around 110 nm, as well.
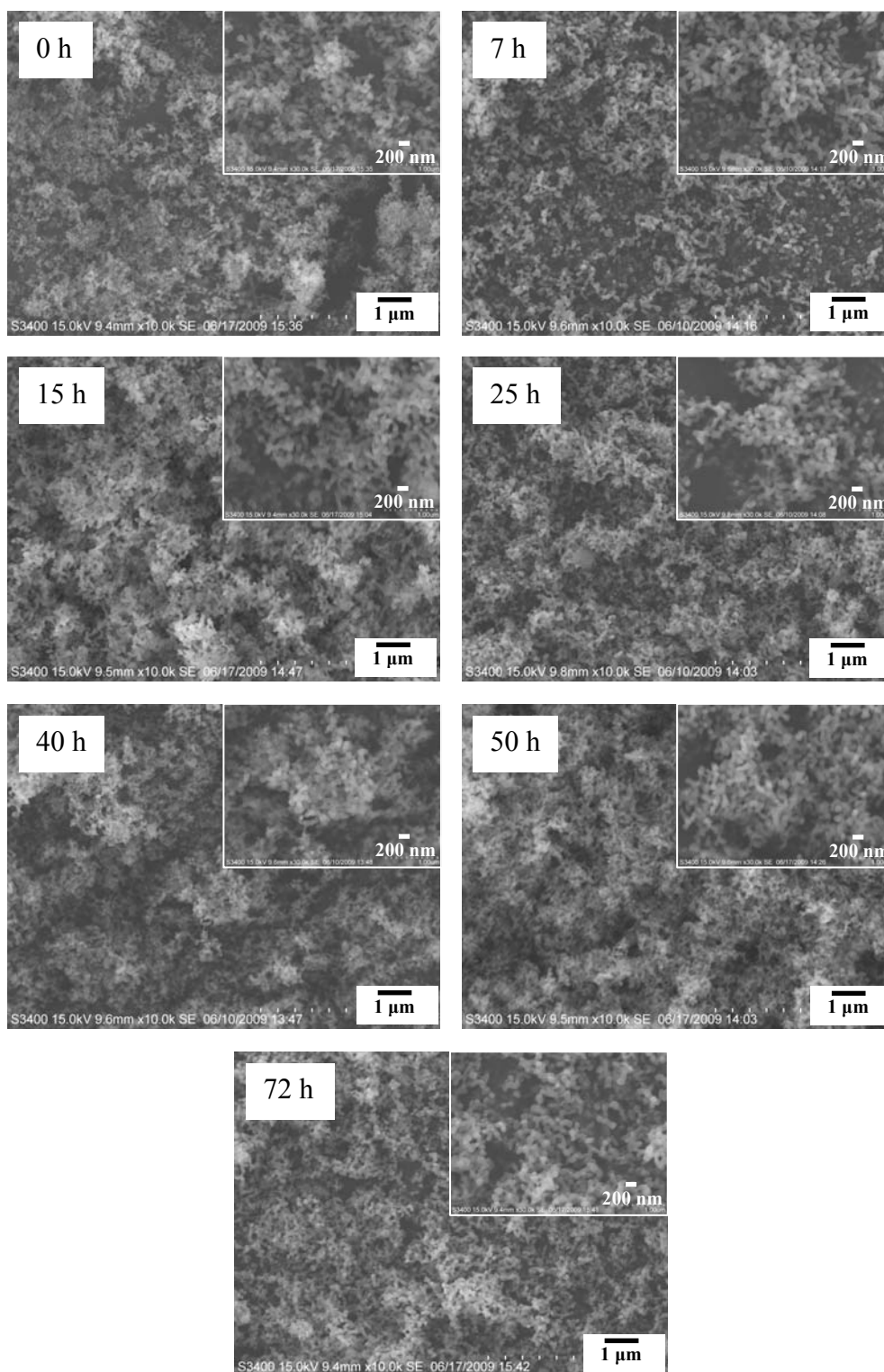
Figure 4.19 SEM micrographs of the alumina products synthesized from Al(acac)₃/RF xerogel which was aged for various aging time and calcined at 1200°C for 2 hours.
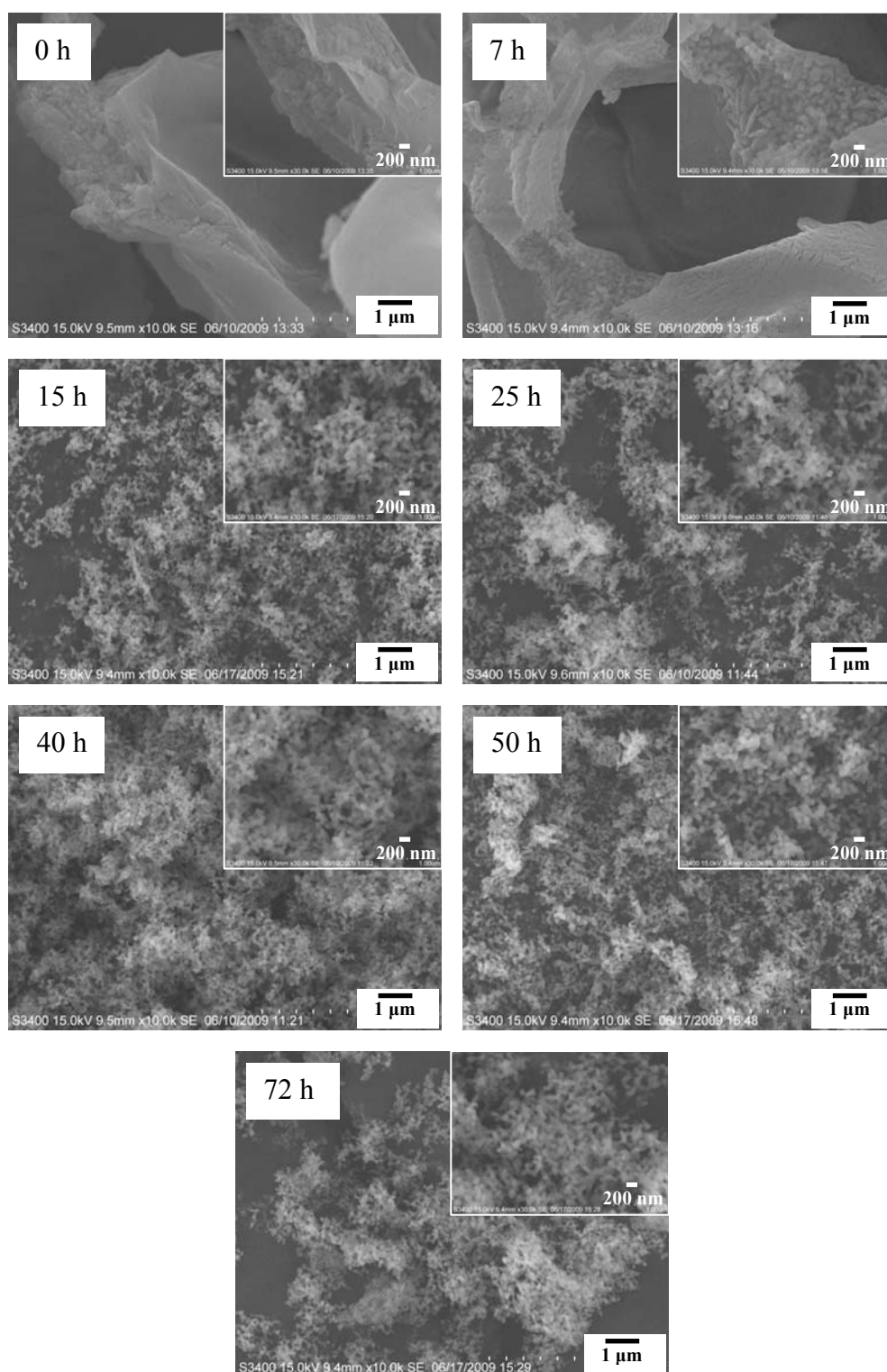
Figure 4.20 SEM micrographs of the alumina products synthesized from Al(acac)₃/RF cryogel which was aged for various aging time and calcined at 1200°C for 2 hours.

Results from the TG and DTA analysis of Al(acac)$_3$/RF gel at various aging times are shown in Figure 4.21. At the aging time of 0 and 7 hours, it is found that there are two decreasing periods which are located at the temperature lower than 100$^{\text{o}}$C and the temperature in the range of 125-150$^{\text{o}}$C. For the first section, the decreased weight is possibly ascribed to the formaldehyde residue in the gel. The second reduction is the result from a degradation of the formaldehyde derivative. For the gel aged in the range of 15-72 hours, two periods of the reduction in weight are observed but the temperature range of the period is different from previously discussed. It indicates the periods at the temperature lower than 100$^{\text{o}}$C and the temperature in the range of 290-600$^{\text{o}}$C. The reduced weight at low temperature (100$^{\text{o}}$C) is caused by the formaldehyde residue as mentioned earlier. At 290-600$^{\text{o}}$C, there is the degradation of resorcinol derivative and RF gel network. These TG/DTA analytical results are in a good agreement with the SEM images. The spherical alumina particles are not completely formed in the first seven hours of the formation as seen in the SEM images (Figure 4.20). This is probably due to the existence of the resorcinol derivative that might be possibly referred to no gel network was performed. In addition, these results are also confirmed by FTIR analysis as described in the next paragraphs.
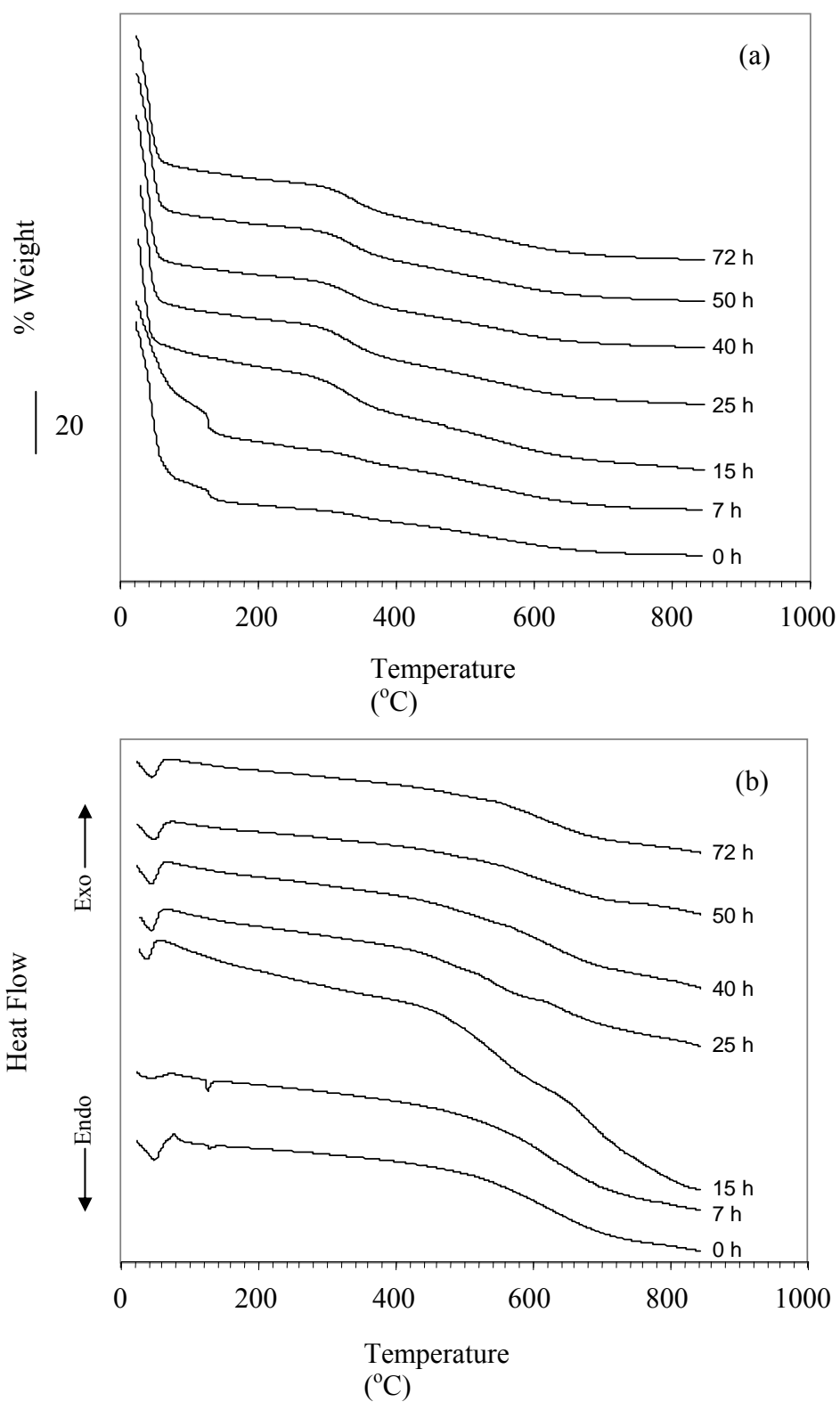
Figure 4.21 TG (a) and DTA (b) analysis of Al(acac)$_3$/RF gel at various aging time.

The formations of RF gel and Al(acac)$_3$/RF network at various aging time are analyzed by means of FTIR technique as illustrated in Figures 4.22 and 4.23, respectively. In general, the reaction between resorcinol and formaldehyde is divided into two steps. The first step is the addition reaction to form resorcinol ethoxy. The IR band at the wavenumber of 959.1 cm^{-1} expresses the pure resorcinol. As seen in Figure 4.22, intensity of this peak decreases with increasing aging time due to the formation of substituted resorcinol. Moreover, the increase in the resorcinol derivative peak presenting at the wavenumber of 974.8 cm^{-1} is also observed. It is found that at the aging time of 50 hours, less pure resorcinol is detected while there is more resorcinol derivative. For the second step of the reaction, the polycondensation reaction of the resorcinol derivatives occurs to form methylene- and methylene ether-bridged compounds as assigned at the wavenumbers of 1475.2 and 1091.9 cm^{-1}, respectively. The methylene bridge is observed since the beginning, while the methylene ether bridge forms after the aging time of 50 hours.

After adding Al(acac)$_3$ into the RF mixture, the obtained Al(acac)$_3$/RF gel was collected at various aging time and then investigated by FTIR. It is found that the peak for pure resorcinol at wavenumber of 962.4 cm^{-1} rapidly decreases, while the substituted resorcinol at wavenumber of 976.1 cm^{-1} is generated. In this case, almost all of the pure resorcinol is converted into the substituted resorcinol at the aging time of 15.5 hours. Thus, the generation of the substituted resorcinol is faster comparing to that in the neat RF mixture. Moreover, the bridges between aromatic rings such as methylene and methylene ether bridges (wavenumbers of 1475.7 and 1095.2 cm^{-1}) are obviously formed at the aging time of 15.5 hours, which is much faster than those of the neat RF system.

Considering the FTIR spectra of the neat RF and Al(acac)$_3$/RF systems, the system with the presence of Al(acac)$_3$ generates the methylene ether bridge faster than that without Al(acac)$_3$. For the neat RF gel, that bridge is formed at the aging time of 50 hours, while it starts to be generated at the aging time of 15.5 hours in the case of Al(acac)$_3$/RF gel. These results correspond to the results from SEM and TG/DTA

techniques that the incomplete gel is obtained at the aging time in the range of 0-7 hours.
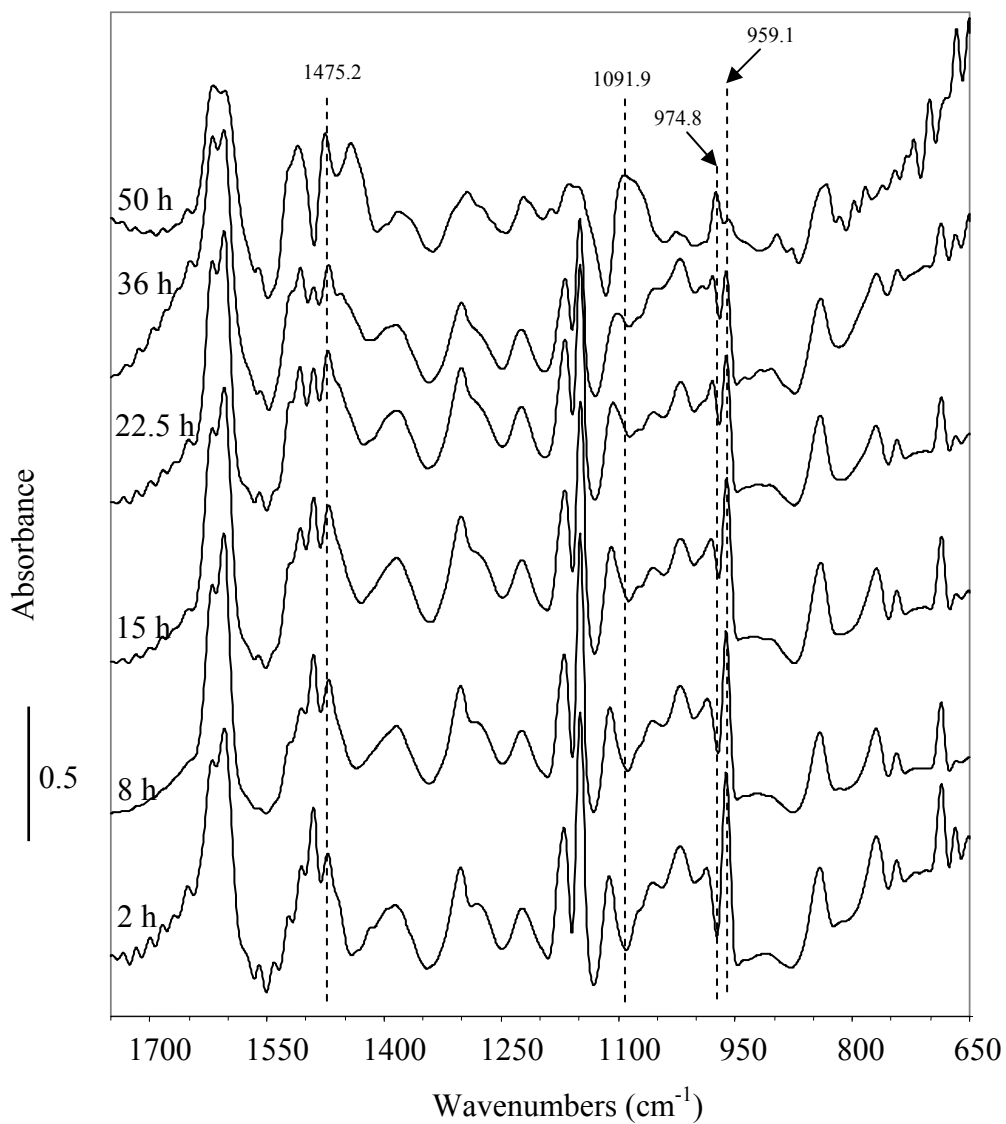
Figure 4.22 Deconvoluted FTIR spectra of RF gel in closed system at various aging time.
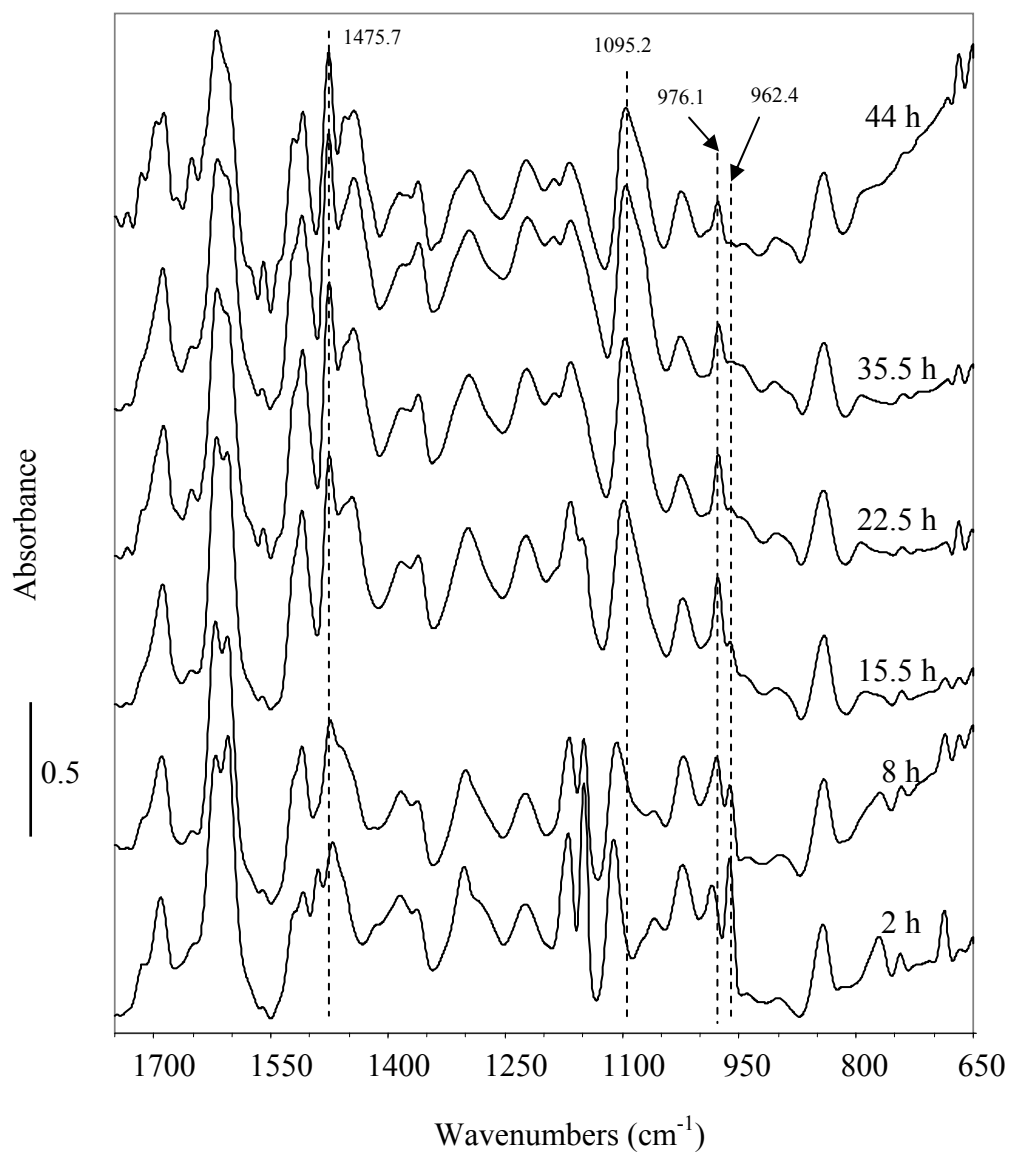
Figure 4.23 Deconvoluted FTIR spectra of Al(acac)$_3$/RF gel in closed system at various aging time.

4.3 Effect of Aging Temperature

In order to investigate the effect of aging temperature, the $Al(acac)_3$/RF gel was aged at different temperatures, i.e. room temperature, 50, 60 and 80^oC, for 3 days. After that, the sample gel was dried by the conventional drying to obtain the $Al(acac)_3$/RF xerogel. Then, the xerogel was calcined at 1200^oC for 2 hours to gain the white powder product. Various techniques were used to characterize the sample, such as SEM, EDX, BET, XRD and FTIR analysis.

Figure 4.24 shows the SEM micrographs of the $Al(acac)_3$/RF xerogels which were aged at various temperatures. It is found that the $Al(acac)_3$/RF xerogel seems to be aggregates of small particles. Size of the constituted particles decreases as the aging temperature is increased. To verify the visual observation, size of 30 random particles were measured using an image processor program (i.e., Semafore v.5.0). From the results, the average size of the grains in the dried is 262, 236, 172 and 109 nm for the aging temperature of room temperature, 50, 60 and 80^oC, respectively.
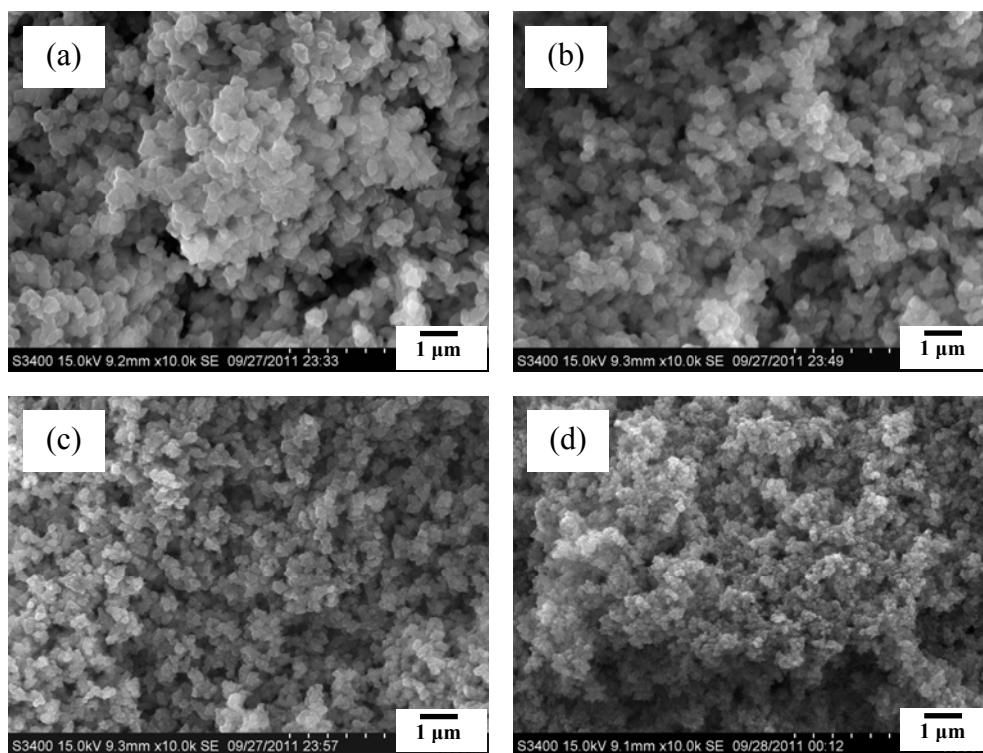
Figure 4.24 SEM micrographs of the Al(acac)$_3$/RF xerogels which were aged at room temperature (a), 50°C (b), 60°C (c) and 80°C (d).

To investigate the shape of carbonaceous material, the gel was pyrolyzed. The results shown in Figure 4.25 are consistent with the case of xerogel. The particle size decreases with the increasing aging temperature of the gel. At room temperature and $50^{o}C$, size of the pyrolyzed carbon particles is 202 and 182 nm, respectively. The particle size of around 97 nm is observed from the pyrolyzed gel aged at 60 and $80^{o}C$.
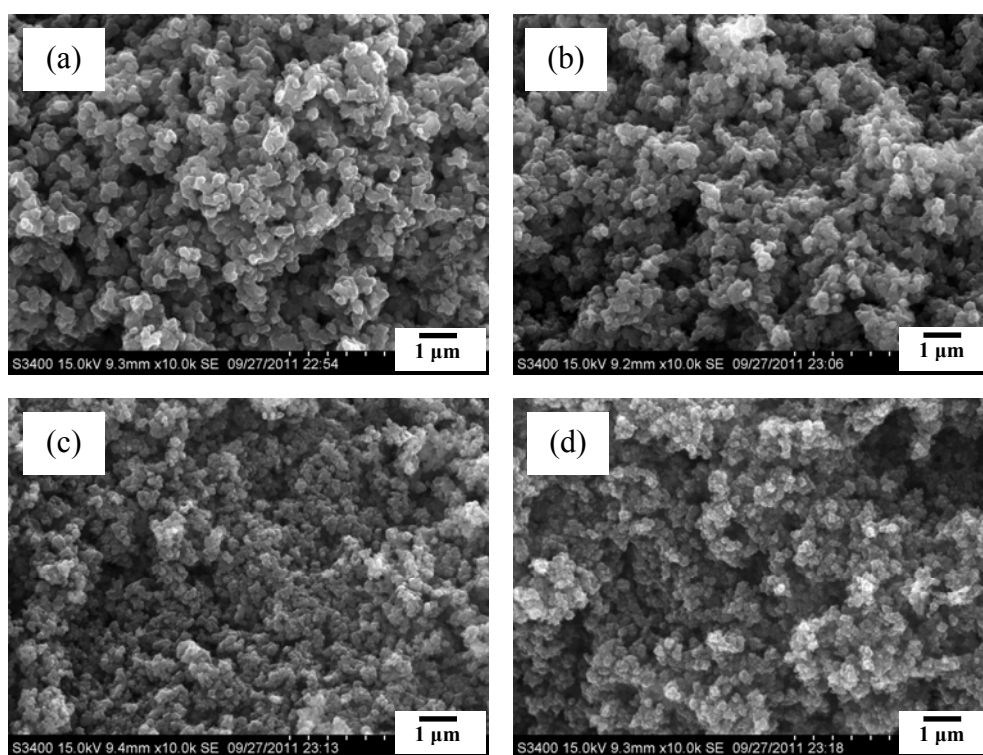
Figure 4.25 SEM micrographs of carbons from the pyrolyzed Al(acac)$_3$/RF xerogels which were aged at room temperature (a), $50^{o}C$ (b), $60^{o}C$ (c) and $80^{o}C$ (d).

After calcining at 1200°C, the alumina was formed as depicted in Figure 4.26. When the gel was aged at room temperature and 50°C, the particle sizes of alumina particles in both products are close to 85 nm. For the aging temperatures of 60 and 80°C, the alumina particle size is around 65 nm which is smaller than the products aged at lower temperature.
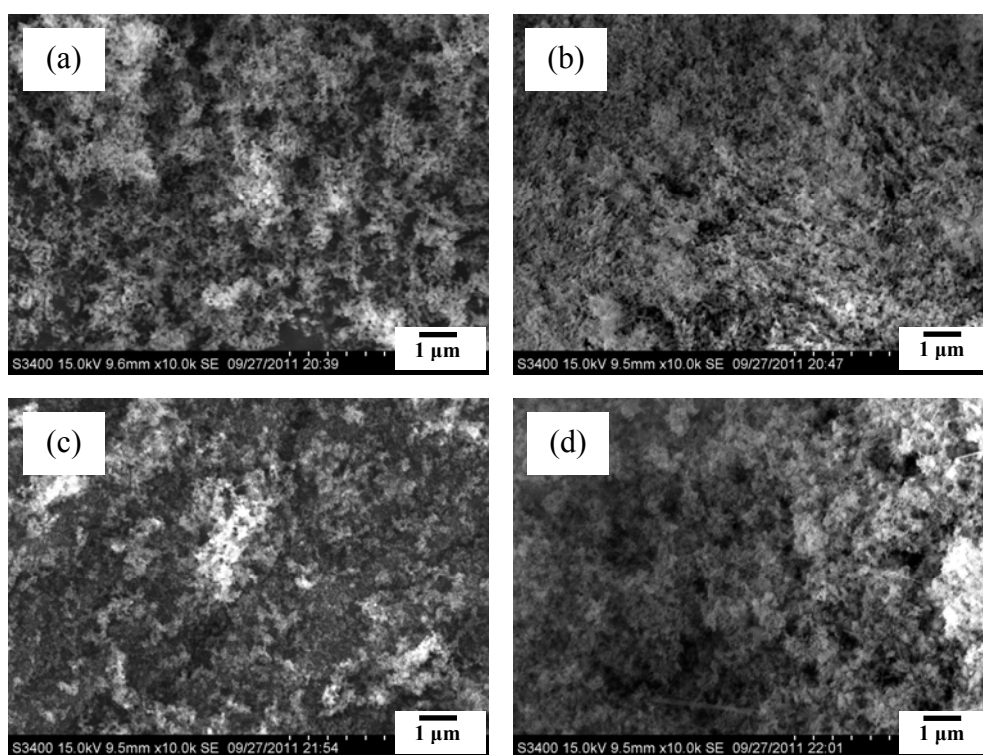
Figure 4.26 SEM micrographs of the alumina products from the Al(acac)$_3$/RF xerogels which were aged at room temperature (a), 50°C (b), 60°C (c) and 80°C (d), and then calcined at 1200°C.

The Al-EDX mapping of Al(acac)$_3$/RF xerogels aged at room temperature, 50, 60 and 80°C are shown in Figure 4.27. It is found that there is a good dispersion of alumina in the gel at all studied temperatures. The white dot in the images represented the aluminium atom, so it indicates that the Al(acac)$_3$ can react and disperse well in the RF gel. This was in a good agreement with the previous research that the AcacH can be used as a filler for improving the dispersion of metal on the catalyst support.
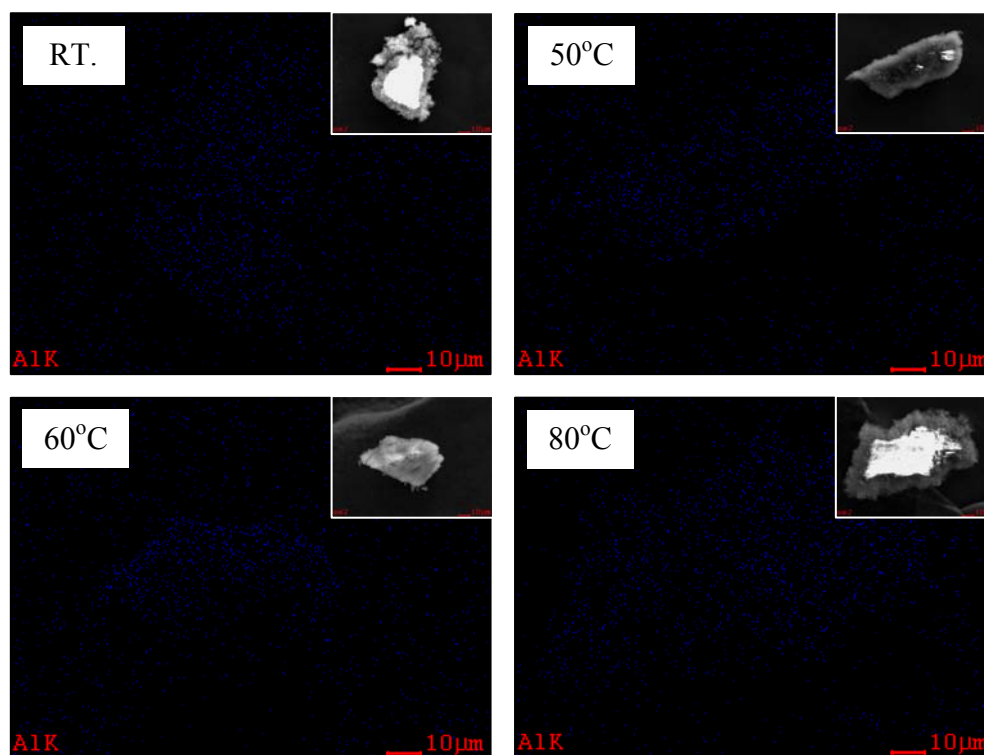
Figure 4.27 Aluminium-EDX mapping of the Al(acac)$_3$/RF xerogels which were aged at room temperature (a), 50°C (b), 60°C (c) and 80°C (d).

N$_2$ adsorption-desorption isotherms of the alumina products synthesized at various aging temperatures are shown in the Figure 4.28. The insets show corresponding pore size distribution. It could be seen that porosity of alumina products synthesized at various temperatures are significantly different. These graphs show the occurrence of Type IV isotherm with Type H3 hysteresis loop at high p/p$_0$ value for all aging temperatures. It is also found that N$_2$ uptake increases and therefore the pore volume is larger, when the aging temperature is increased. The pore volume is 0.044, 0.129, 0.237 and 0.291 cm^3/g for the samples aged at room temperature, 50, 60 and 80°C, respectively. Considering the pore size distribution, the pore size of alumina is in the mesopore range, i.e., 2-50 nm, with large pore diameter of 20-50 nm. The surface area of the alumina product is 67.2, 68.7, 47.8 and 18.8 m^2/g for the product aged at 80, 60, 50°C and room temperature, respectively. Thus, the aging temperature affects the alumina product surface. The largest surface area achieved is 68.7 m^2/g even though the alumina is calcined at high temperature of 1200°C.
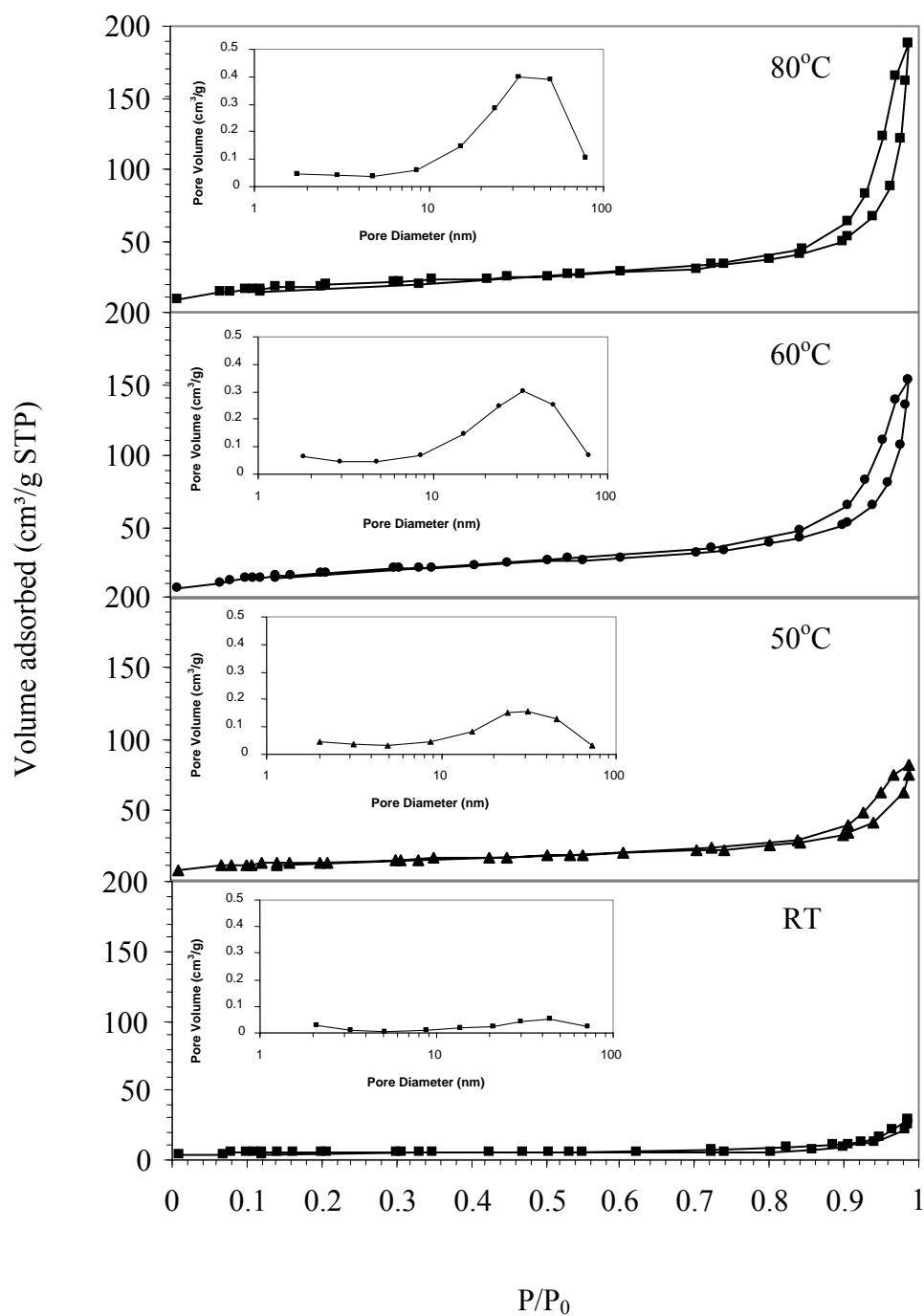
Figure 4.28 N$_2$ adsorption-desorption isotherms and pore size distributions of the alumina products from the Al(acac)$_3$/RF xerogels which were aged at various temperatures and then calcined at 1200°C.

Phase transitions of product synthesized at the calcination temperatures of 600 and 1200°C are shown in Figures 4.29 and 4.30, respectively. Considering both calcination temperatures, the phase transitions were monitored for the sample aged for 40 hours and 3 days.

After being calcined at 600°C, XRD patterns reveal that γ phase is obtained when the gel is aged for 40 hours at room temperature, 50 and 80°C, but, amorphous phase is observed for the sample aged at 60°C. For the gel aged for 3 days, γ phase is also obtained from the gel aged at the temperature of 50°C. On the other hand, the amorphous phase is detected when the gel is aged at room temperature and 80°C. Interestingly, there are two strong peaks at 2θ of 38.68 and 49.04 that could not be easily assigned to a specific phase of alumina.

For the samples calcined at 1200°C, XRD patterns show that the pure phase of α alumina is obtained only when the gel is at room temperature, regardless of the aging time. The rest of the samples are α alumina mixed with γ alumina. The content of each phase depends upon the combination of aging temperature and time. For the samples being aged for 40 hours at temperature of 50 and 80°C, it is obvious that the majority phase is α alumina with the trace of γ alumina. On the contrary, at the aging temperature of 60°C, the majority phase is γ alumina with slight trace of α alumina. After aging the gel for 3 days, the pure α alumina phase is obtained when the gel aging is performed at room temperature. For 50°C of aging temperature, the majority phase is α alumina and there is a small amount of γ alumina phase. In contrast, it is apparent that the high formation of γ alumina with a trace of α alumina is obtained at both aging temperatures of 60 and 80°C.
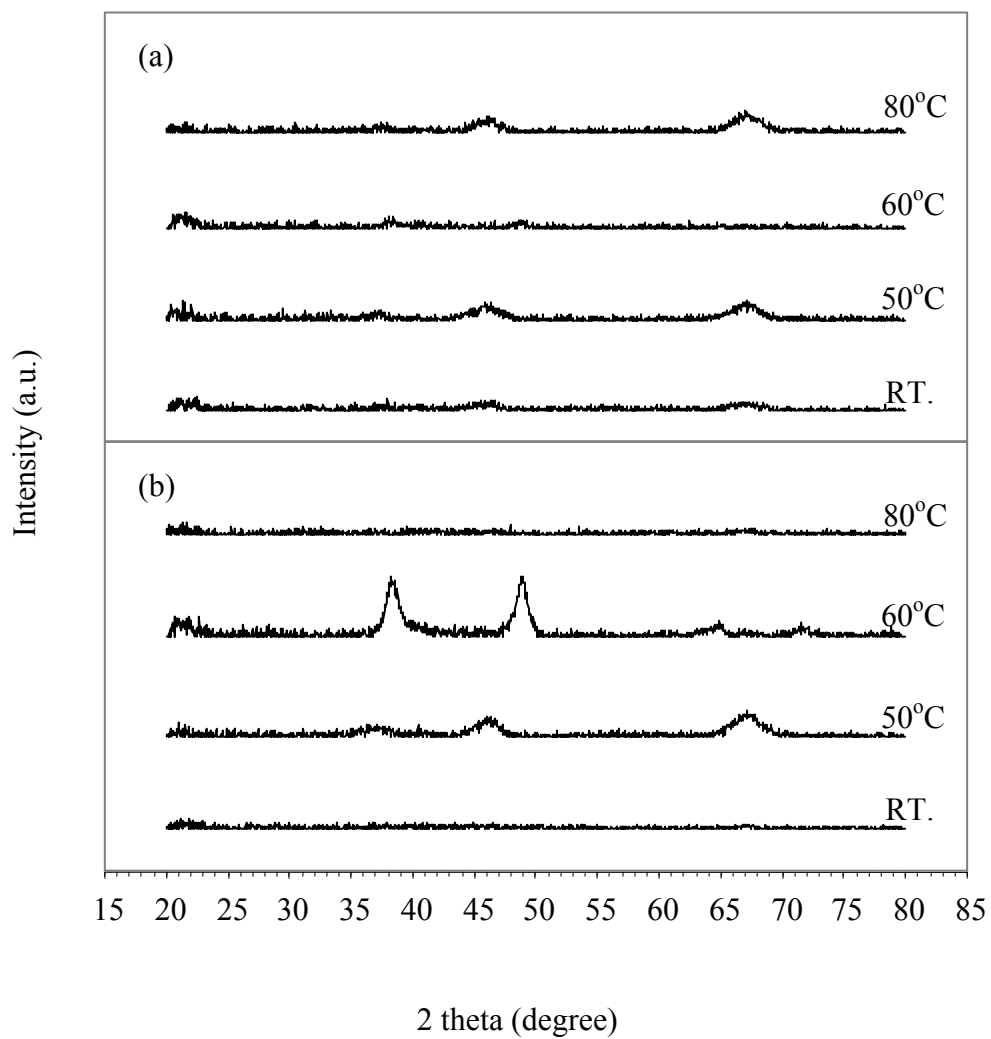
Figure 4.29 XRD patterns of the alumina products from the Al(acac)$_3$/RF xerogels which were aged for 40 hours (a) and 3 days (b) at various temperatures and then calcined at at 600°C.
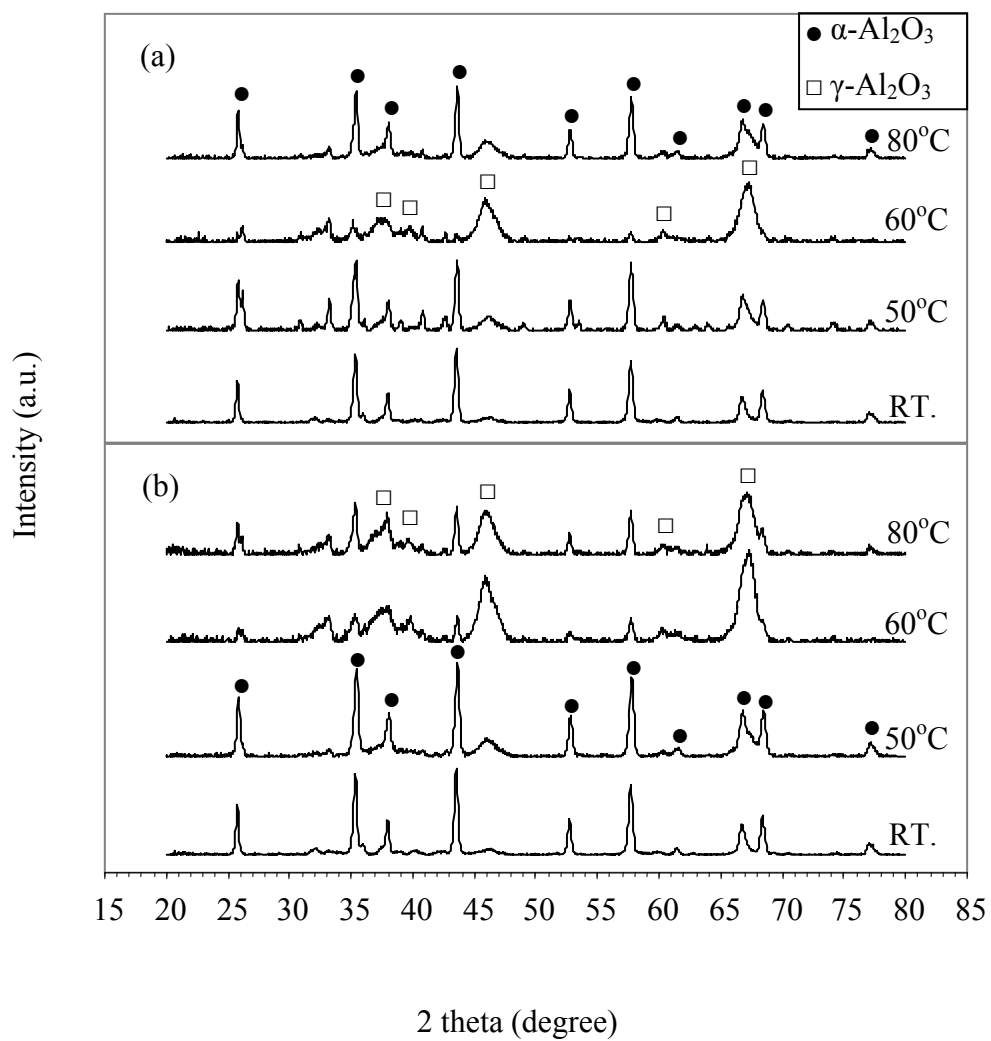
Figure 4.30 XRD patterns of the alumina products from the Al(acac)$_3$/RF xerogels which were aged for 40 hours (a) and 3 days (b) at various temperatures and then calcined at 1200°C.

The chemical properties of the Al(acac)$_3$/RF xerogels aged at various times were investigated by FTIR analysis, as shown in Figure 4.33. The IR spectra were monitored in the range of 1750-650 cm^{-1}. The strong absorption peaks at 1611.9 and 1475.8 cm^{-1} are assigned to C-C bondings of aromatic ring stretching vibration and methylene bridge (-CH$_2$-) stretching vibration. A degree of linkage, namely polymerization degree, is represented by the intensity ratio of the methylene bridge stretching to the aromatic ring stretching. It is found that the linkage degree increases with the increase in aging temperature. The linkage degree is 0.94, 1.07, 1.05 and 1.17 when the aging temperature is room temperature, 50°C, 60°C and 80°C, respectively.
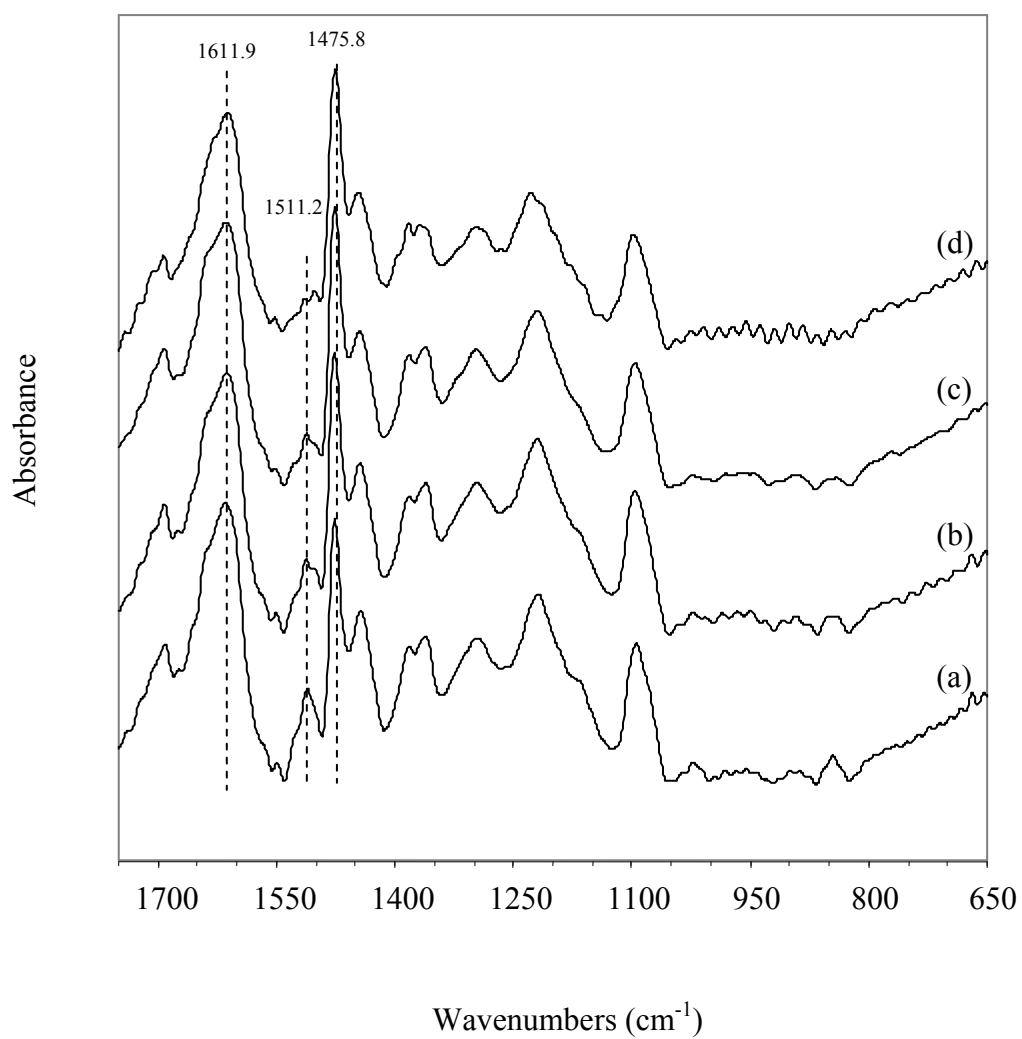
Figure 4.31 Deconvoluted FTIR spectra of Al(acac)$_3$/RF xerogels which were aged at room temperature (a), 50°C (b), 60°C (c) and 80°C (d).

4.4 Effect of Aluminium Content

In order to study the effect of the amount of aluminium precursor in the RF mixture, various molar ratios of aluminium acetylacetonate to resorcinol (A/R) were used, i.e. 0.005, 0.01, 0.05, 0.08 and 0.1. The $Al(acac)_3$/RF mixture was aged at room temperature in a closed system. After aging gel for 5 days, the sample gel was dried by the conventional drying process and then calcined at 1200^oC to obtain the white powder product. Many techniques were used to characterize the sample such as SEM, XRD and FTIR.

Figure 4.32 shows SEM micrographs of the $Al(acac)_3$/RF dried gel. The morphology of the gel significantly depends on the $Al(acac)_3$ content. As the $Al(acac)_3$ content is increased, the structure of the sample gel changes from collection of nano sphere through bicontinuous structure to particle aggregates. Analyzing the aggregated particle size by Semafore v.5 program, the average particle size of the $Al(acac)_3$/RF dried gel is 46, 66, 306, 616 and 937 nm when the sample gel is synthesized with A/R molar ratio of 0.005, 0.01, 0.05, 0.08 and 0.1, respectively. From these results, it could be seen that the aggregated particle size increases as the amount of the $Al(acac)_3$ precursor increases.
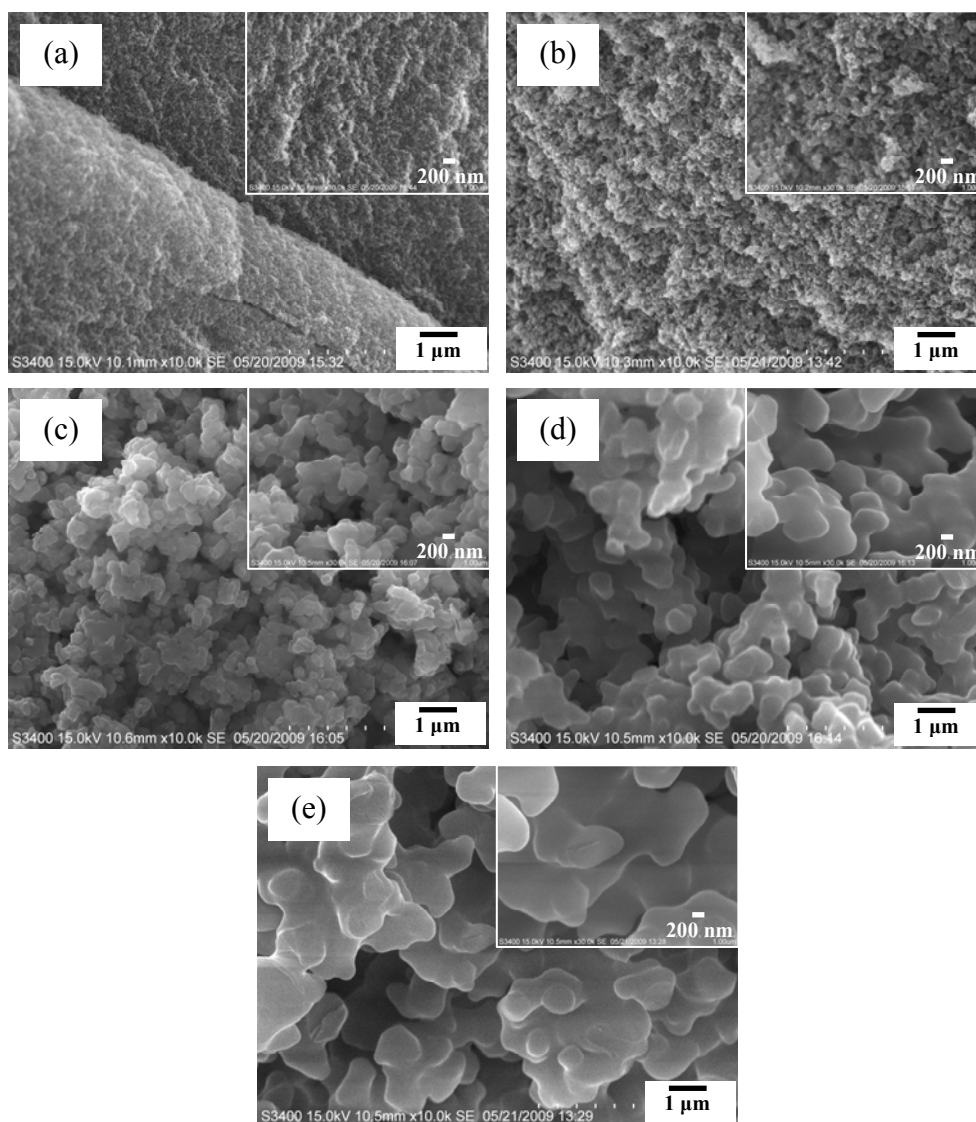
Figure 4.32 SEM micrographs of the Al(acac)₃/RF xerogels which were prepared using the aluminium contents (A/R molar ratio) of 0.005 (a), 0.01 (b), 0.05 (c), 0.08 (d) and 0.1 (e).

To obtain the white alumina product, the Al(acac)₃/RF gel was calcined at 1200°C. Morphologies and phase transitions of the calcined product are presented in Figures 4.33 and 4.34, respectively. It is observed that, unlike the dried gel, the

particle size of the calcined product is not significantly dependent on the content of aluminium precursor.
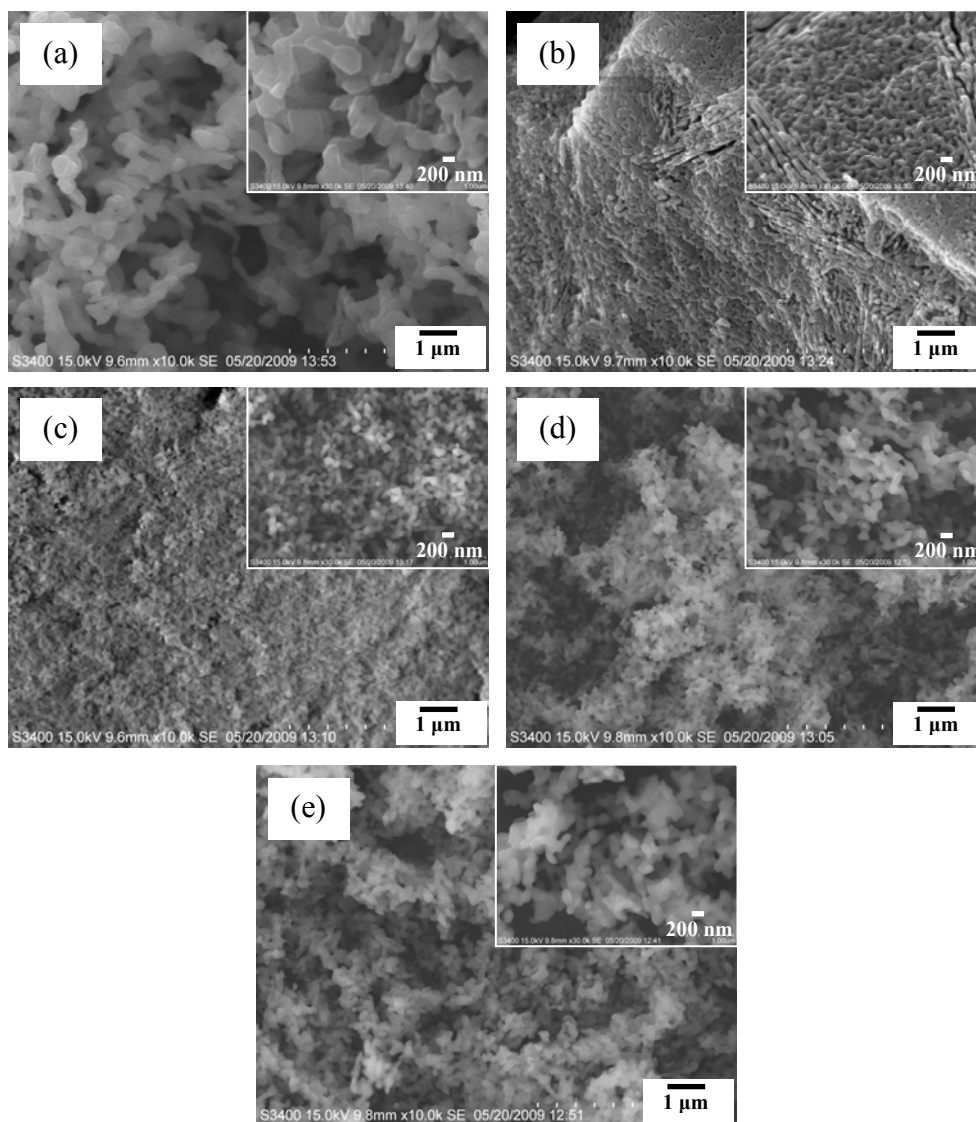
Figure 4.33 SEM micrographs of the alumina products which were prepared using the aluminium contents (A/R molar ratio) of 0.005 (a), 0.01 (b), 0.05 (c), 0.08 (d) and 0.1 (e) and calcined at 1200°C.

At the A/R molar ratio of 0.005, the obtained particle size is around 416 nm. The particle size is steeply reduced to 127 nm when the molar ratio is slightly increased to 0.01. However, the results from XRD analysis show that the calcined products synthesized with A/R ratio of 0.005 and 0.01 are not the alumina, but it may be sodium aluminate powder. This is believed that the aluminium atoms loaded into the RF mixture are not enough to create the alumina (Al_2O_3) product as seen in Figures 4.34 (a) and (b).
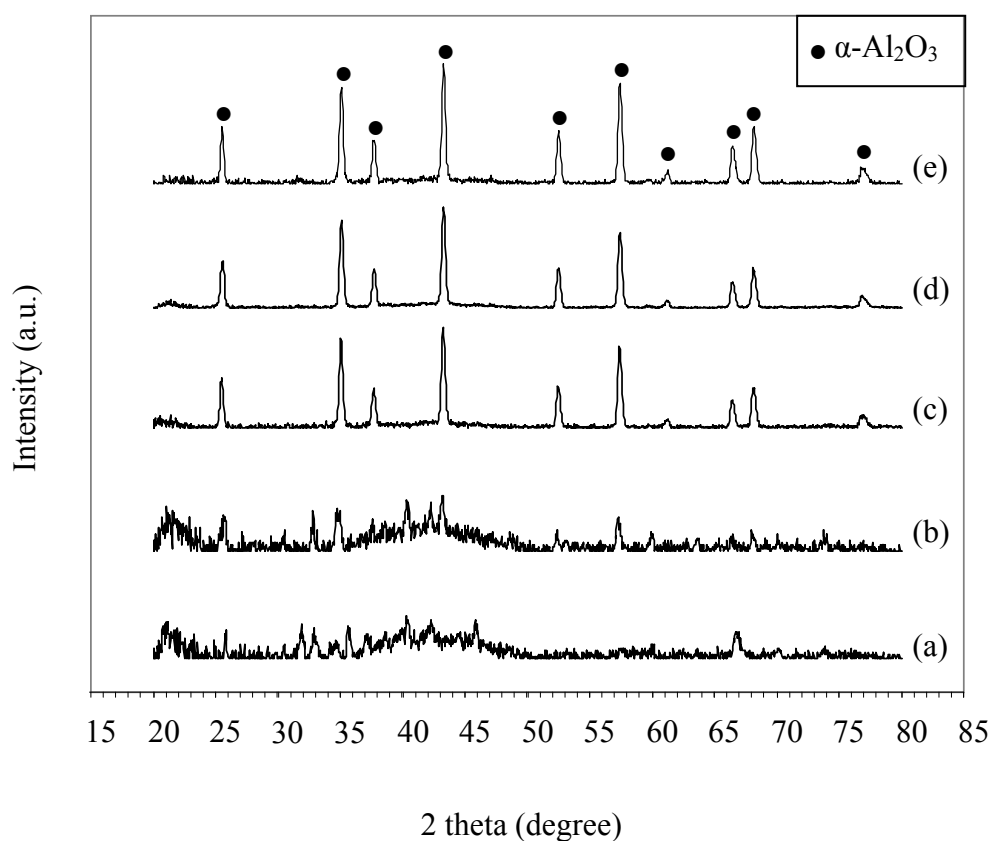
Figure 4.34 XRD patterns of the calcined products from the $Al(acac)_3$/RF gels aged for 5 days which were prepared using the aluminium contents (A/R molar ratio) of 0.005 (a), 0.01 (b), 0.05 (c), 0.08 (d) and 0.1 (e).

FTIR spectra of the Al(acac)$_3$/RF gels produced using various contents of aluminium precursor are shown in Figure 4.35. The characteristic absorption bands of RF structure are observed at 1615.7 cm^{-1} due to aromatic ring stretching vibration, at 1508.9 cm^{-1} caused by C=C aromatic ring vibration, at 1475.8 cm^{-1} from methylene bridge between aromatic ring and at 1382.6 cm^{-1} due to –OH in plane bending vibration. Moreover, the signals for methylene ether bridge between aromatic rings at 1095.6 cm^{-1} and aliphatic hydroxyl vibration at 1021.3 cm^{-1} are detected, while the strong absorption band at 1693.2 cm^{-1} is also observed which is corresponding to the stretching vibration of C=O group (keto form of AcacH ligand) bonded with hydroxyl group by hydrogen bonding. From these results, it is clear that the Al(acac)$_3$ in the RF gel catalyzes the polycondensation of RF gel. The observed degree of linkage is increased, corresponding to the increased intensity ratio of bridge vibration to aromatic ring vibration, with increasing the Al(acac)$_3$ content.
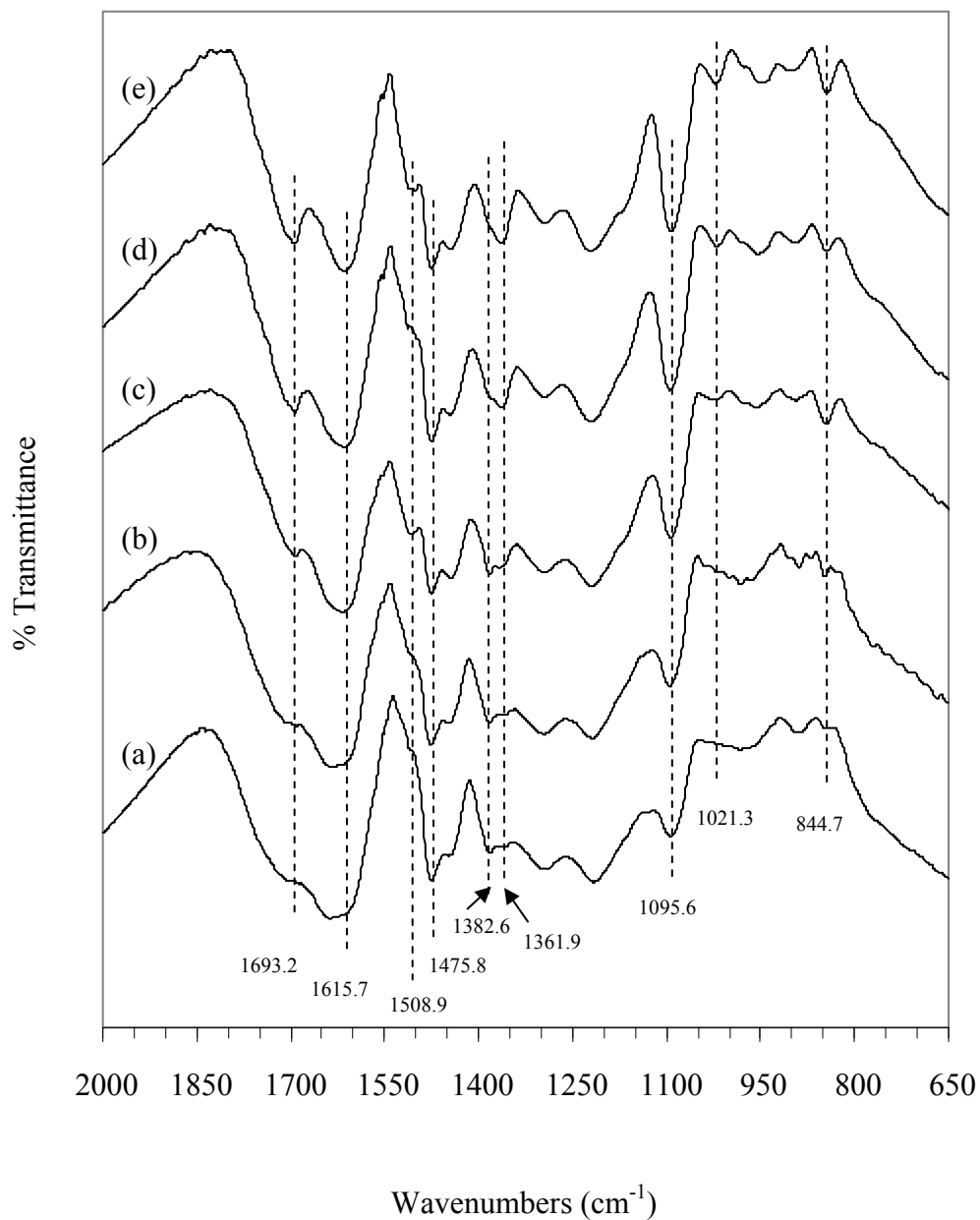
Figure 4.35 FTIR spectra of the Al(acac)$_3$/RF gels aged for 5 days which were prepared using the aluminium contents (A/R molar ratio) of 0.005 (a), 0.01 (b), 0.05 (c), 0.08 (d) and 0.1 (e).

4.5 Effect of Type of Catalyst Employed in RF Gel

To investigate the effect of the catalyst employed in RF gel, several types of catalyst such as acetic acid, ascorbic acid, formic acid, nitric acid, oxalic acid, sodium carbonate and tartaric acid were used to catalyze the polymerization of RF gel in the system of $Al(acac)_3$/RF mixture.

Considering this effect on the morphology of the gained alumina, the products calcined at $1200^{o}C$ were analyzed by SEM technique. The images are shown in Figure 4.36. It is found that there is a slight difference in shape for all employed catalysts. The smallest particle size of the alumina product, which is 116 nm, is achieved from the system using sodium carbonate as the catalyst.

From these results, it could be concluded that the type of catalyst does not affect the shape of the calcined alumina product. However, the suitable catalyst for alumina production at high temperature is sodium carbonate due to a small size of alumina grains obtained.
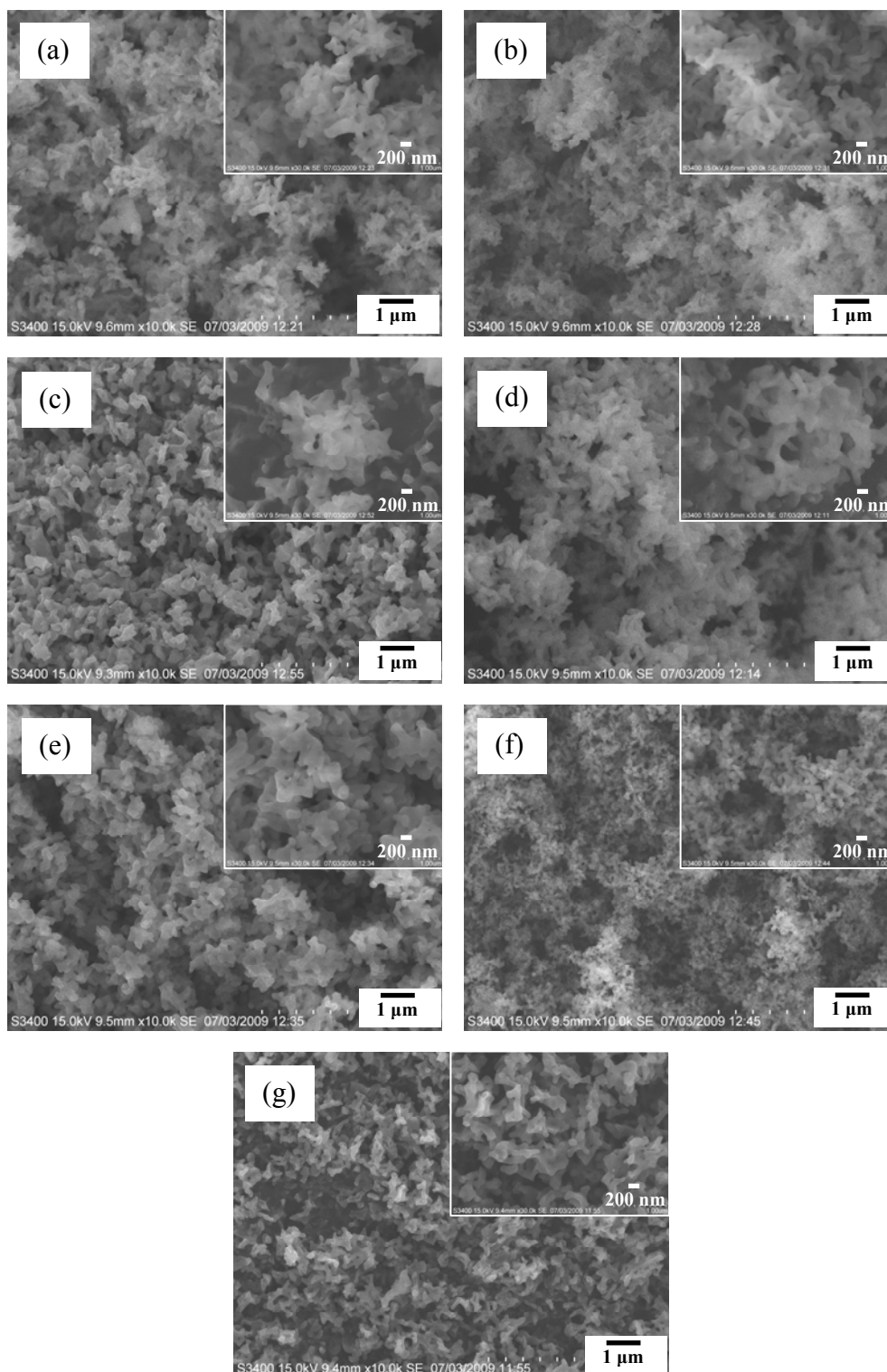
Figure 4.36 SEM micrographs of the alumina products from the Al(acac)$_3$/RF gels catalyzed by acetic acid (a), ascorbic acid (b), formic acid (c), nitric acid (d), oxalic acid (e), sodium carbonate (f) and tartaric acid (g).

Figure 4.37 shows N_2 adsorption-desorption isotherms of the alumina products prepared from Al(acac)$_3$/RF gels with different types of catalysts. It is found that all products, except the one catalyzed by sodium carbonate, seem to be a nonporous structure with surface area of 5.85, 7.13, 10.34, 11.90, 11.02 and 13.70 m^2/g and pore volume of 0.0074, 0.0186, 0.0136, 0.0197, 0.0232 and 0.0279 cm^3/g for the sample catalyzed by ascorbic acid, oxalic acid, nitric acid, tartaric acid, formic acid and acetic acid, respectively. However, the pore size distribution shown as the inset reveals that there is small number of pores in the alumina product with the pore size diameters in the range of 20-70 nm.

As catalyzed by sodium carbonate, isotherm of the obtained alumina exhibited in Type IV with H3 hysteresis loop, which suggests the mesoporosity nature of the product. High surface area and pore volume comparing to those of other samples, which are 26.89 m^2/g and 0.0748 cm^3/g, respectively, are gained even after calcining at 1200°C, as seen in the Figure 4.37 (a).

Phase transitions of the alumina products calcined at 1200°C are shown in Figure 4.38. It is found that XRD patterns of all products, except the case using sodium carbonate, exhibit a pure phase of α alumina. When sodium carbonate is using, α phase with a small amount of γ phase is observed.
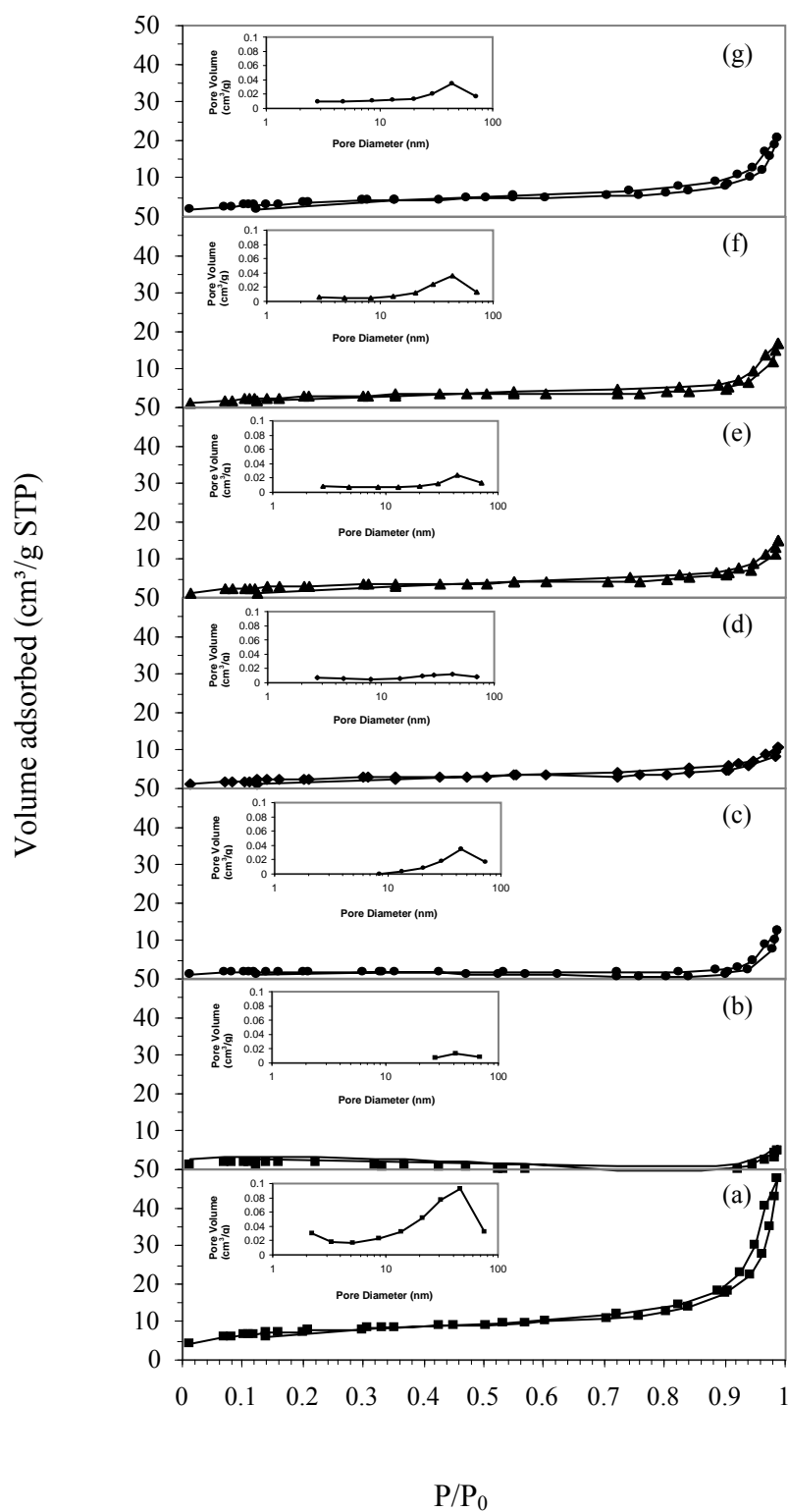
Figure 4.37 N$_2$ adsorption-desorption isotherms of the alumina products prepared from the Al(acac)$_3$/RF gels catalyzed by sodium carbonate (a), ascorbic acid (b), oxalic acid (c), nitric acid (d), tartaric acid (e), formic acid (f) and acetic acid (g).
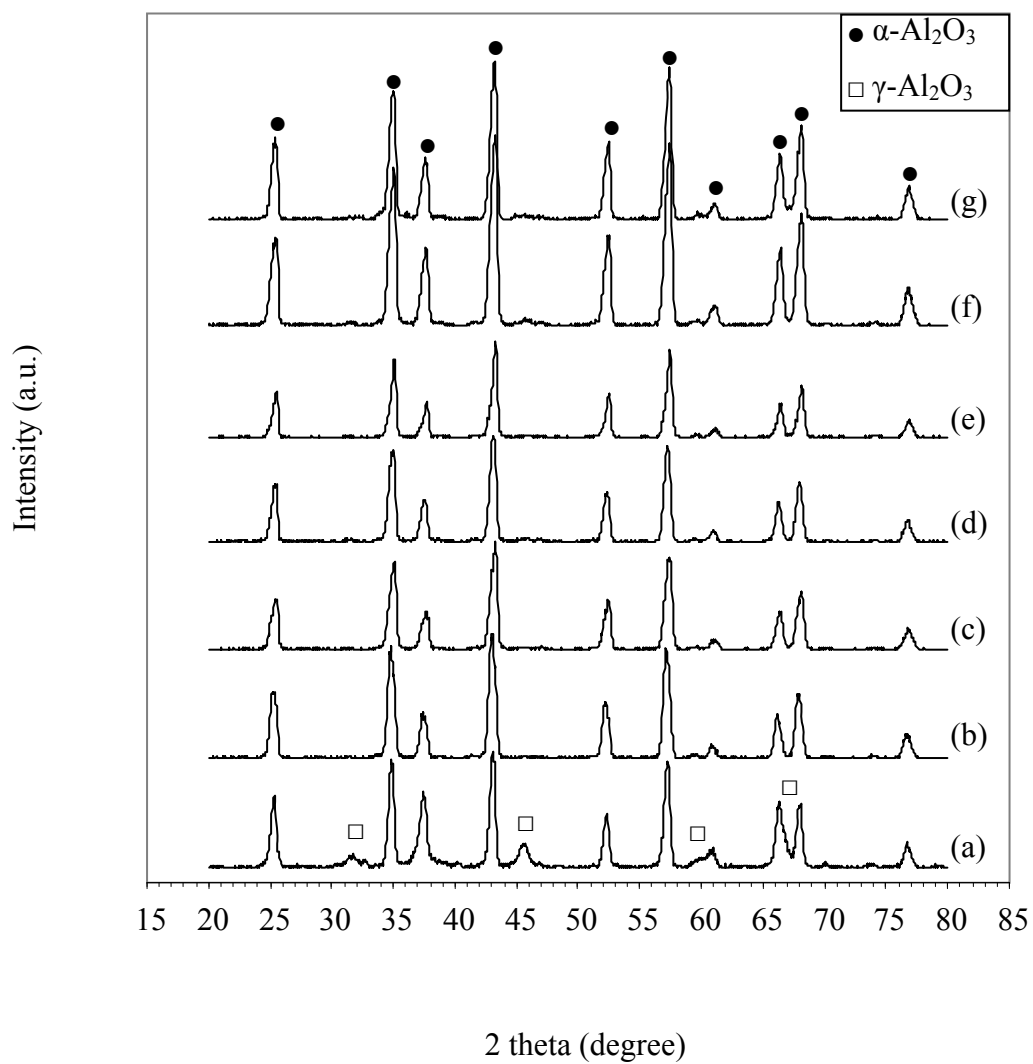
Figure 4.38 XRD patterns of the alumina products prepared from the Al(acac)₃/RF gels catalyzed by sodium carbonate (a), ascorbic acid (b), oxalic acid (c), nitric acid (d), tartaric acid (e), formic acid (f) and acetic acid (g).

For chemical property analysis, FTIR spectra were obtained in the range of 1750-650 cm^{-1}. Various catalysts, i.e. sodium carbonate, ascorbic acid, oxalic acid, nitric acid, tartaric acid, formic acid and acetic acid, were added into RF mixture and aged for 5 hours. The products were consequently collected and analyzed by FTIR method as shown the spectra in Figure 4.39. All sample gels show all main absorption peaks including peak at 1619.3 cm^{-1} corresponding to aromatic ring stretching, at 1407.4 cm^{-1} due to –OH in plane bending, and at 1694.0 cm^{-1} referring to C=O bonded with -OH by hydrogen bonding. A peak shoulder at 963.2 cm^{-1} indicates the presence of unsubstituted resorcinol while a peak at 977.8 cm^{-1} appears due to substituted aromatic ring. It could be explained that reactions, which produce the resorcinol derivative and generate the initial gel network, take place. Moreover, a peak at 1472.0 cm^{-1} indicating the formation of methylene bridge vibration between aromatic rings is also observed.

After aging the gel for 72 hours, the FTIR spectra were investigated again as shown in Figure 4.40. All important peaks which are previously discussed are observed as well. However, the absence of the unsubstituted resorcinol band at 963.2 cm^{-1} indicates the complete of the reaction. Only a peak at 977.2 cm^{-1} attributing to the substituted benzene ring is found. Furthermore, the spectra of absorption band at 1475.1 and 1086 cm^{-1} are presented. It is clear that there is a progress in the polycondensation to form the methylene and methylene ether bridges.

From these results, it could be concluded that the type of catalyst does not affect the overall reactions because all catalysts could catalyze the polycondensation to form the methylene and methylene ether linkages between aromatic rings and produce water as a by-product. However, there is slightly difference in the amount of water formed, as indicated by the intensity of spectra at 1649.8 cm^{-1}.
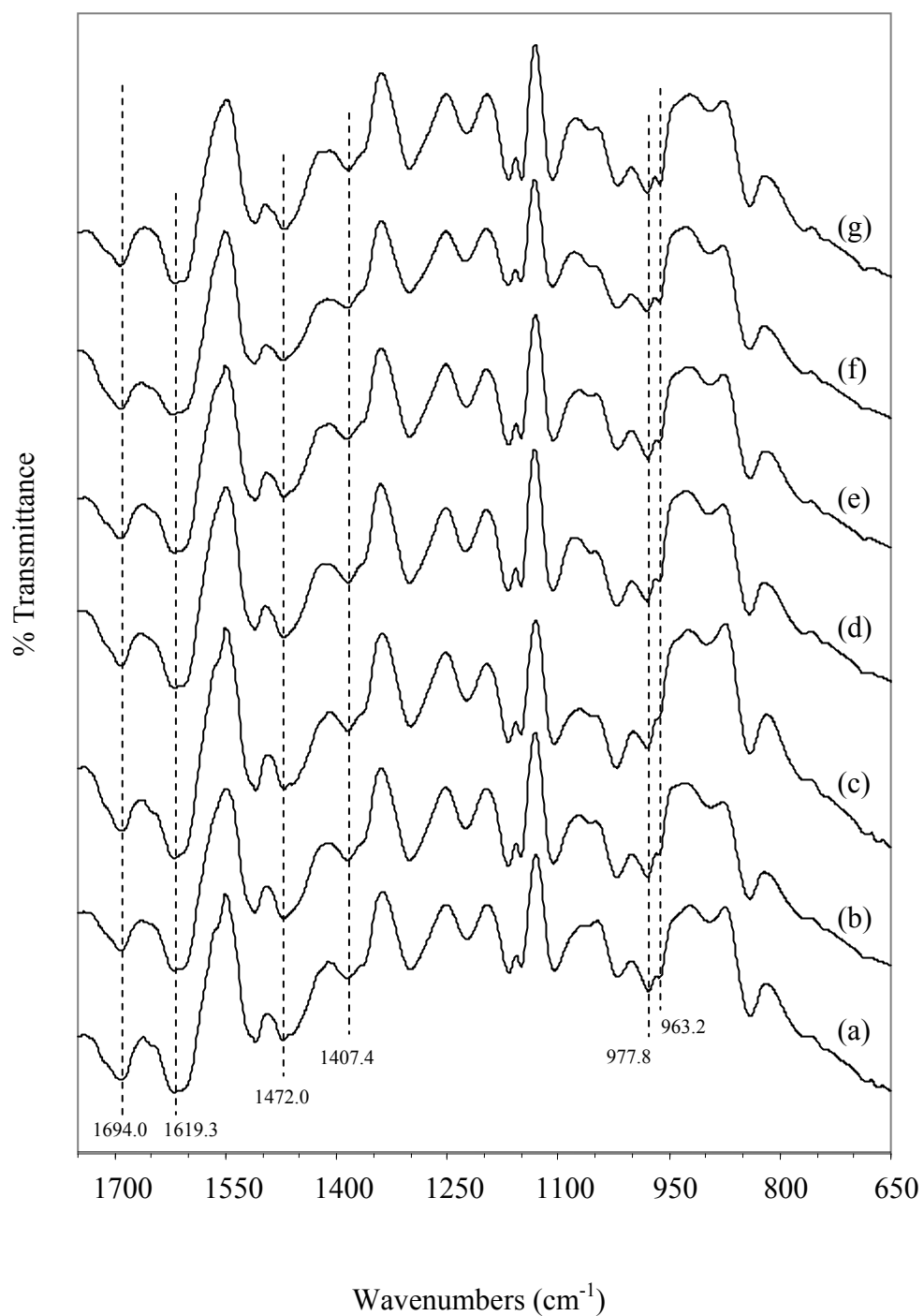
Figure 4.39 FTIR spectra of the Al(acac)$_3$/RF gels for 5 hours catalyzed by sodium carbonate (a), ascorbic acid (b), oxalic acid (c), nitric acid (d), tartaric acid (e), formic acid (f) and acetic acid (g).
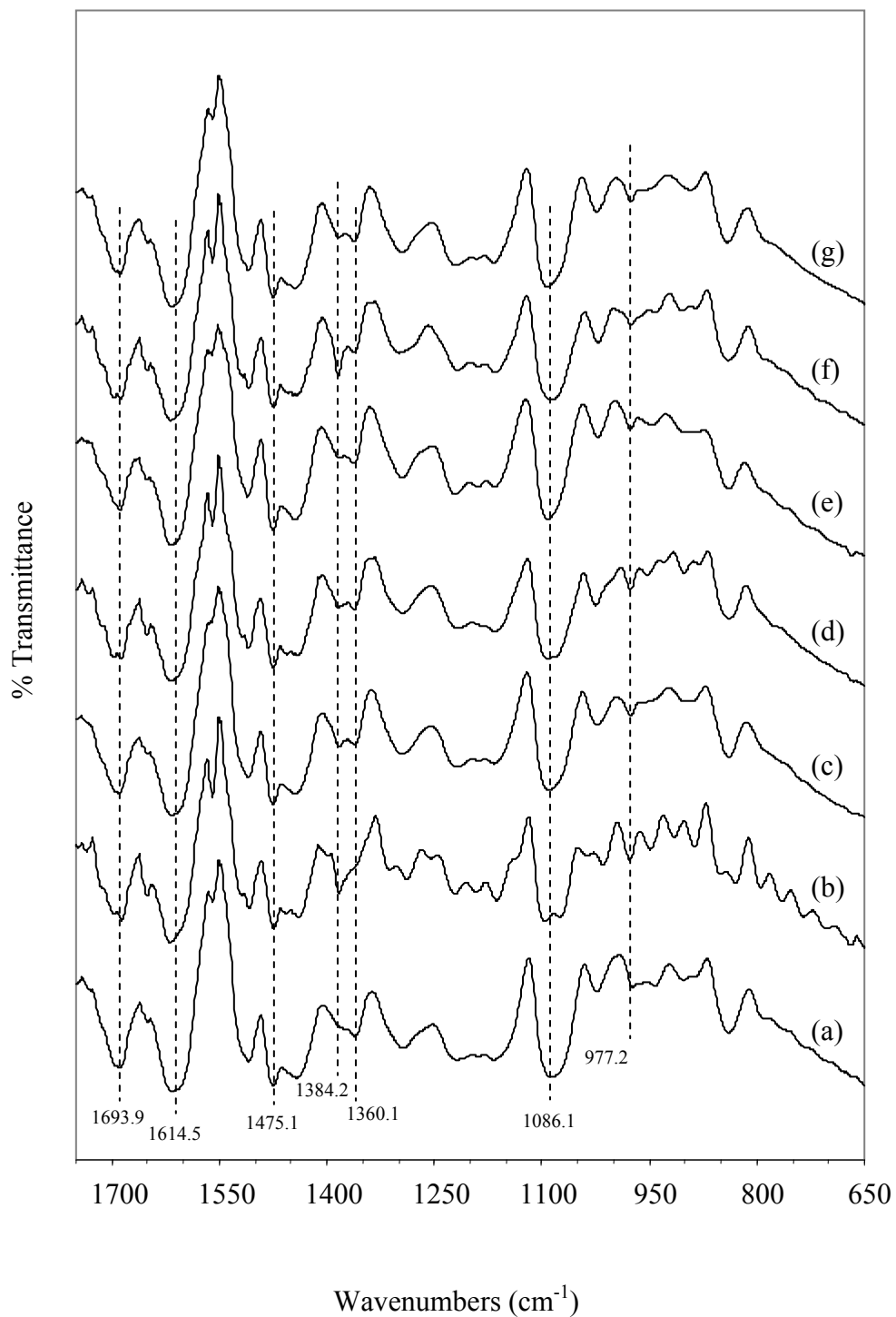
Figure 4.40 FTIR spectra of the Al(acac)$_3$/RF gels for 72 hours catalyzed by sodium carbonate (a), ascorbic acid (b), oxalic acid (c), nitric acid (d), tartaric acid (e), formic acid (f) and acetic acid (g).

4.6 Effect of Type of Aluminium Precursor

To investigate the effect of the aluminium precursor type in RF gel, several types of precursors such as aluminium acetylacetonate (Al(acac)$_3$), aluminium acetate and aluminium nitrate were used as an aluminium source in Al/RF gel.

Morphologies of products after calcining at 1200°C were investigated by SEM technique as shown the images in Figure 4.41. It was found that the shape of product significantly depends on the type of aluminium precursor. For aluminium acetylacetonate, the shape of alumina product was observed as worm-like structure having size of 121 nm. With aluminium acetate, the alumina product was found as aggregated particle with particle size of 230 nm approximately. Moreover, the sheet shape of alumina, with size around 950 nm, was obtained when aluminium nitrate was used as the aluminium source.

From these results, it could be concluded that the type of aluminium precursor affects the morphology of alumina product. The size of alumina synthesized from aluminium acetylacetonate was smaller than those synthesized from aluminium acetate and aluminium nitrate. Porous properties, phase transformation of alumina product and also the chemical properties of the sample gels were investigated in the next topic.
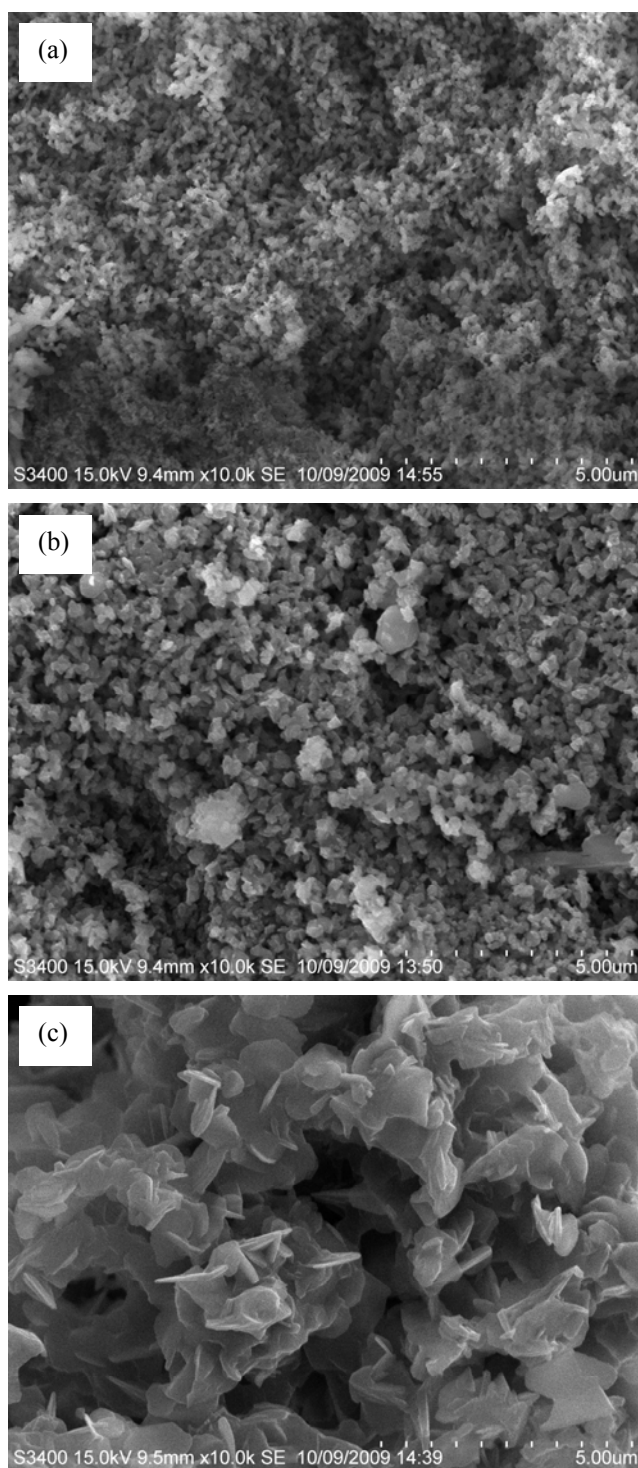
Figure 4.41 SEM micrographs of the alumina products after calcining at 1200°C synthesized by using (a) aluminium acetylacetonate, (b) aluminium acetate and (c) aluminium nitrate precursor.

To explain the textural property of alumina prepared with various aluminium precursors, N_2 adsorption-desorption isotherms and pore size distributions on alumina product were plotted. Moreover, in order to investigate the effect of the calcination temperature on the evolution of textural property, the alumina product was calcined at various temperature in range of 900-1200°C.

Using aluminium acetylacetonate as an aluminium source, the N_2 sorption isotherm and pore size distribution of the synthesized alumina are shown in Figure 4.42. It was found that the nature of isotherm exhibits the characteristic of Type IV with H3 hysteresis loop for all calcination temperature. As shown in the shape of isotherm, there was a small slope at relative pressure from 0 to 0.05, which could be attributed to a broad pore size distribution in the micropore range. For a sharp slope at relative pressure from 0.8 to 0.98, this indicated the presence of mesopore with large pore diameter due to having a hysteresis loop. The pore size distribution showed that the alumina product has pore size in the range of 20-60 nm. By calcining at 1200°C, the surface area and pore volume of alumina product were 18.82 m^2/g and 0.0447 cm^3/g, respectively.

In the case that aluminium acetate was used as an aluminium precursors, the N_2 sorption isotherm and pore size distribution of alumina product were shown in Figure 4.43. It was found that the shape of isotherm is in Type IV with H3 hysteresis loop for calcining at 900-1100°C. It suggested that the obtained alumina is a mesoporous particle. It showed that the alumina product has a narrow pore size distribution in the range of 3-20 nm, but a wide pore size distribution in the range of 5-70 nm for calcinating at 1100°C is observed. Considering the shape of isotherm at calcination temperature of 1200°C, there was a small amount of N_2 uptake and the hysteresis loop was not present, indicating nonporous material. The surface area and pore volume of alumina product were 6.24 m^2/g and 0.0105 cm^3/g, respectively.

For using aluminium nitrate as an aluminium source, the N_2 sorption isotherm and pore size distribution of the synthesized alumina are shown in Figure 4.44. It was found that the shape of isotherm is similar to Type IV with H4 hysteresis loop for all

calcination temperatures. This could be implied that the obtained alumina is a mesoporous nature with wide pore distribution (2-70 nm), while its isotherm shape is slit-like shape. This result agreed with the result shown in SEM image (Figure 4.41(c)). The surface area and pore volume of alumina product were 27.90 m^2/g and 0.1207 cm^3/g, respectively.
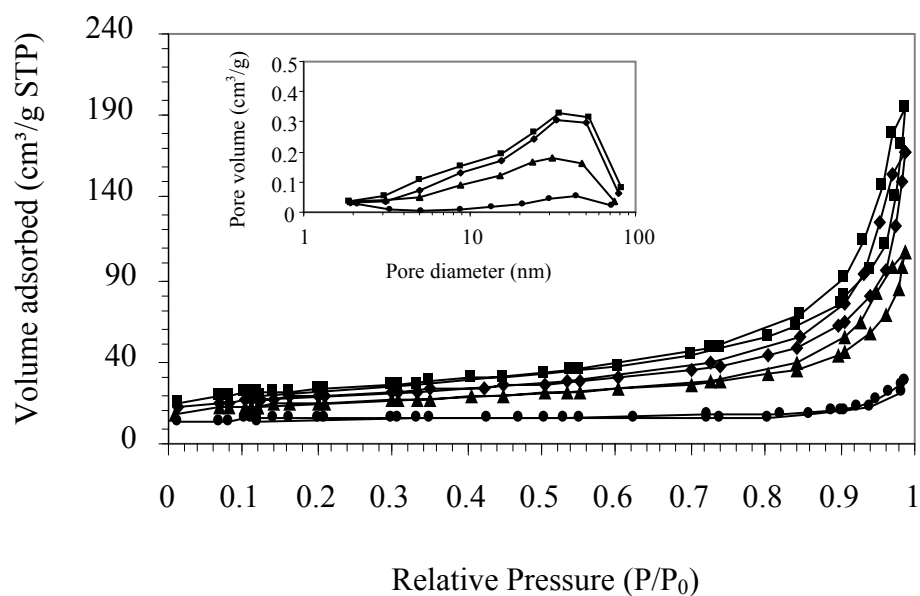
Figure 4.42 N$_2$ sorption of the alumina products synthesized by aluminium acetylacetonate precursor after calcining at 900-1200°C.
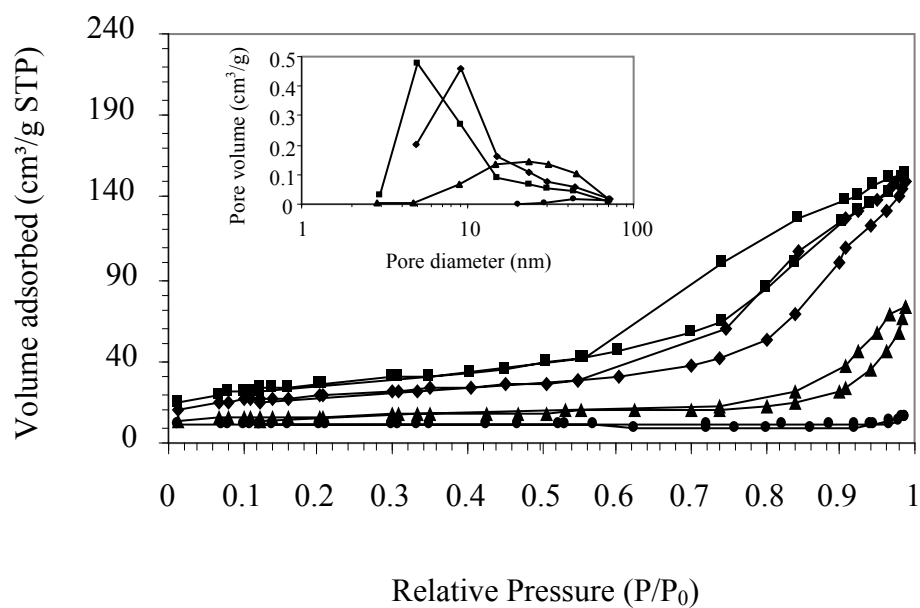
Figure 4.43 N_2 sorption of the alumina products synthesized by aluminium acetate precursor after calcining at 900-1200°C.
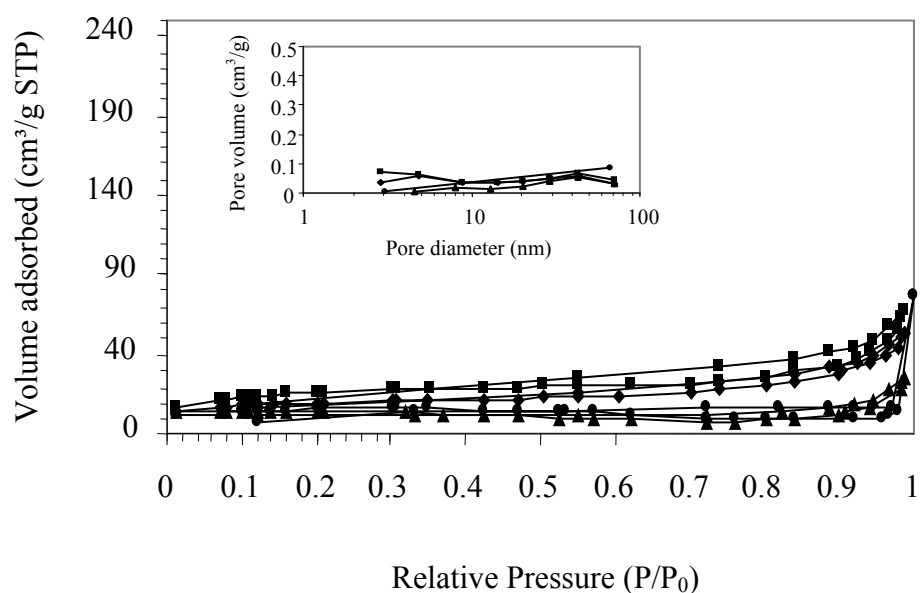
Figure 4.44 N_2 sorption of the alumina products synthesized by aluminium nitrate precursor after calcining at 900-1200°C.

Phase transitions and phase transformations of the alumina products at temperature in the range of 900 to 1200°C were investigated by XRD analysis.

XRD patterns of the alumina synthesized using aluminium acetylacetonate, aluminium acetate and aluminium nitrate as a precursor are shown in Figures 4.45, 4.46 and 4.47, respectively. For all cases, it was observed that the sequence of phase transformation starts with γ alumina and subsequently transforms to the thermodynamically stable phase, α alumina, at temperature around 1100°C. These results indicated that the major phase is α alumina and the minor phase is γ alumina. The intensity of γ phase of alumina was slightly different for each precursor, indicating the variation in retarding the transformation to α alumina. In case that aluminium acetylacetonate was used as aluminium precursor, its amount of γ phase was higher compared to other types of aluminium sources at temperature of 1100°C, while the complete transformation to α phase was obtained at 1200°C. These conditions were the desirable ones which the γ and α phase were maximized at 1100°C and 1200°C, respectively. It could be therefore concluded that the aluminium acetylacetonate is suitable for employing as a source of aluminium in high temperature synthesis.
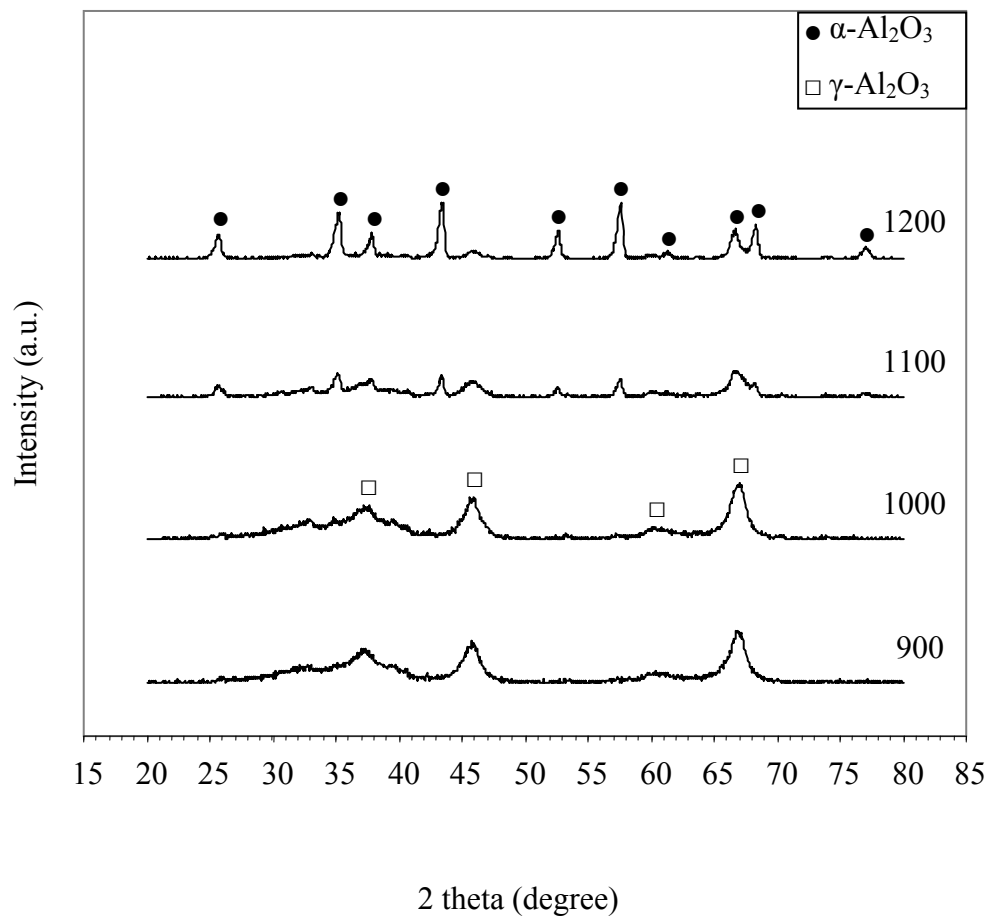
Figure 4.45 XRD patterns of the alumina products synthesized by aluminium acetylacetonate precursor after calcining at 900-1200°C.
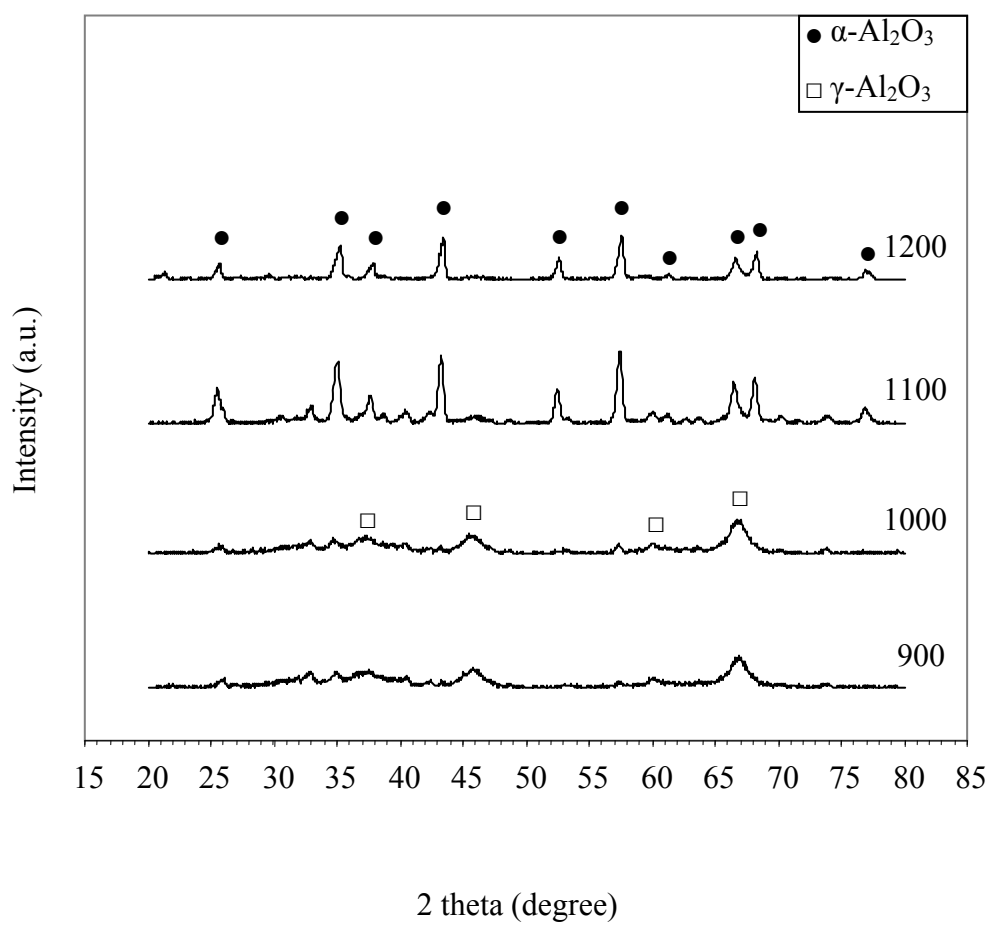
Figure 4.46 XRD patterns of the alumina products synthesized by aluminium acetate precursor after calcining at 900-1200°C.
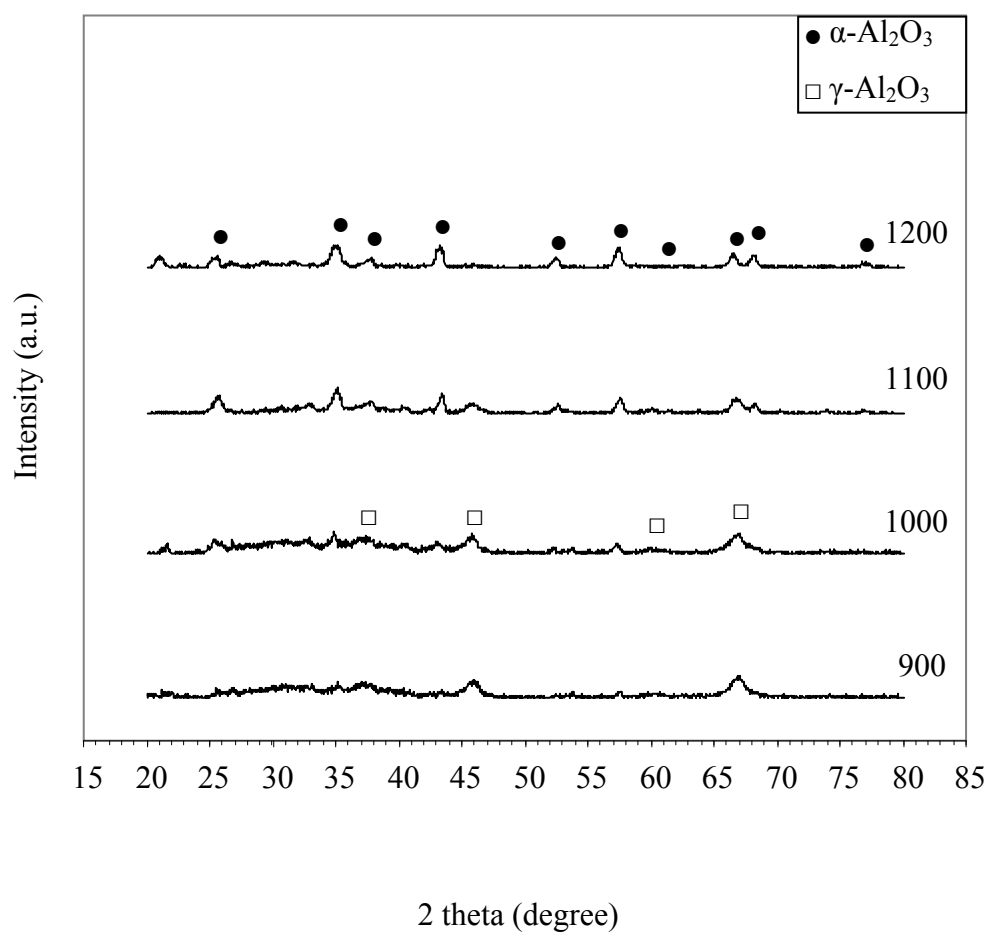
Figure 4.47 XRD patterns of the alumina products synthesized by aluminium nitrate precursor after calcining at 900-1200°C.

To evaluate the chemical bonding, the FTIR spectra ranging from 650 to 1750 cm^{-1} of aluminium acetylacetonate/RF gel, aluminium acetate/RF gel and aluminium nitrate/RF gel are shown in Figure 4.48, 4.49 and 4.50, respectively.
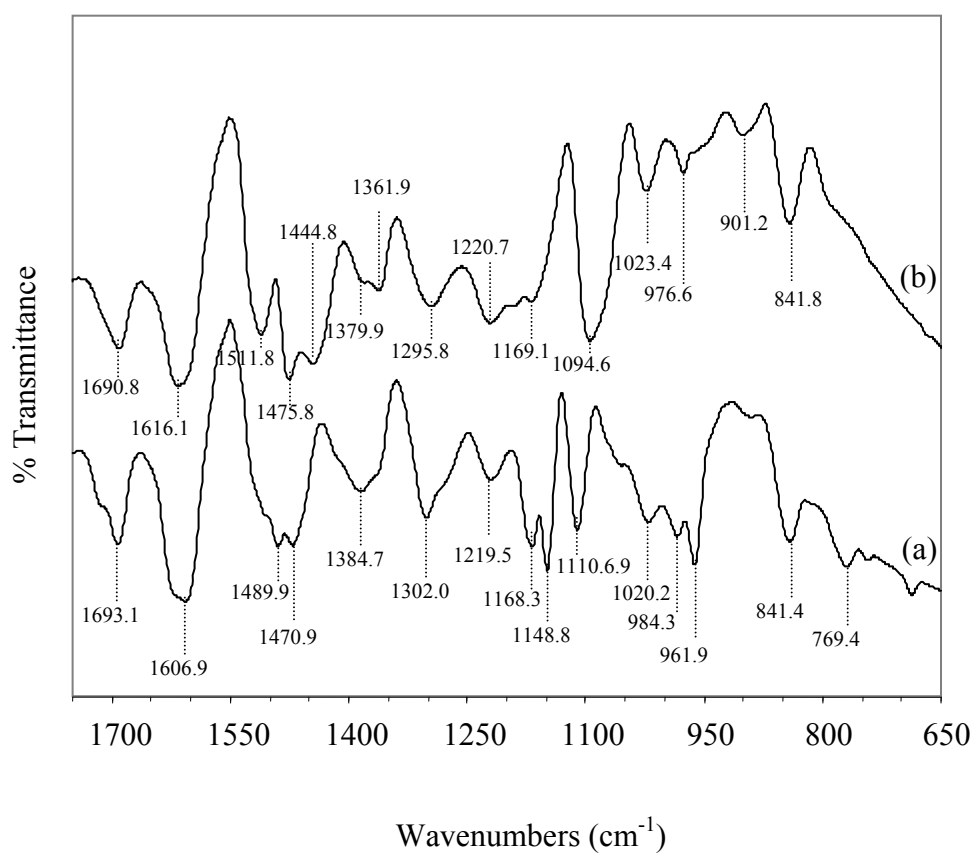
Figure 4.48 FTIR spectra of the aluminium acetylacetonate/RF gel aged at (a) 0 and (b) 3 days.
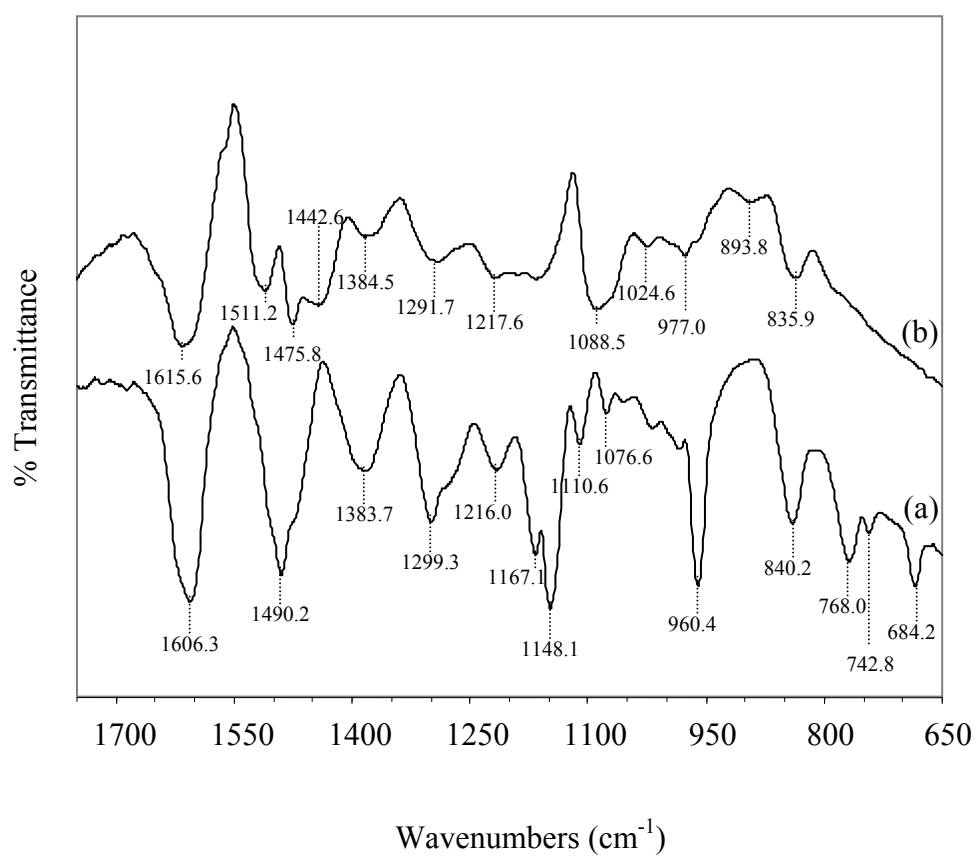
Figure 4.49 FTIR spectra of the aluminium acetate/RF gel aged at (a) 0 and (b) 3 days.
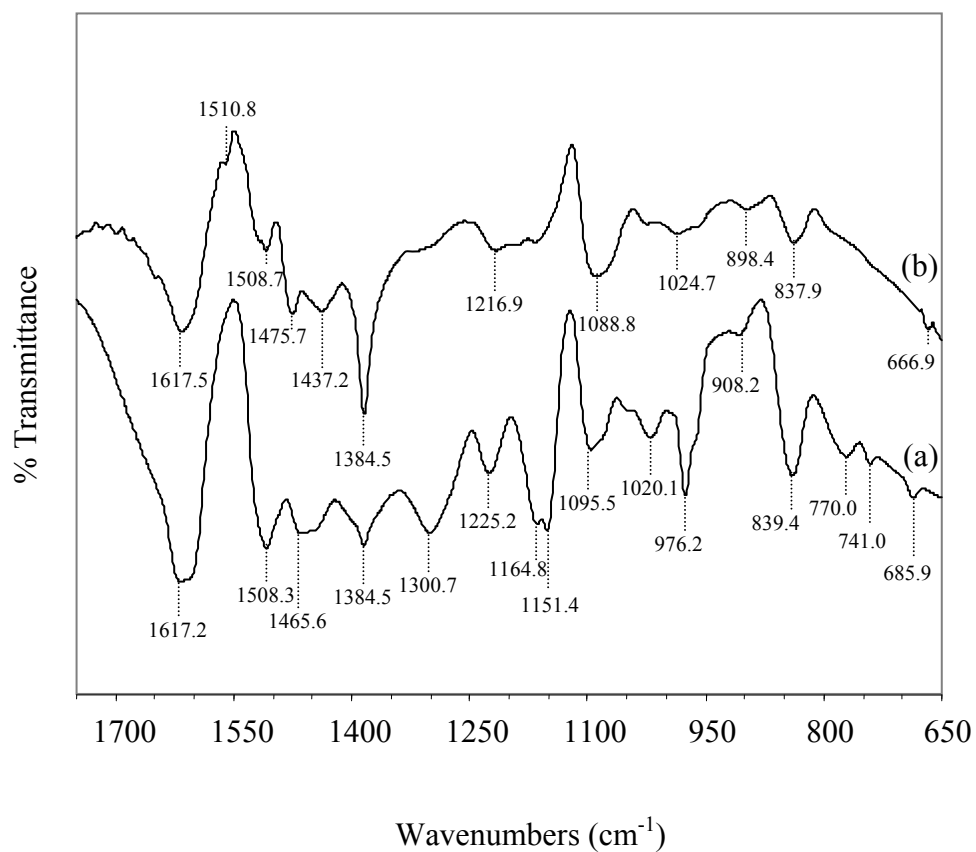
Figure 4.50 FTIR spectra of the aluminium nitrate/RF gel aged at (a) 0 and (b) 3 days.

4.7 Effect of Moisture Content on porosity of carbon derived from resorcinol-formaldehyde gel

Porous carbon derived from resorcinol-formaldehyde (RF) gel has been extensively studied because of its potential in various applications such as adsorbents, catalyst supports and electrode devices (Moreno-Castilla and Maldonado-Hódar, 2005). The preparation of such carbon is mainly consisted of the synthesis of RF gel, gel aging, drying and pyrolysis of the gel. In the drying step, although the conventional evaporative drying is commonly used to dry the RF gel (Job et al., 2004), significant reduction of the surface area and pore volume are often observed because of the pores collapses by capillary forces. Therefore, it is the aim of this research to investigate the effect of aging condition, i.e., the humidity, so that the gel can retain its porous structure during the conventional drying. This is a simple strategy to maintain the textural properties of the gel, comparing to other methods such as changing the gel composition (Al-Muhtaseb and Ritter, 2003, Léonard et al., 2008) or adding surfactant (Bruno et al., 2010).

For experimental procedure, the RF gel was prepared according to the method reported by Tonanon et al. (Tonanon et al., 2005). Briefly, resorcinol (9 g) and sodium carbonate (0.01 g) were dissolved in 10 ml of distilled water. Then, 12.5 ml of 37% formaldehyde aqueous solution with methanol as a stabilizing agent was added to the solution. After homogenizing, the mixture was aged under different level of humidity at 25°C for 3 days in a closed system. The relative humidity (RH) in the aging system was controlled to be 8%, 52.9%, 75.3% or 100% by placing an open container filled with silica gel, saturated solution of $Mg(NO_3)_2$, saturated solution of NaCl or water, respectively, into the aging chamber (Soykeabkaew et al., 2004). After aging, the obtained RF gels were dried at 110°C in a conventional oven for 24 h. For the pyrolysis, the dried RF xerogels were heated from room temperature to 250°C at a constant heating rate of 10°C/min under N_2 flow and kept at that temperature for 2 h. Then, the temperature was raised to 750°C using the same heating rate and maintained at 750°C for 4 h. The textural and microstructural properties of the samples were analyzed by N_2 sorption analysis and scanning electron microscope.

The chemical functional groups within the gel were also analyzed by Fourier-transform infrared spectroscopy. The Fourier self-deconvolution was applied to enhance resolution of peaks.

Micrographs in Figure 4.51 clearly show that the humidity level in the aging of the RF gel significantly affects morphology of the carbon products. Although the morphology of the products aged at 52.9% and 75.3% RH is similar to the conventional RF-derived carbon xerogel reported in literature that was aged in uncontrolled atmosphere (Al-Muhtaseb and Ritter, 2003), the carbon gels synthesized from the RF gel aged in low humidity, i.e. 8% RH, appears nonporous. On the other hand, when the humidity of the aging atmosphere was saturated, highly porous product with surface area of 564 m^2/g was obtained. It should be noted that the surface area of this product is comparable to those obtained by using freeze drying (Tonanon et al., 2005).
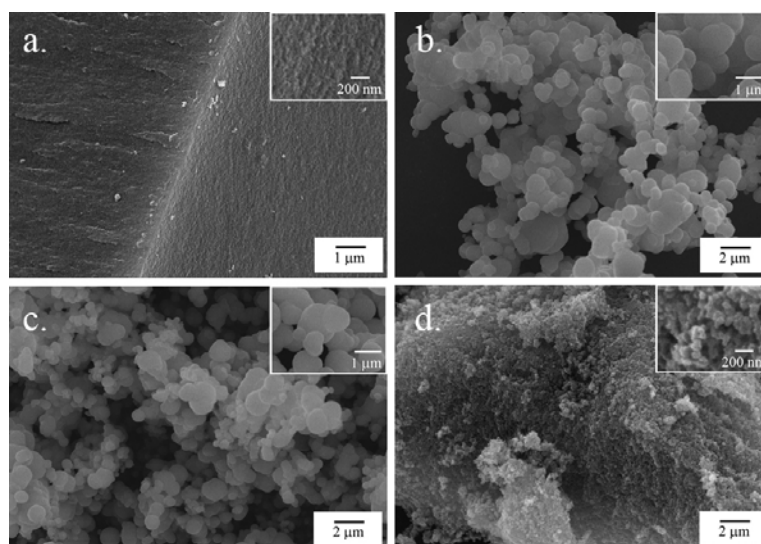
Figure 4.51 SEM micrographs of pyrolyzed carbon prepared from RF gel that was aged under humidity of 8% (a), 52.9% (b), 75.3% (c) and 100% (d).

The N_2 adsorption-desorption isotherms of all carbon products are shown in Figure 4.52. All products, except the one aged in 8% RH, show type IV isotherm, which suggests the mesoporosity nature of the products. It is also indicated from the sudden uptake of N_2 at low relative pressure in the isotherm that the products contain micropores within the structure as well. As shown in the inset of Figure 4.52, both surface area and pore size of the carbon product are increased when the humidity of the aging atmosphere is increased. It coincides with the fact that water content in the RF hydrogel after aging was found to be 30.1%, 54.3%, 89.7% and 160.5% (based on mass of the dried gel) for the gel aged in 8%, 52.9%, 75.3% and 100% RH, respectively. Therefore, it is suggested that the water content within the RF hydrogel during the aging is crucial for the formation of the pores. For the RF gel aged at 8% RH, significant amount of water evaporated out of the gel in the early stage of aging, while the structure of the pores had not yet been fully developed. Hence, the pores collapsed during aging and drying, resulting in low surface area and low pore volume of the pyrolyzed product. On the other hand, for the gel aged in high humidity, great extent of polycondensation of the RF network was achieved while water was still retained in the RF hydrogel, resulting in strengthen porous structure.
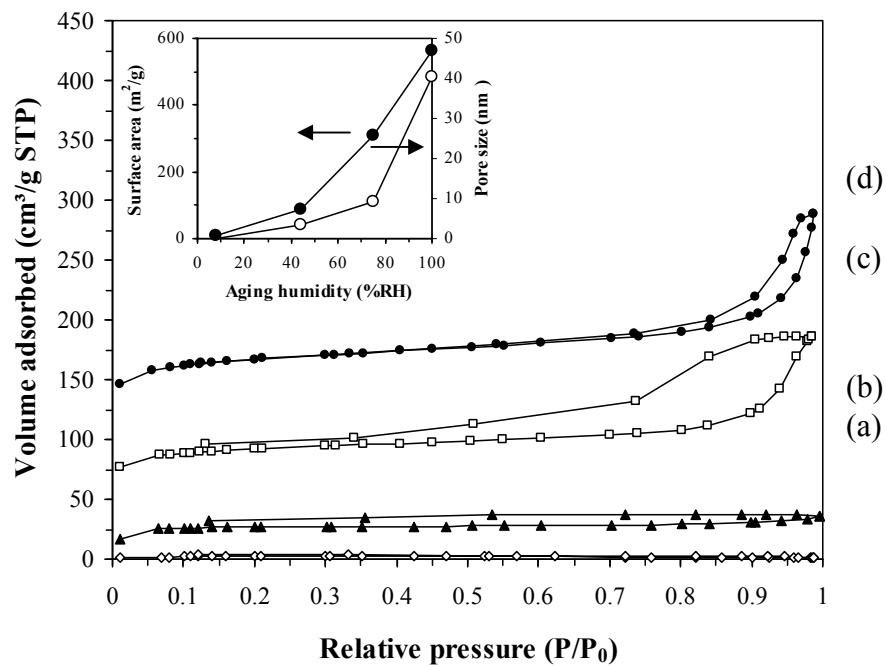
Figure 4.52 N$_2$ adsorption-desorption isotherms of carbon products prepared from RF gel that was aged under humidity of 8% (a), 52.9% (b), 75.3% (c) and 100% (d).

The previous discussion is supported by the results from FTIR analysis. The FTIR spectra of all samples show similar features, as shown by the representative spectra in Figure 4.53a, e.g., the signals located at 977, 1092, 1475 and 1605 cm^{-1} corresponding to stretching vibrations of 1, 2, 4-substituted resorcinol, C-O-C of methylene ether bridge, CH$_2$ of methylene bridge and aromatic ring, respectively (Poljanšek and Krajnc, 2005). Both methylene and methylene ether bridges are cross-linking bonds formed between aromatic rings due to polycondensation of the substituted resorcinol in the RF gel. According to Figure 4.53b, the intensity ratio of the methylene bridge with respect to aromatic ring (I_{1475}/I_{1605}) generally increases as the aging progresses. Nevertheless, the rate of increase in the formation of the bridge depends upon the aging environment. Comparing between the samples aged in 8% and 100% RH, greater amount of methylene bridge is formed initially when the gel is aged in low humidity, but the gel aged in 100% RH eventually shows greater extent of polycondensation afterward, during which the water content in the gel is still high. It should be noted that the use of such intensity ratio eliminates the effect of sample size taken in the FTIR measurement. Hence the data from different samples can be quantitatively compared.
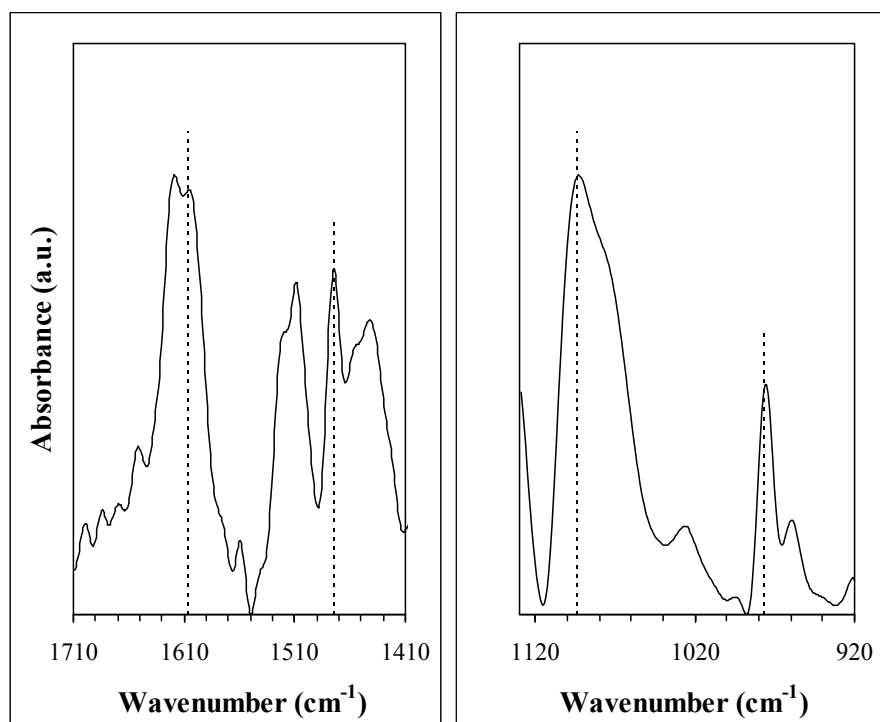
(a)
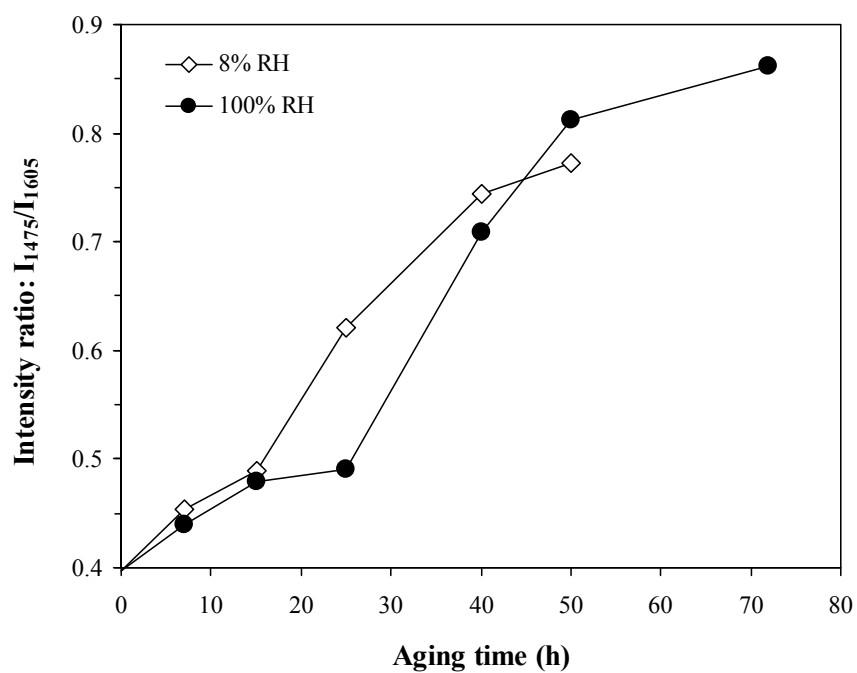
(b)

Figure 4.53 (a) Representative FTIR spectra of the RF hydrogel. (b) Ratio of the FTIR signals from methylene bridge to that of aromatic ring of the RF hydrogel during aging.

In summary, it is possible to enhance the surface area and pore volume of carbon xerogels derived from RF gel by using the very simple technique, i.e., aging the RF gel under high level of humidity. By keeping water within the hydrogel, the RF gel network can be formed with high enough mechanical strength to withstand capillary pressure and avoid the collapse of the structure during the drying. The obtained product can have high surface area comparable to those that are dried using complicated techniques such as freeze drying or super critical drying.

CHAPTER V

CONCLUSIONS AND RECOMENDATIONS

5.1 Conclusions

The conclusions of present research are the following:

1. Porous alumina can be successfully synthesized using resorcinol-formaldehyde gel as a template. High surface area of product, as high as 68 m^2/g, is obtained, even after calcination at 1200°C.

2. Aluminium acetylacetonate is more suitable for synthesizing alumina by this method than aluminium acetate and aluminium nitrate.

3. Properties of alumina product depend on various conditions such as aging time, aging temperature, aluminium content, type of catalyst and type of aluminium precursor.

5.2 Recommendations for the Future Studies

Regarding the previous conclusions, the following recommendations for the future studies are proposed.

1. Effect of drying methods such as freeze dry and supercritical dry should be investigated and compared to obtain the higher surface area of alumina product.

2. Ultrasonication should be applied during aging gel to obtain the higher surface area of alumina product.

REFERENCES

Al-Muhtaseb, S.A., and Ritter, J.A. preparation and properties of resorcinol-formaldehyde organic and carbon gels. Advanced Materials 15 (2003): 101-114.

Amin, A.S., and Zareh, M.M. Acetylacetone-formaldehyde reagent for the spectrophotometric determination of some sulfa drugs in pure and dosage forms. Microchimica Acta 124 (1996): 227-233.

Bahlawane, N., and Watanabe, T. New sol-gel route for the preparation of pure alpha-alumina at 950 degrees C. Journal of the American Ceramic Society 83 (2000): 2324-2326.

Bai, P., Wu, P., Yan, Z., and Zhao, X.S. A reverse cation-anion double hydrolysis approach to the synthesis of mesoporous γ-Al$_2$O$_3$ with a bimodal pore size distribution. Microporous and Mesoporous Materials 118 (2009): 288-295.

Boissière, C., et al. Nanocrystalline Mesoporous γ-Alumina Powders "UPMC1 Material" Gathers Thermal and Chemical Stability with High Surface Area. Chemistry of Materials 18 (2006): 5238-5243.

Brinker, C.J., and Scherer, G.W. Sol−Gel Science: The Physics and Chemistry of Sol-Gel Processing. Academic Press, 1989.

Brinker, C.J., and Scherer, G.W. Sol−Gel Science. Berlin: Springer, 1990.

Bruno, M.M., Cotella, N.G., Miras, M.C., and Barbero, C.A. A novel way to maintain resorcinol-formaldehyde porosity during drying: Stabilization of the sol-gel nanostructure using a cationic polyelectrolyte. Colloids and Surfaces A: Physicochemical and Engineering Aspects 362 (2010): 28-32.

Cava, S., et al. Structural characterization of phase transition of Al_2O_3 nanopowders obtained by polymeric precursor method. Materials Chemistry and Physics 103 (2007): 394-399.

Charles, R.G., and Pawlikowski, M.A. Comparative Heat Stabilities of Some Metal Acetylacetonate Chelates. The Journal of Physical Chemistry 62 (1958): 440-444.

Coleman, N.J., and Hench, L.L. A gel-derived mesoporous silica reference material for surface analysis by gas sorption 1. Textural features. Ceramics International 26 (2000): 171-178.

Czakkel, O., Marthi, K., Geissler, E., and László, K. Influence of drying on the morphology of resorcinol-formaldehyde-based carbon gels. Microporous and Mesoporous Materials 86 (2005): 124-133.

Dhere, S.L., Bangi, U.K.H., Latthe, S.S., and Venkateswara Rao, A. Enhancement in hydrophobicity of silica films using metal acetylacetonate and heat treatment. Journal of Physics and Chemistry of Solids 72 (2011): 45-49.

Diaz-Acosta, I., Baker, J., Cordes, W., and Pulay, P. Calculated and Experimental Geometries and Infrared Spectra of Metal Tris-Acetylacetonates: Vibrational Spectroscopy as a Probe of Molecular Structure for Ionic Complexes. Part I. The Journal of Physical Chemistry A 105 (2000): 238-244.

Dumeignil, F., et al. Modification of structural and acidic properties of sol-gel-prepared alumina powders by changing the hydrolysis ratio. Applied Catalysis A: General 241 (2003): 319-329.

Durairaj, R.B. Resorcinol: chemistry, technology, and applications. Springer, 2005.

Dynys, F.W., and Halloran, J.W. Alpha Alumina Formation in Alum-Derived Gamma Alumina. Journal of the American Ceramic Society 65 (1982): 442-448.

Ecsedi, Z., Lazau, I., and Pacurariu, C. Microstructural analysis of the effects of polyvinyl alcohol content on the porosity of sol-gel derived alumina ceramics. Microporous and Mesoporous Materials 118 (2008): 453-457.

ElKhatat, A.M., and Al-Muhtaseb, S.A. Advances in Tailoring Resorcinol-Formaldehyde Organic and Carbon Gels. Advanced Materials 23 (2011): 2887-2903.

Fessi, S., and Ghorbel, A. Preparation of Alumina Supported Palladium Catalysts by Sol-Gel Method. Journal of Sol-Gel Science and Technology 19 (2000): 417-420.

Gairola, A., Kunte, G.V., Umarji, A.M., and Shivashankar, S.A. Determination of the enthalpies of sublimation and evaporation from thermogravimetric data: Application to metalorganic complexes of Al and Cr. Thermochimica Acta 488 (2009): 17-20.

Garcia-Vergara, S.J., Skeldon, P., Thompson, G.E., and Habazaki, H. Behaviour of a fast migrating cation species in porous anodic alumina. Corrosion Science 50 (2008): 3179-3184.

Gocmez, H., and Özcan, O. Low temperature synthesis of nanocrystalline α-Al_2O_3 by a tartaric acid gel method. Materials Science and Engineering: A 475 (2008): 20-22.

Grenier-Loustalot, M.-F., Larroque, S., and Grenier, P. Phenolic resins: 5. Solid-state physicochemical study of resoles with variable FP ratios. Polymer 37 (1996a): 639-650.

Grenier-Loustalot, M.-F., Larroque, S., Grenier, P., and Bedel, D. Phenolic resins: 3. Study of the reactivity of the initial monomers towards formaldehyde at constant pH, temperature and catalyst type. Polymer 37 (1996b): 939-953.

Grenier-Loustalot, M.-F., Larroque, S., Grenier, P., and Bedel, D. Phenolic resins: 4. Self-condensation of methylolphenols in formaldehyde-free media. Polymer 37 (1996c): 955-964.

Grenier-Loustalot, M.-F., Larroque, S., Grenier, P., Leca, J.-P., and Bedel, D. Phenolic resins: 1. Mechanisms and kinetics of phenol and of the first polycondensates towards formaldehyde in solution. Polymer 35 (1994): 3046-3054.

Grenier-Loustalot, M.F., Larroque, S., Grande, D., Grenier, P., and Bedel, D. Phenolic resins: 2. Influence of catalyst type on reaction mechanisms and kinetics. Polymer 37 (1996d): 1363-1369.

Inagaki, M. Pores in carbon materials-Importance of their control. Xinxing Tan Cailiao/ New Carbon Materials 24 (2009): 193-222.

Ishizaki, K., Komarneni, S., and Nanko, M. Porous Materials: Process Technology and Applications. Kluwer Academic Publishers, 1998.

Jing, C., Xu, X., and Hou, J. Preparation of compact Al_2O_3 film on metal for oxidation resistance by polyvinylpyrrolidone. Journal of Sol-Gel Science and Technology 43 (2007): 321-327.

Jirglová, H., and Maldonado-Hódar, F.J. Chemical Interactions of Surface-Active Agents with Growing Resorcinol-Formaldehyde Gels. Langmuir 26 (2010): 16103-16109.

Job, N., Pirard, R., Marien, J., and Pirard, J.-P. Porous carbon xerogels with texture tailored by pH control during sol-gel process. Carbon 42 (2004): 619-628.

Khaleel, A., and Al-Mansouri, S. Meso-macroporous γ-alumina by template-free sol-gel synthesis: The effect of the solvent and acid catalyst on the microstructure and textural properties. Colloids and Surfaces A: Physicochemical and Engineering Aspects 369 (2010): 272-280.

Kim, S.-M., Lee, Y.-J., Jun, K.-W., Park, J.-Y., and Potdar, H.S. Synthesis of thermo-stable high surface area alumina powder from sol-gel derived boehmite. Materials Chemistry and Physics 104 (2007): 56-61.

Kim, Y., Kim, C., Kim, P., and Yi, J. Effect of preparation conditions on the phase transformation of mesoporous alumina. Journal of Non-Crystalline Solids 351 (2005): 550-556.

Kritikaki, A., and Tsetsekou, A. Fabrication of porous alumina ceramics from powder mixtures with sol-gel derived nanometer alumina: Effect of mixing method. Journal of the European Ceramic Society 29 (2009): 1603-1611.

Léonard, A., Blacher, S., Crine, M., and Jomaa, W. Evolution of mechanical properties and final textural properties of resorcinol-formaldehyde xerogels during ambient air drying. Journal of Non-Crystalline Solids 354 (2008): 831-838.

Liang, C., Sha, G., and Guo, S. Resorcinol-formaldehyde aerogels prepared by supercritical acetone drying. Journal of Non-Crystalline Solids 271 (2000): 167-170.

Lin, C., and Ritter, J.A. Effect of synthesis pH on the structure of carbon xerogels. Carbon 35 (1997): 1271-1278.

Lin, Y.-S., and Burggraaf, A.J. Preparation and Characterization of High-Temperature Thermally Stable Alumina Composite Membrane. Journal of the American Ceramic Society 74 (1991): 219-224.

Lippens, B.C., and Steggerdo, J.J. Physical and chemical aspects of adsorbents and catalysts. New York: Academic Press, 1970.

Maekawa, H., Esquena, J., Bishop, S., Solans, C., and Chmelka, B.F. Meso/Macroporous Inorganic Oxide Monoliths from Polymer Foams. Advanced Materials 15 (2003): 591-596.

Mahmoud, M.E., Osman, M.M., Hafez, O.F., and Elmelegy, E. Removal and preconcentration of lead (II), copper (II), chromium (III) and iron (III) from wastewaters by surface developed alumina adsorbents with immobilized 1-nitroso-2-naphthol. Journal of Hazardous Materials 173 (2010): 349-357.

Mark, J.E., West, R., and Allcock, H.R. Inorganic Polymers. 2nd ed. Oxford University Press, 1989.

Moreno-Castilla, C., and Maldonado-Hódar, F.J. Carbon aerogels for catalysis applications: An overview. Carbon 43 (2005): 455-465.

Morterra, C., and Magnacca, G. A case study: Surface chemistry and surface structure of catalytic aluminas, as studied by vibrational spectroscopy of adsorbed species. Catalysis Today 27 (1996): 497-532.

Parida, K.M., Pradhan, A.C., Das, J., and Sahu, N. Synthesis and characterization of nano-sized porous gamma-alumina by control precipitation method. Materials Chemistry and Physics 113 (2009): 244-248.

Pekala, R.W. Organic aerogels from the polycondensation of resorcinol with formaldehyde. Journal of Materials Science 24 (1989): 3221-3227.

Pekala, R.W., Alviso, C.T., and LeMay, J.D. Organic aerogels: A new type of ultrastructured polymer. 1991.

Pekala, R.W., and Schaefer, D.W. Structure of organic aerogels. 1. Morphology and scaling. Macromolecules 26 (1993): 5487-5493.

Pizzi, A., Horak, R.M., Ferreira, D., and Roux, D.G. Condensates of phenol, resorcinol, phloroglucinol, and pyrogallol as model compounds of flavonoid A- and B-rings with formaldehyde. Journal of Applied Polymer Science 24 (1979): 1571-1578.

Poljanšek, I., and Krajnc, M. Characterization of Phenol-Formaldehyde Prepolymer Resins by In Line FT-IR Spectroscopy. Acta Chimica Slovenica 52 (2005): 238-244.

Raff, R.A.V., and Silverman, B.H. Kinetics of the Uncatalyzed Reactions between Resorcinol and Formaldehyde. Industrial & Engineering Chemistry 43 (1951): 1423-1427.

Ramanathan, S., Bhat, R., Upadhyaya, D., and Roy, S. Alumina ceramics by sol-gel technique. Bulletin of Materials Science 17 (1994): 95-103.

Ray, J.C., You, K.-S., Ahn, J.-W., and Ahn, W.-S. Mesoporous alumina (I): Comparison of synthesis schemes using anionic, cationic, and non-ionic surfactants. Microporous and Mesoporous Materials 100 (2007): 183-190.

Reddy, D.J.P., Rajulu, A.V., Arumugam, V., and Naresh, M.D. Effects of Resorcinol On the Mechanical Properties of Soy Protein Isolate Films. Journal of Plastic Film and Sheeting 25 (2009): 221-233.

Regalbuto, J. Catalyst Preparation: Science and Engineering CRC Press, 2006.

Saunders, K.J. Organic polymer chemistry: an introduction to the organic chemistry of adhesives, fibres, paints, plastics and rubbers. 2nd ed. Chapman and Hall, 1988.

Schaefer, D.W., Pekala, R., and Beaucage, G. Origin of porosity in resorcinol-formaldehyde aerogels. Journal of Non-Crystalline Solids 186 (1995): 159-167.

Šebenik, A., Osredkar, U., and Vizovišek, I. Study of the reaction between resorcinol and formaldehyde. Polymer 22 (1981): 804-806.

Shen, C., and Shaw, L. FTIR analysis of the hydrolysis rate in the sol–gel formation of gadolinia-doped ceria with acetylacetonate precursors. Journal of Sol-Gel Science and Technology 53 (2010): 571-577.

Shi, L., and Wong, N.B. Preparation and characterization of alumina membranes and alumina-titania composite membranes. Journal of Materials Research 14 (1999): 3599-3603.

Shirodker, M., Borker, V., Nather, C., Bensch, W., and Rane, K.S. Synthesis and structure of tris (acetylacetonato) aluminum(III). Indian Journal of Chemistry: Section A 49 (2010): 1607-1611.

Sing, K.S.W., et al. Reporting Physisorption Data for Gas/Solid Systems. Pure and Applied Chemistry 57 (1985): 603-619.

Slabzhennikov, S.N., Ryabchenko, O.B., and Kuarton, L.A. Interpretation of the IR spectra of aluminum, gallium, and indium tris(acetylacetonates). Russian Journal of Coordination Chemistry 32 (2006): 545-551.

Sohn, J.R., and Lee, S.I. An Infrared Spectroscopic Study of Acetylacetone Adsorbed on Layer Silicates Containing Various Interlayer Cations. Journal of Industrial and Engineering Chemistry 3 (1997): 198-202.

Soykeabkaew, N., Supaphol, P., and Rujiravanit, R. Preparation and characterization of jute- and flax-reinforced starch-based composite foams. Carbohydrate Polymers 58 (2004): 53-63.

Streitwieser, A., and Heathcock, C.H. Introduction to organic chemistry. New York: Macmillan, 1976.

Studart, A.R., Gonzenbach, U.T., Tervoort, E., and Gauckler, L.J. Processing Routes to Macroporous Ceramics: A Review. Journal of the American Ceramic Society 89 (2006): 1771-1789.

Tamon, H., and Ishizaka, H. SAXS Study on Gelation Process in Preparation of Resorcinol-Formaldehyde Aerogel. Journal of Colloid and Interface Science 206 (1998): 577-582.

Tamon, H., and Ishizaka, H. Influence of Gelation Temperature and Catalysts on the Mesoporous Structure of Resorcinol-Formaldehyde Aerogels. Journal of Colloid and Interface Science 223 (2000): 305-307.

Tayyari, S.F., and Milani-nejad, F. Vibrational assignment of acetylacetone. Spectrochimica Acta Part A: Molecular and Biomolecular Spectroscopy 56 (2000): 2679-2691.

Tikhov, S.F., Fenelonov, V.B., Zaikovskii, V.I., Potapova, Y.V., and Sadykov, V.A. The three-dimensional microporous structure of alumina synthesized through the aluminum hydrothermal oxidation route. Microporous and Mesoporous Materials 33 (1999): 137-142.

Tokudome, Y., Fujita, K., Nakanishi, K., Miura, K., and Hirao, K. Synthesis of Monolithic Al$_2$O$_3$ with Well-Defined Macropores and Mesostructured Skeletons via the Sol-Gel Process Accompanied by Phase Separation. Chemistry of Materials 19 (2007): 3393-3398.

Tonanon, N., et al. Improvement of mesoporosity of carbon cryogels by ultrasonic irradiation. Carbon 43 (2005): 525-531.

Varagnat, J. Encyclopedia of Chemical Technology. Vol. 13, New York: Wiley.

Werstler, D.D. Quantitative 13C n.m.r. characterization of aqueous formaldehyde resins: 2. Resorcinol-formaldehyde resins. Polymer 27 (1986): 757-764.

Xu, B., et al. Synthesis of mesoporous alumina with highly thermal stability using glucose template in aqueous system. Microporous and Mesoporous Materials 91 (2006): 293-295.

Yao, N., et al. Ultrasonic Synthesis of Silica-Alumina Nanomaterials with Controlled Mesopore Distribution without Using Surfactants. Langmuir 18 (2002): 4111-4117.

Yeung, K.L., Sebastian, J.M., and Varma, A. Mesoporous alumina membranes: Synthesis, characterization, thermal stability and nonuniform distribution of catalyst. Journal of Membrane Science 131 (1997): 9-28.

Yoldas, B.E. Alumina Sol Preparation from Alkoxides. American Ceramic Society Bulletin 54 (1975): 289-290.

Yu, H.A., Kaneko, T., Yoshimura, S., and Otani, S. A turbostratic carbon with high specific surface area from 1,4-benzenedimethanol. Carbon 34 (1996): 676-678.

Zhang, W.-j., He, Y.-q., and Qi, Q. Synthesize of porous TiO$_2$ thin film of photocatalyst by charged microemulsion templating. <u>Materials Chemistry and Physics</u> 93 (2005): 508-515.

Zhang, Y., Liang, H., Zhao, C., and Liu, Y. Macroporous alumina monoliths prepared by filling polymer foams with alumina hydrosols. <u>Journal of Materials Science</u> 44 (2009): 931-938.

Zhang, Z.Y. Catalytic Effect of Aluminum Acetylacetonate on Hydrolysis and Polymerization of Methyltrimethoxysilane. <u>Langmuir</u> 13 (1997): 473-476.

APPENDIX

CALCULATION OF THE CRYSTALLITE SIZE

Calculation of the crystallite size by Debye-Scherrer equation

The crystallite size was calculated from the width at half-height of the diffraction peak of XRD pattern using the Debye-Scherrer equation.

From Scherrer equation:

$$D = \frac{K\lambda}{\beta \cos \theta} \tag{A.1}$$

where   D = Crystallite size, Å

K = Crystallite-shape factor = 0.9

λ = X-ray wavelength, 1.5418 Å for CuKα

θ =   Observed peak angle, degree

β =   X-ray diffraction broadening, radian

The X-ray diffraction broadening (β) is the pure width of a powder diffraction, free of all broadening due to the experimental equipment. Standard α-alumina is used to observe the instrumental broadening since its crystallite size is larger than 2000 Å. The X-ray diffraction broadening (β) can be obtained by using Warren's formula.

From Warren's formula:

$$\beta^2 = B_M^2 - B_S^2 \tag{A.2}$$

$$\beta = \sqrt{B_M^2 - B_S^2}$$

Where B_M = The measured peak width in radians at half peak height.

B_S =   The corresponding width of a standard material.

Example: Calculation of the crystallite size of titania

The half-height width of 101 diffraction peak $= 0.93125^{o}$

$\qquad\qquad\qquad\qquad\qquad\qquad\qquad\qquad = 0.01625$ radian

The corresponding half-height width of peak of α-alumina $= 0.004$ radian

The pure width $\qquad = \sqrt{B_M^2 - B_S^2}$

$\qquad\qquad\qquad = \sqrt{0.01625^2 - 0.004^2}$

$\qquad\qquad\qquad = 0.01577$ radian

$\beta \quad = \quad 0.01577$ radian

$2\theta \quad = \quad 25.56^{o}$

$\theta \quad = \quad 12.78^{o}$

$\lambda \quad = \quad 1.5418$ Å

The crystallite size $\quad = \quad \dfrac{0.9 x\, 1.5418}{0.01577 \ \cos 12.78} \quad = \quad 90.15$Å

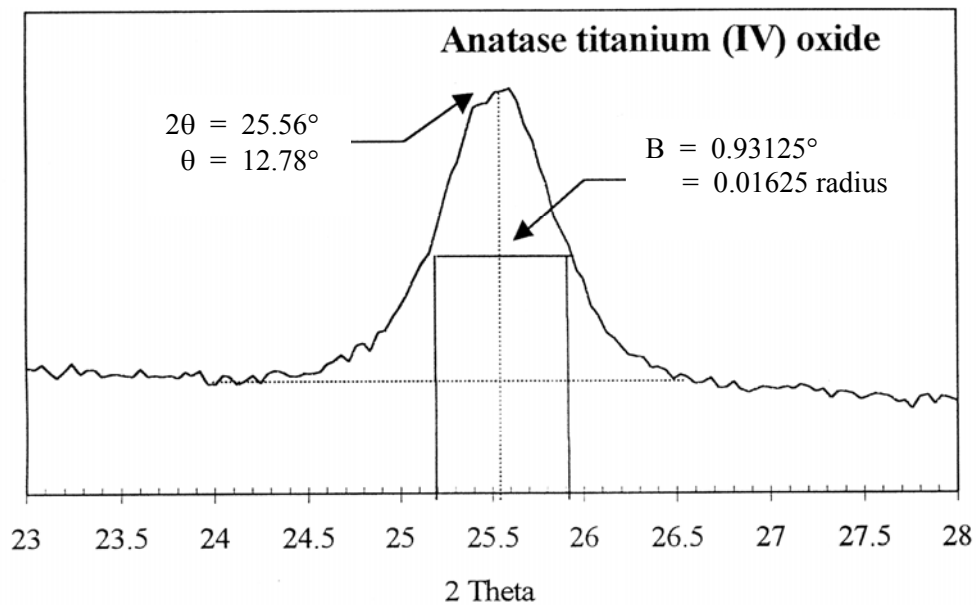$\qquad\qquad\qquad\qquad\qquad = \qquad 9$ nm

Figure A.1 The 101 diffraction peak of titania for calculation of the crystallite size
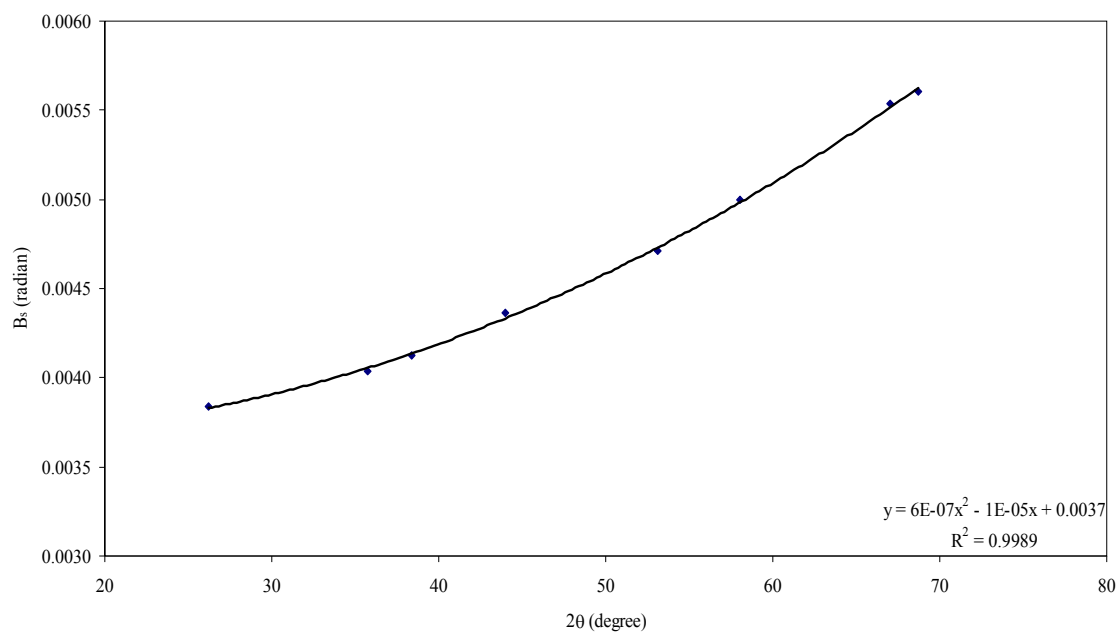
Figure A.2 The plot indicating the value of line broadening due to the equipment. The data were obtained by using α-alumina as standard.

VITA

Miss Pamornrat Chantam was born on December 9, 1981 in Nakornratchasima, Thailand. She finished high school from Pakchong School, Nakornratchasima in 1998. She received the Bachelor's Degree in Chemical Engineering from Suranaree University of Technology in December 2004. She entered the Master of Engineering in Chemical Engineering at Chulalongkorn University in June, 2005. She subsequently continued studying Doctoral degree of Chemical Engineering, Chulalongkorn University since May 2007.